

BWR Anticipated Transients Without Scram in the MELLLA+ Expanded Operating Domain

Part 2:
Sensitivity Studies for Events
Leading to Instability

AVAILABILITY OF REFERENCE MATERIALS IN NRC PUBLICATIONS

NRC Reference Material

As of November 1999, you may electronically access NUREG-series publications and other NRC records at NRC's Library at www.nrc.gov/reading-rm.html. Publicly released records include, to name a few, NUREG-series publications; *Federal Register* notices; applicant, licensee, and vendor documents and correspondence; NRC correspondence and internal memoranda; bulletins and information notices; inspection and investigative reports; licensee event reports; and Commission papers and their attachments.

NRC publications in the NUREG series, NRC regulations, and Title 10, "Energy," in the *Code of Federal Regulations* may also be purchased from one of these two sources.

1. The Superintendent of Documents

U.S. Government Publishing Office
Mail Stop IDCC
Washington, DC 20402-0001
Internet: bookstore.gpo.gov
Telephone: (202) 512-1800
Fax: (202) 512-2104

2. The National Technical Information Service

5301 Shawnee Rd., Alexandria, VA 22312-0002
www.ntis.gov
1-800-553-6847 or, locally, (703) 605-6000

A single copy of each NRC draft report for comment is available free, to the extent of supply, upon written request as follows:

Address: **U.S. Nuclear Regulatory Commission**
Office of Administration
Publications Branch
Washington, DC 20555-0001
E-mail: distribution.resource@nrc.gov
Facsimile: (301) 415-2289

Some publications in the NUREG series that are posted at NRC's Web site address www.nrc.gov/reading-rm/doc-collections/nuregs are updated periodically and may differ from the last printed version. Although references to material found on a Web site bear the date the material was accessed, the material available on the date cited may subsequently be removed from the site.

Non-NRC Reference Material

Documents available from public and special technical libraries include all open literature items, such as books, journal articles, transactions, *Federal Register* notices, Federal and State legislation, and congressional reports. Such documents as theses, dissertations, foreign reports and translations, and non-NRC conference proceedings may be purchased from their sponsoring organization.

Copies of industry codes and standards used in a substantive manner in the NRC regulatory process are maintained at—

The NRC Technical Library

Two White Flint North
11545 Rockville Pike
Rockville, MD 20852-2738

These standards are available in the library for reference use by the public. Codes and standards are usually copyrighted and may be purchased from the originating organization or, if they are American National Standards, from—

American National Standards Institute

11 West 42nd Street
New York, NY 10036-8002
www.ansi.org
(212) 642-4900

Legally binding regulatory requirements are stated only in laws; NRC regulations; licenses, including technical specifications; or orders, not in NUREG-series publications. The views expressed in contractor-prepared publications in this series are not necessarily those of the NRC.

The NUREG series comprises (1) technical and administrative reports and books prepared by the staff (NUREG-XXXX) or agency contractors (NUREG/CR-XXXX), (2) proceedings of conferences (NUREG/CP-XXXX), (3) reports resulting from international agreements (NUREG/IA-XXXX), (4) brochures (NUREG/BR-XXXX), and (5) compilations of legal decisions and orders of the Commission and Atomic and Safety Licensing Boards and of Directors' decisions under Section 2.206 of NRC's regulations (NUREG-0750).

DISCLAIMER: This report was prepared as an account of work sponsored by an agency of the U.S. Government. Neither the U.S. Government nor any agency thereof, nor any employee, makes any warranty, expressed or implied, or assumes any legal liability or responsibility for any third party's use, or the results of such use, of any information, apparatus, product, or process disclosed in this publication, or represents that its use by such third party would not infringe privately owned rights.



United States Nuclear Regulatory Commission

Protecting People and the Environment

NUREG/CR-7180
BNL-NUREG-105327-2014

BWR Anticipated Transients Without Scram in the MELLLA+ Expanded Operating Domain

Part 2: Sensitivity Studies for Events Leading to Instability

Manuscript Completed: April 2014

Date Published: June 2015

Prepared by:

Lap-Yan Cheng, Joo Seok Baek, Arantxa Cuadra, Arnold Aronson,
David Diamond, and Peter Yarsky*

Nuclear Science and Technology Department
Brookhaven National Laboratory

*U.S. Nuclear Regulatory Commission

Tarek Zaki, NRC Project Manager

NRC Job Codes V6150 and F6018

Office of Nuclear Regulatory Research

ABSTRACT

This is the second in a series of reports on the response of a BWR/5 boiling water reactor, operating in the expanded operating domain “MELLLA+,” to anticipated transients without reactor scram (ATWS). Herein, ATWS events initiated by a turbine trip are considered at two points in the fuel cycle: the beginning of cycle (BOC), and at peak hot excess reactivity (PHE, close to the middle of the cycle). We evaluate the effects of modeling the gap conductance (between the fuel pellet and clad), the turbine bypass fraction, and the initial core flow rate. We compare two limiting fixed values of gas-gap conductance, a low value of $5,000 \text{ W/m}^2\text{-K}$ at BOC and a high value of $161,000 \text{ W/m}^2\text{-K}$ at PHE with corresponding base cases that utilize a dynamic gas-gap model. We analyze two turbine bypass fractions, viz., 10% and 25% at PHE, and compare them with the 100% bypass base case. A reduced core flow of 75% of the rated core flow is analyzed at PHE and compared with the base case of 85%.

The simulations were carried out using the TRACE/PARCS code system and models developed for a previous study with all relevant BWR/5 systems. Modeling in the core is particularly detailed (four types of fuel rods are included in each fuel assembly, and 382 thermal-hydraulic channels to represent all assemblies, taking into account half-core symmetry) so as to capture the complex neutronic thermal-hydraulic coupling during periods of instability.

The study offers insights into the behavior of the reactor during these events, including the impact of the operator’s assumed actions on its oscillatory behavior due to instabilities in the reactor, and on its eventual shutdown. It shows the effect of gap conductance, turbine bypass fraction, and initial flow rate.

TABLE OF CONTENTS

ABSTRACT.....	iii
TABLE OF CONTENTS.....	v
LIST OF FIGURES.....	vii
LIST OF TABLES.....	ix
ACKNOWLEDGMENTS.....	xi
ACRONYMS.....	xiii
1 INTRODUCTION.....	1-1
1.1 Background.....	1-1
1.2 Objectives.....	1-1
1.3 Methodology.....	1-2
1.4 Organization of Report.....	1-3
2 SENSITIVITY STUDIES FOR TURBINE TRIP EVENTS.....	2-1
2.1 Gap Conductance Modeling.....	2-1
2.1.1 Initial Conditions.....	2-2
2.1.2 Sequence of Events.....	2-3
2.1.3 Steamline Flow.....	2-5
2.1.4 Core Power and Dome Pressure.....	2-7
2.1.5 Core Flow.....	2-13
2.1.6 Feedwater Flow and RPV Water Level.....	2-16
2.1.7 Boron Inventory in Core.....	2-18
2.1.8 Liquid Subcooling of Core Flow.....	2-20
2.1.9 Fuel Rod Cladding Temperature.....	2-21
2.1.10 Ratio of Power to Product of Flow and Enthalpy.....	2-23
2.1.11 Additional Figures-of-Merit.....	2-24
2.1.12 Summary.....	2-26
2.2 Effect of Turbine Bypass Fraction at PHE.....	2-28
2.2.1 Bypass Fractions.....	2-28
2.2.2 Initial Conditions.....	2-28
2.2.3 Sequence of Events.....	2-29
2.2.4 Steamline Flow and Dome Pressure.....	2-29
2.2.5 Core Power.....	2-31
2.2.6 Core Flow.....	2-34
2.2.7 Feedwater Flow and RPV Water Level.....	2-35
2.2.8 Boron Inventory in Core.....	2-37
2.2.9 Liquid Subcooling of Core Flow.....	2-37
2.2.10 Fuel Rod Cladding Temperature.....	2-38
2.2.11 Ratio of Power to Product of Flow and Enthalpy.....	2-39
2.2.12 Additional Figures-of-Merit.....	2-40
2.2.13 Summary.....	2-42
2.3 Effect of Initial Core Flow Rate at PHE.....	2-43
2.3.1 Core Flow Rates at PHE.....	2-43
2.3.2 Initial Conditions.....	2-43
2.3.3 Sequence of Events.....	2-43
2.3.4 Steamline Flow.....	2-45
2.3.5 Core Power and Dome Pressure.....	2-45
2.3.6 Core Flow.....	2-47
2.3.7 Feedwater Flow and RPV Water Level.....	2-48
2.3.8 Boron Inventory in Core.....	2-51
2.3.9 Liquid Subcooling of Core Flow.....	2-51

2.3.10	Fuel Rod Cladding Temperature.....	2-52
2.3.11	Ratio of Power-to-Product-of-Flow-and-Enthalpy.....	2-54
2.3.12	Additional Figures-of-Merit.....	2-54
2.3.13	Summary.....	2-56
3	Summary and Conclusions.....	3-1
4	References.....	4-1
Appendix A - Modeling of Gap Conductance.....		A-1

LIST OF FIGURES

Figure 2.1	Steamline Mass Flow Rate - Effect of Low Gas-Gap Conductance at BOC.....	2-6
Figure 2.2	Steamline Mass Flow Rate - Effect of High Gas-Gap Conductance at PHE	2-6
Figure 2.3	Core Power - Effect of Low Gas-Gap Conductance at BOC	2-7
Figure 2.4	Core Power - Effect of High Gas-Gap Conductance at PHE.....	2-8
Figure 2.5	Gap Conductance Calculated by the Dynamic Gas-Gap Model	2-8
Figure 2.6	Total Reactivity for the Two PHE Cases.....	2-9
Figure 2.7	Moderator Reactivity for the Two PHE Cases.....	2-10
Figure 2.8	Doppler Reactivity for the Two PHE Cases	2-10
Figure 2.9	Boron Reactivity for the Two PHE Cases	2-11
Figure 2.10	Fuel Centerline and Cladding Temperatures in Channel 245 at BOC.....	2-12
Figure 2.11	Fuel Centerline and Cladding Temperatures in Channel 243 at PHE	2-12
Figure 2.12	Change of Fuel Centerline Temperatures in Channel 243 in Northeast Quadrant at PHE.....	2-13
Figure 2.13	RPV Pressure - Effect of Low Gas-Gap Conductance at BOC	2-14
Figure 2.14	RPV Pressure - Effect of High Gas-Gap Conductance at PHE	2-14
Figure 2.15	Core Flow Rate - Effect of Low Gas-Gap Conductance at BOC	2-15
Figure 2.16	Core Flow Rate - Effect of High Gas-Gap Conductance at PHE.....	2-15
Figure 2.17	Feedwater Flow Rate - Effect of Low Gas-Gap Conductance at BOC	2-16
Figure 2.18	Feedwater Flow Rate - Effect of High Gas-Gap Conductance at PHE.....	2-17
Figure 2.19	Downcomer Water Level - Effect of Low Gas-Gap Conductance at BOC.....	2-17
Figure 2.20	Downcomer Water Level - Effect of High Gas-Gap Conductance at PHE.....	2-18
Figure 2.21	Boron Inventory in Reactor Core - Effect of Low Gas-Gap Conductance at BOC	2-19
Figure 2.22	Boron Inventory in Reactor Core - Effect of High Gas-Gap Conductance at PHE.....	2-19
Figure 2.23	Liquid Subcooling at the Core Inlet - Effect of Low Gas-Gap Conductance at BOC	2-20
Figure 2.24	Liquid Subcooling at the Core Inlet - Effect of High Gas-Gap Conductance at PHE.....	2-21
Figure 2.25	Maximum Cladding Temperature among all Fuel Bundles - Effect of Low Gas-Gap Conductance at BOC.....	2-22
Figure 2.26	Maximum Cladding Temperature among All Fuel Bundles - Effect of High Gas-Gap Conductance at PHE	2-22
Figure 2.27	Ratio of Power to Product of Flow and Enthalpy (FOM1) in Limiting Bundles - Effect of Low Gas-Gap Conductance at BOC.....	2-23
Figure 2.28	Ratio of Power to Product of Flow and Enthalpy (FOM1) in Limiting Bundles - Effect of High Gas-Gap Conductance at PHE	2-24
Figure 2.29	Power Oscillation Modes - Low Gas-Gap Conductance at BOC.....	2-25
Figure 2.30	Power Oscillation Modes - High Gas-Gap Conductance at PHE	2-26
Figure 2.31	Steamline Mass Flow Rate - Effect of Turbine Bypass Fraction at PHE	2-30
Figure 2.32	RPV Pressure - Effect of Turbine Bypass Fraction at PHE.....	2-31
Figure 2.33	Core Power - Effect of Turbine Bypass Fraction at PHE.....	2-32
Figure 2.34	Core Power at PHE with 10% Bypass Fraction (Case 2A).....	2-32
Figure 2.35	Core Power at PHE with 25% Bypass Fraction (Case 2B).....	2-33
Figure 2.36	Core Power at PHE with 100% Bypass Fraction (Case 2).....	2-33
Figure 2.37	Core Power - Effect of Turbine Bypass Fraction at BOC	2-34
Figure 2.38	Core Flow Rate - Effect of Turbine Bypass Fraction at PHE.....	2-35
Figure 2.39	Feedwater Flow Rate - Effect of Turbine Bypass Fraction at PHE.....	2-36
Figure 2.40	Downcomer Water Level - Effect of Turbine Bypass Fraction at PHE.....	2-36

Figure 2.41	Boron Inventory in Reactor Core - Effect of Turbine Bypass Fraction at PHE...	2-37
Figure 2.42	Liquid Subcooling at Core Inlet - Effect of Turbine Bypass Fraction at PHE	2-38
Figure 2.43	Maximum Cladding Temperature among All Fuel Bundles - Effect of Turbine Bypass Fraction at PHE	2-39
Figure 2.44	Ratio of Power-to-Product-of-Flow-and-Enthalpy (FOM1) in Limiting Bundles - Effect of Turbine Bypass Fraction at PHE.....	2-40
Figure 2.45	Power Oscillation Modes - 10% Turbine Bypass at PHE.....	2-41
Figure 2.46	Power Oscillation Modes - 25% Turbine Bypass Fraction at PHE	2-42
Figure 2.47	Steamline Mass Flow Rate - Effect of Core Flow at PHE	2-45
Figure 2.48	Core Power - Effect of Core Flow at PHE.....	2-46
Figure 2.49	Void Reactivity - Effect of Core Flow at PHE	2-46
Figure 2.50	RPV Pressure - Effect of Core Flow at PHE	2-47
Figure 2.51	Reactor Core Flow Rate - Effect of Core Flow at PHE.....	2-48
Figure 2.52	Feedwater Flow Rate - Effect of Core Flow at PHE.....	2-49
Figure 2.53	Downcomer Water Level - Effect of Core Flow at PHE.....	2-50
Figure 2.54	Coolant Mass in Ring 1 Separators - Effect of Core Flow at PHE.....	2-50
Figure 2.55	Boron Inventory in Reactor Core - Effect of Core Flow at PHE.....	2-51
Figure 2.56	Liquid Subcooling at Core Inlet - Effect of Core Flow at PHE	2-52
Figure 2.57	Maximum Cladding Temperature among all Fuel Bundles - Effect of Core Flow at PHE	2-53
Figure 2.58	Local Peak Power - Effect of Core Flow at PHE.....	2-53
Figure 2.59	Ratio of Power to Product of Flow and Enthalpy (FOM1) in Limiting Bundles - Effect of Core Flow at PHE.....	2-54
Figure 2.60	Power Oscillation Modes - 75% Core Flow at PHE	2-55

LIST OF TABLES

Table 1.1	Simulation Conditions of ATWS-I Cases.....	1-2
Table 2.1	Simulation Conditions - Effect of Gap Conductance Modeling	2-1
Table 2.2	Comparison of Steady-State Thermal-Hydraulic Parameters - Effect of Gap Conductance Modeling	2-2
Table 2.3	Comparison of Initial Fuel Temperatures - Effect of Gap Conductance Modeling	2-3
Table 2.4	Sequence of Events - Effect of Gap Conductance Modeling.....	2-4
Table 2.5	Figures-of-Merit Associated with the Evolution of Power Instability - Effect of Gas-Gap Modeling	2-25
Table 2.6	Turbine Bypass Fractions and Simulation Conditions	2-28
Table 2.7	Comparison of Steady-State Thermal-Hydraulic Parameters - Effect of Turbine Bypass Fraction at PHE	2-28
Table 2.8	Sequence of Events - Effect of Turbine Bypass Fraction at PHE.....	2-29
Table 2.9	Figures-of-Merit Associated with Evolution of Power Instability - Effect of Turbine Bypass Fraction at PHE	2-40
Table 2.10	Initial Core Flow Rate at PHE and Simulation Conditions	2-43
Table 2.11	Comparison of Steady-State Thermal-Hydraulic Parameters - Effect of Core Flow Rate at PHE	2-43
Table 2.12	Sequence of Events - Effect of Core Flow Rate at PHE.....	2-44
Table 2.13	Figures-of-Merit Associated with Evolution of Power Instability - Effect of Core Flow Rate at PHE	2-55

ACKNOWLEDGMENTS

This project was a joint effort of Brookhaven National Laboratory (BNL) and U.S. Nuclear Regulatory Commission staff. The authors wish to thank the Project Manager, Tarek Zaki, and his predecessor, Istvan Frankl, for their support and technical feedback. We greatly appreciated the efforts of the staff in the Office of Nuclear Regulatory Research, Reactor Systems Code Development Branch, to quickly assess and implement improvements, as they were identified, in the computer codes used in the project. We also appreciate the work done by Lynda Fitz in finalizing this document and providing administrative support.

ACRONYMS

3D	Three Dimensional
ADF	Assembly Discontinuity Factor
ADS	Automatic Depressurization System
ATWS	Anticipated Transient Without SCRAM
ATWS-ED	Anticipated Transient Without SCRAM with Emergency Depressurization
ATWS-I	Anticipated Transient Without SCRAM with Instability
BNL	Brookhaven National Laboratory
BOC	Beginning-of-Cycle
BWR	Boiling Water Reactor
CB	Control Block in TRACE Input
CONTAN	Containment Component in TRACE Input
CST	Condensate Storage Tank
DC	Downcomer
DW	Drywell
DWO	Density-Wave Oscillation
ED	Emergency Depressurization
EOFPL	End-of-Full-Power-Life
EPU	Extended Power Uprate
FCT	Fuel Centerline Temperature
FCW	Flow Control Window
FOM	Figure-of-Merit
FW	Feedwater
GE	General Electric
GEH	GE Hitachi
HCTL	Heat Capacity Temperature Limit
MELLLA+	Maximum Extended Load Line Limit Analysis Plus
MSIV	Main Steam Isolation Valve
NRC	U.S. Nuclear Regulatory Commission
OLTP	Original Licensed Thermal Power
PARCS	Purdue Advanced Reactor Core Simulator
PCT	Peak Clad Temperature
PHE	Peak-Hot-Excess-Reactivity
RCIC	Reactor Core Isolation Cooling
RPS	Reactor Protection System
RPT	Recirculation Pump Trip
RPV	Reactor Pressure Vessel
RWL	Reactor Water Level
SETS	Stability Enhancing Two-Step method
S-I	Semi-Implicit Numerics
SLCS	Standby Liquid Control System
SP	Suppression Pool
SRV	Safety Relief Valve
TAF	Top-of-Active Fuel
TBV	Turbine Bypass Valve
TRACE	TRAC-RELAP Advanced Computational Engine
TSV	Turbine Stop Valve
UH	Void History
UHSPH	Void History Spectrally Corrected
WR	Water Rod

1 INTRODUCTION

1.1 Background

In recent years, the operating power of boiling water reactors (BWRs) has been increased; sometimes to 120% of the original licensed thermal power (OLTP). This places them in an expanded operating domain and changes how they maneuver in the power-flow operating map. One option being pursued, the “maximum extended load line limit analysis plus” (MELLLA+) operation [1], raises questions about how the plant will respond to anticipated transients without scram (ATWS). This report is one of a series of several reports that describes how these events were simulated with state-of-the-art codes, and gives the results of that analysis.

In a previous report [2] we discussed how MELLLA+ operation affects the power-flow operating map, and its impact in an ATWS event. If the initiating event is a turbine trip, then after the recirculation pumps have automatically tripped, the reactor evolves to a relatively high power-to-flow condition, and specifically to a region of the power-flow map wherein unstable power oscillations are likely to occur. If these power oscillations are left unmitigated, the fuel may be damaged. Additionally, the severity of the power oscillations may hamper the effectiveness of mitigation strategies. For example, ATWS events typically are mitigated by the injection of dissolved neutron absorber (boron) through the standby liquid control system; the occurrence of an oscillation-induced reversal of core inlet flow may reduce the rate at which this soluble absorber is delivered to the reactor core.

ATWS scenarios initiated by closure of the main steamline isolation valves are also of concern. In these events, the amount of energy being placed into containment during the mitigation period may be excessive. This thermal load may exhaust the available pressure suppression capacity of the containment wetwell and this would prompt an emergency depressurization according to standard emergency operating procedures. An emergency depressurization poses several problems: (1) The reactor has undergone a beyond-design-basis event, and the fuel may have been damaged; (2) the pressure suppression capacity of the containment has been exhausted; and, (3) the boundary of reactor coolant pressure has been bypassed by manually opening the automatic depressurization system’s valves. These events are detailed in our companion reports [3, 4].

1.2 Objectives

ATWS events leading to instability (ATWS-I) were studied in our previous report [2] for a typical BWR/5 plant. Table 1.1 summarizes the specific cases considered with a turbine trip as the initiating event. We gained significant insight as to the reactor’s behavior and the ability to mitigate events initiated by turbine trip with reactor trip assumed to fail. In the present study, the objective is to understand the sensitivity of events initiated by a turbine trip to fuel gap conductance, initial flow rate, and turbine bypass capacity as a fraction of nuclear boiler rating (hereafter bypass fraction) at a different point in the fuel cycle.

Table 1.1 Simulation Conditions of ATWS-I Cases

Case ID	Exposure ¹	Power ² % of OLTP	Flow Rate, % ³	Bypass Capacity, % ⁴	Spectral History ⁵
1	BOC	120	85	100	UH
1A	BOC	120	85	10	UH
1B	BOC	120	85	25	UH
1F	BOC	120	85	50	UH
2	PHE	120	85	100	UH
2G	PHE	120	85	100	UHSPH
3	EOFPL	120	105	100	UH

¹ BOC, PHE, and EOFPL, respectively, represent beginning-of-cycle, peak-hot-excess-reactivity, and end-of-full-power-life.

² Power of 120% is 3,988 MWt.

³ Core flow rate of 100% is 13,670.8 kg/s.

⁴ Bypass capacity is the percentage of normal steam flow to the turbine.

⁵ UH and UHSPH, respectively, stand for void history and spectrally corrected void history as discussed in Section 3.2.5 in [2].

1.3 Methodology

The methodology used in the present study is the same as that we used in our original study [2], where it is explained in detail. Our basic tool is TRACE/PARCS that couples the modeling of thermal-hydraulics throughout all relevant reactor components (TRACE) with the modeling of neutronics in the core (PARCS). The code package was assessed for its applicability to ATWS [5], and our earlier study [2] provided additional insights into its capability. Indeed, one of the objectives of that study was to further evaluate the capabilities of TRACE/PARCS to calculate the phenomena associated with BWR ATWS and reactor stability events; this evaluation also is documented in [2].

The development of the models used in the current analysis is detailed in [2]. Reactor systems/components that are modeled are the steamline, including the turbine bypass and stop valves, safety/relief valves, and main steam isolation valves; the recirculation loop, including recirculation pumps; the feedwater and reactor water level control; the reactor core isolation cooling with option to draw from the condensate storage tank or the suppression pool; the standby liquid control system; the primary containment (drywell and wetwell) with the pool cooler; and the vessel, including the core, steam separator/dryer, and jet pumps.

The core requires special attention and each fuel bundle is represented in the neutronics model, albeit two bundles share the same thermal-hydraulic channel. Nuclear data for each bundle are a function of the thermal-hydraulic variables and the presence of control blades or soluble boron. Models for three different times in the fuel cycle are available, (beginning-of-cycle (BOC), peak-hot-excess-reactivity (PHE), and end-of-full-power-life (EOFPL)); however, herein we consider only the first two statepoints. Within each bundle four different types of fuel rods are modeled. In the present study changes were made to the gap conductance and Appendix A explains how we obtained the values used.

The validity of these models is in part assessed by comparing steady state results for power distributions with those obtained by the vendor GE-Hitachi. Those results are documented in [2].

1.4 Organization of Report

Chapter 2 gives the analysis of the sensitivity calculations, including our consideration of the effect of gap conductance, bypass fraction, and initial flow rate. Conclusions are provided in Chapter 3 and references in Chapter 4. Appendix A contains an explanation of our modeling of gap conductance.

2 SENSITIVITY STUDIES FOR TURBINE TRIP EVENTS

Sensitivity studies were undertaken to evaluate the effects of the gap (between the fuel pellet and clad) conductance modeling, turbine bypass fractions at PHE, and the initial core flow rates at PHE. We compared two fixed limiting values of gas-gap conductance, a low value of 5,000 W/m²-K at BOC and a high value of 161,000 W/m²-K at PHE (Appendix A states how these values were selected) with corresponding base cases that utilize the dynamic gas-gap model. The turbine bypass fractions analyzed are 10% and 25%; these two sensitivity cases are compared with the 100% bypass base case at PHE. The reduced core flow at 75% of rated core flow is analyzed and compared with the base case of 85% core flow at PHE. This rate for the PHE base case (85%) represents the nominal MELLLA+ operating condition, and the reduced flow at 75% corresponds to the low-low flow setpoint.

2.1 Gap Conductance Modeling

Four cases are considered: the case with gas-gap conductance of 5,000 W/m²-K at BOC, the case with 161,000 W/m²-K at PHE, and two reference cases with the TRACE dynamic gas-gap model at BOC and PHE. Our objective was to investigate the effect of low and high gap conductance on the reactor's instability. The two fixed limiting conductance values were obtained from generic calculations performed previously for BWR 10x10 fuel rods [6]. Appendix A describes our selection of the low and high gap conductance values and their implementation in the TRACE model. We note that the gas-gap conductance is modeled as a heat transfer coefficient U,

$$U = \kappa/\Delta x$$

where,

κ = fuel rod gas-gap thermal conductivity

Δx = width of fuel rod gas-gap

All cases have 100% turbine bypass capacity. The turbine stop valve (TSV) is closed in 0.1 s on a turbine trip at 10 s into the simulation time, and then reopens fully in 1.0 s to simulate the bypass paths with 100% turbine bypass. Table 2.1 shows the simulation conditions of the two sensitivity cases, 1C and 2C, together with the two reference cases, 1 and 2.

Table 2.1 Simulation Conditions - Effect of Gap Conductance Modeling

Case ID	Exposure	Power, % of OLTP	Core Flow Rate, %	Bypass Capacity, %	Gap Conductance
1	BOC	120	85	100	Dynamic ¹
1C	BOC	120	85	100	5,000 W/m ² -K ²
2	PHE	120	85	100	Dynamic ¹
2C	PHE	120	85	100	161,000 W/m ² -K ³

¹ Dynamic gas-gap model is considered with elastic cladding deformation and the clad rupture model off.

² Low limit value of gas-gap conductance.

³ High limit value of gas-gap conductance.

2.1.1 Initial Conditions

The reference values for initial conditions are given in Chapter 3 of [2]. The differences of key thermal-hydraulic parameters between the reference and the TRACE calculated values (at the end of the 10 s TRACE/PARCS null transient calculation) are given in Table 2.2. As shown in this table, the calculated steady state values are in good agreement with the reference ones as gap conductance does not impact these parameters.

Any small differences in the initial values shown in Table 2.2 reflect the core's initial power being disturbed by random noise in moderator density imposed in the PARCS calculation at five seconds into the null transient.

Table 2.2 Comparison of Steady-State Thermal-Hydraulic Parameters – Effect of Gap Conductance Modeling

Effect of Low Fixed Gas-Gap Conductance Value (BOC Cases)				
Parameter	Dynamic (Case 1)		Low Limit Value (Case 1C)	
	TRACE Value	Diff. (%)	TRACE Value	Diff. (%)
Core Power (MWt)	3988	0	3988	0
Steam Dome Pressure (kPa)	7143	0.10	7141	0.07
Main Steamline Flow (kg/s)	2222	0	2218	-0.18
Total Core Flow (kg/s)	11614	-0.05	11622	0.02
Feedwater Flow (kg/s)	2220	-0.09	2218	-0.18
Feedwater Temperature (K)	500	0	500	0
Downcomer Level (m)	14.32	-0.97	14.32	-0.97
Effect of High Fixed Gas-Gap Conductance Value (PHE Cases)				
Parameter	Dynamic (Case 2)		High Limit Value (Case 2C)	
	TRACE Value	Diff. (%)	TRACE Value	Diff. (%)
Core Power (MWt)	3988	0	3988	0
Steam Dome Pressure (kPa)	7141	0.07	7141	0.07
Main Steamline Flow (kg/s)	2218	-0.18	2218	-0.18
Total Core Flow (kg/s)	11631	0.09	11617	-0.03
Feedwater Flow (kg/s)	2218	-0.18	2218	-0.18
Feedwater Temperature (K)	500	0	500	0
Downcomer Level (m)	14.32	-0.97	14.32	-0.97

While the main steady-state thermal-hydraulic parameters remain unchanged for different gap conductance models, the fuel temperatures change significantly. Table 2.3 shows the steady-state core-averaged fuel and average fuel centerline temperatures along with the gap conductance for each case. For those dynamic gas-gap conductance ones, the conductance varies from node to node; Table 2.3 shows the range of values as calculated by TRACE. The fuel temperatures (both average and centerline) are higher for the dynamic conductance cases than for the fixed conductance cases, indicating that, on average, gas-gap conductance is higher for the latter, both at BOC and PHE.

Table 2.3 Comparison of Initial Fuel Temperatures - Effect of Gap Conductance Modeling

Effect of Low Fixed Gas-Gap Conductance Value (BOC Cases)		
Parameter	Dynamic (Case 1)	Low Limit Value (Case 1C)
Gap Conductance (W/m ² -K)	700 – 6,000	5,000 ¹
Average Fuel Temperature (K)	1249.1	1131.3
Average Fuel Centerline Temperature (K)	1460.0	1322.7
Effect of High Fixed Gas-Gap Conductance Value (PHE Cases)		
Parameter	Dynamic (Case 2)	High Limit Value (Case 2C)
Gap Conductance (W/m ² -K)	600 – 6,000	161,000
Average Fuel Temperature (K)	1314	1001
Average Fuel Centerline Temperature (K)	1534	1167

¹We note that based on the calculated steady-state core-average fuel temperatures, the assumed low fixed gap conductance of 5,000 W/m²-K effectively is higher than the average value calculated by the dynamic-gap model.

2.1.2 Sequence of Events

The timing of the sequence of events in the cases with the fixed-gap conductance values generally is similar to that in the cases with the dynamic gas-gap model. Table 2.4 shows the time sequence for the events; detailed discussions about the system's behavior are presented in the following sections. The table also notes instances wherein the sequence differs for different cases.

Table 2.4 Sequence of Events - Effect of Gap Conductance Modeling

Effect of Low Fixed Gas-Gap Conductance Value (BOC Cases)	
Time (s)	Event
0.0	<ul style="list-style-type: none"> Null transient simulation starts.
10.0	<ul style="list-style-type: none"> Null transient simulation ends. Turbine trip is initiated by closing the TSV. Recirculation pumps are tripped on the turbine trip. Feedwater temperature starts decreasing.
10.1	<ul style="list-style-type: none"> TSV closes completely and starts opening again to simulate 100% turbine bypass flow.
11.1	<ul style="list-style-type: none"> TSV (simulating bypass) completes opening and its open area provides the predetermined steam flow fraction shown in Table 2.1.
~ 11.4	<ul style="list-style-type: none"> Steam flow starts decreasing.
~ 13.0	<ul style="list-style-type: none"> Feedwater flow starts decreasing.
~ 95	<ul style="list-style-type: none"> Power oscillation (instability) starts in Case 1. ~ 102 s in Case 1C.
120	<ul style="list-style-type: none"> Reduction in water level is initiated and the setpoint of the normal water level control system is reduced linearly to top-of-active-fuel (TAF) over 180 s.
130	<ul style="list-style-type: none"> Boron injection is initiated and linearly ramped to full flow at 190 s.
~ 143	<ul style="list-style-type: none"> Noticeable bi-modal oscillation of the core power is initiated in Case 1. ~ 144 s in Case 1C.
~ 158	<ul style="list-style-type: none"> Downcomer water level begins decreasing.
~ 160	<ul style="list-style-type: none"> Boron starts accumulating in the core.
~ 181	<ul style="list-style-type: none"> Peak cladding temperature of ~1,373 K occurs in Case 1. ~ 1,287 K at 184 s in Case 1C.
~ 234	<ul style="list-style-type: none"> Power oscillation ends in Case 1C. ~ 245 s in Case 1.
400	<ul style="list-style-type: none"> Simulation ends.
Effect of High Fixed Gas-Gap Conductance Value (PHE Cases)	
Time (s)	Event
0.0	<ul style="list-style-type: none"> Null transient simulation starts.
10.0	<ul style="list-style-type: none"> Null transient simulation ends. Turbine trip is initiated by closing the TSV. Recirculation pumps are tripped on the turbine trip. Feedwater temperature starts decreasing.
10.1	<ul style="list-style-type: none"> TSV closes completely and starts opening again to simulate 100% turbine bypass flow.
11.1	<ul style="list-style-type: none"> TSV (simulating bypass) completes opening and its open area provides the predetermined steam flow fraction of 100% as shown in Table 2.1.
~11.4	<ul style="list-style-type: none"> Steam flow starts decreasing.
~12.3	<ul style="list-style-type: none"> Feedwater flow starts decreasing.
~77	<ul style="list-style-type: none"> Power oscillation (instability) starts in Case 2C. ~95 s in Case 2.
120	<ul style="list-style-type: none"> Water level reduction is initiated by reducing the setpoint of the normal water level control system linearly to TAF over 180 s.
130	<ul style="list-style-type: none"> Boron injection is initiated and linearly ramped to full flow at 190 s.

~131	<ul style="list-style-type: none"> Downcomer water level begins decreasing but very slowly in Case 2C. Noticeable reduction of DC water level starts at around 177.7 s. At ~163 s, DC water level begins declining in Case 2.
~144	<ul style="list-style-type: none"> Noticeable bi-modal oscillation of the core power is initiated in Case 2. ~146 s in Case 2C.
~160	<ul style="list-style-type: none"> Boron starts accumulating in the core.
~163	<ul style="list-style-type: none"> Peak cladding temperature of ~1,690 K occurs in Case 2. ~640 K at 175 s in Case 2C. No significant temperature increase (less than 70 K) is predicted.
~218	<ul style="list-style-type: none"> Power oscillation ends in Case 2C. ~240 s in Case 2.
400	<ul style="list-style-type: none"> Simulation ends.

2.1.3 Steamline Flow

Figure 2.1 compares steamline flow rates for the two BOC cases. In the legend, “Dynamic” and “Low Gap Conductance” represent the cases, respectively, with the dynamic gas-gap model, and the low fixed value of the gas-gap conductance of 5,000 W/m²-K. The steam flow’s behavior is almost identical in the two cases.

Comparison of steamline flow rates for the two PHE cases is shown in Figure 2.2. In the legend, “High Gap Conductance” represents the case with the high fixed value of the gas-gap conductance of 161,000 W/m²-K. The behavior of the steam flow is almost the same in the two cases until it reaches a maximum at 11.4 s; then, TRACE predicts a lesser steam flow with high gap conductance than with the dynamic gas-gap model. This difference is caused by a lower core power in the former than in the latter. We offer a detailed discussion about the power behavior in the next section.

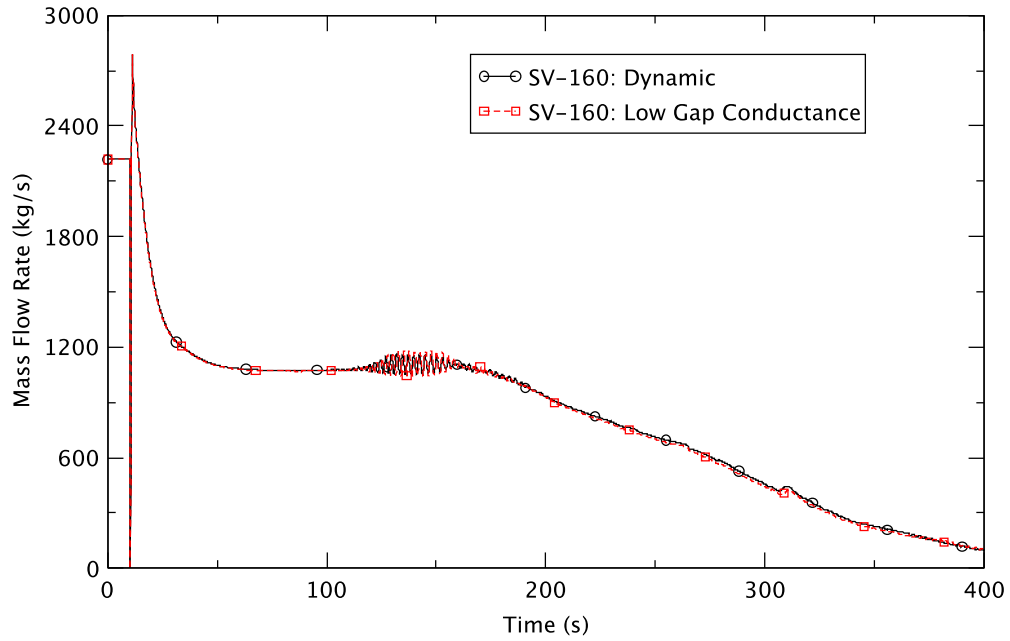


Figure 2.1 Steamline Mass Flow Rate - Effect of Low Gas-Gap Conductance at BOC

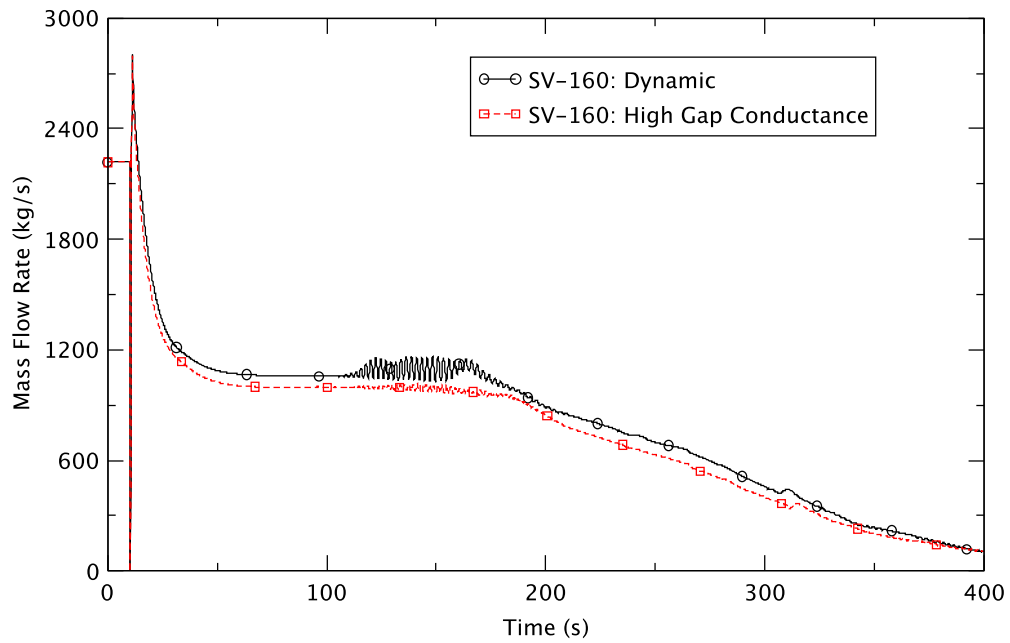


Figure 2.2 Steamline Mass Flow Rate - Effect of High Gas-Gap Conductance at PHE

2.1.4 Core Power and Dome Pressure

Figure 2.3 and Figure 2.4 compare reactor core powers for the cases at BOC and PHE, respectively. While the former show a very similar general trend, the reactor power behavior is very different in the PHE cases. With high gas-gap conductance, TRACE predicts that the reactor power will be lower in general, and much more stable without large oscillatory behavior, than the case with the dynamic gas-gap model. The low gas-gap conductance at BOC does not significantly affect the power behavior.

Figure 2.5 illustrates the order-of-magnitude of the gap conductance calculated by the dynamic gas-gap model for the two reference cases at BOC and PHE. The two channel numbers, 245 and 243, correspond to the two channels with the maximum first harmonic for BOC and PHE, respectively. The axial node of 20 is close to the middle of the fuel rod. We note that for the BOC case, the fixed low gap conductance value of $5,000 \text{ W/m}^2\text{-K}$ is within the range of values calculated by the dynamic gas-gap model. Thus, the BOC gap conductance sensitivity case is expected to have similar transient responses as in the BOC reference case.

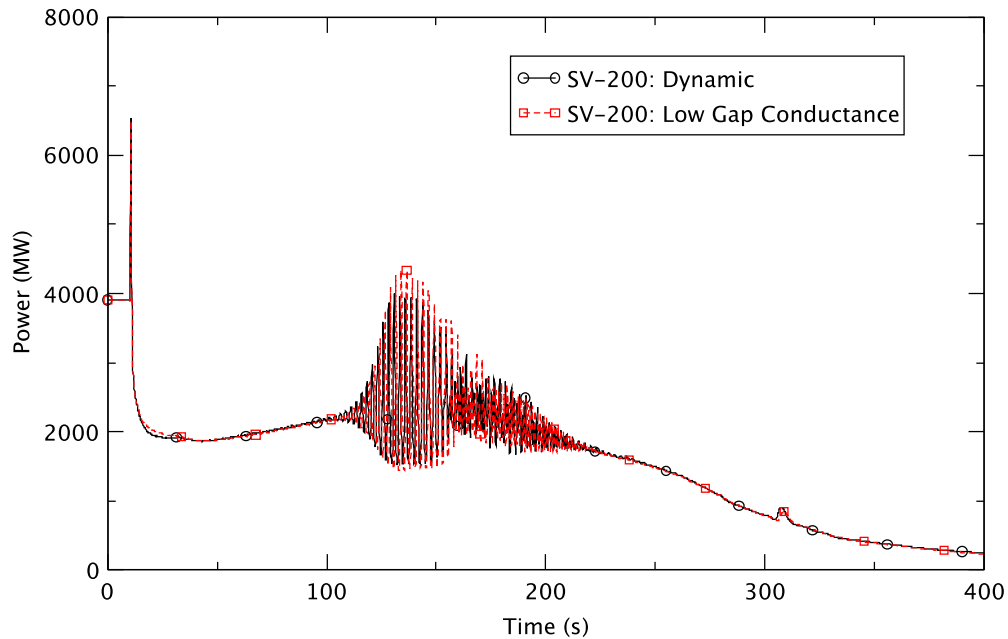


Figure 2.3 Core Power - Effect of Low Gas-Gap Conductance at BOC

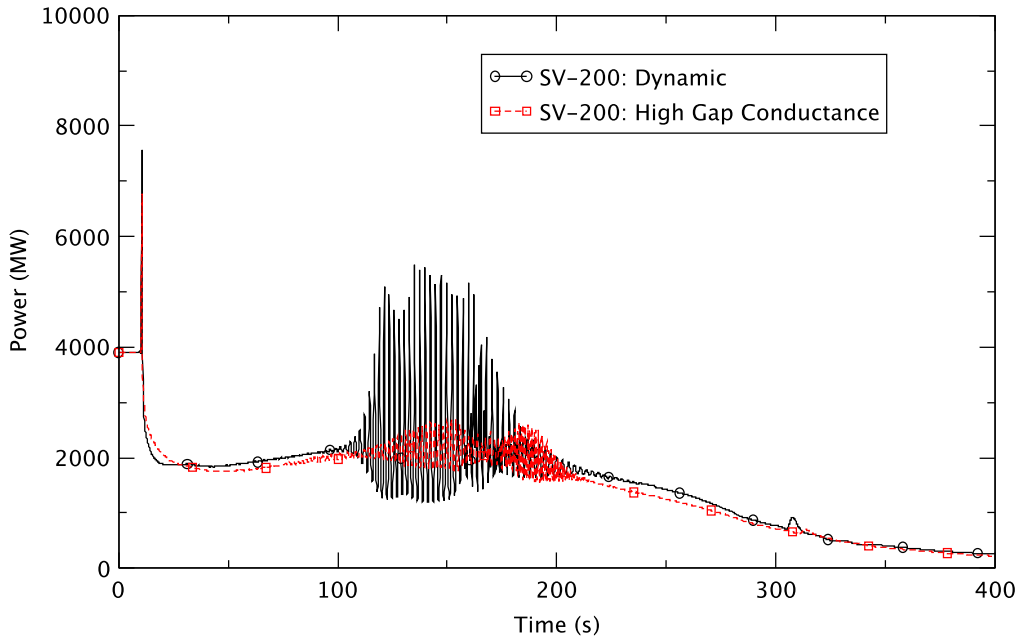


Figure 2.4 Core Power - Effect of High Gas-Gap Conductance at PHE

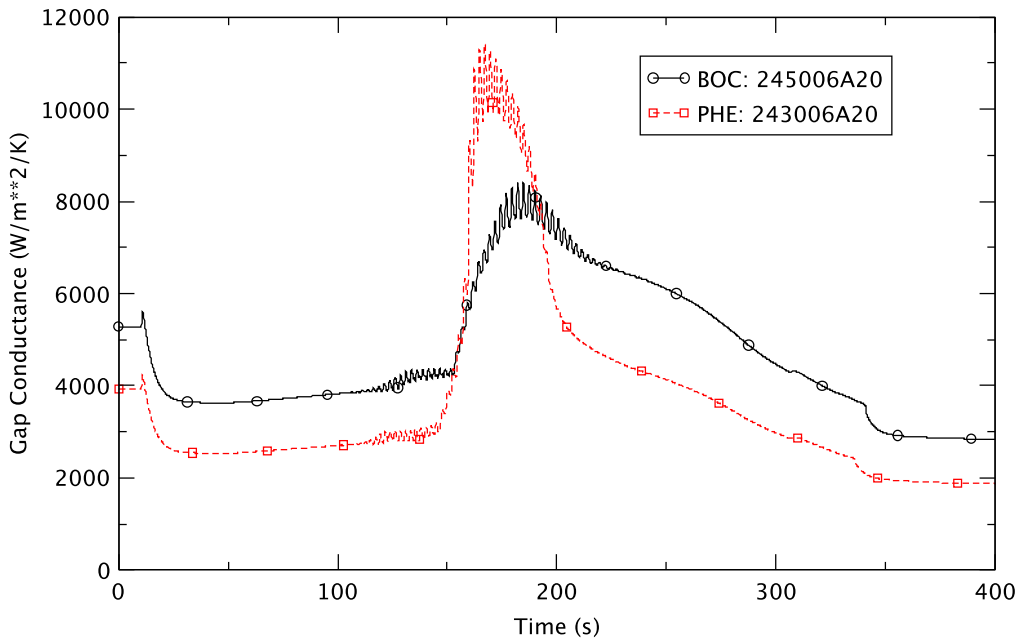


Figure 2.5 Gap Conductance Calculated by the Dynamic Gas-Gap Model

For the PHE case, the gap conductance calculated by the dynamic gas-gap model is an order-of-magnitude lower than the value of the fixed high gap conductance of $161,000 \text{ W/m}^2\text{-K}^1$ assumed for the sensitivity case. These drastically different gap conductance values lead to significantly different transient responses for the two PHE cases. The transient behavior of the high gap conductance sensitivity case and the reference case can be explained by the transient reactivity response. The total reactivity for each of the two PHE cases is shown in Figure 2.6. The curve labeled the dynamic gap represents the reference case and that labeled high gap conductance represents the sensitivity case. As is evident, the amplitude of reactivity fluctuations is higher in the reference case than the sensitivity case. This difference is attributed primarily to the moderator reactivity feedback, as shown in Figure 2.7. The Doppler reactivity for the two PHE cases is depicted in Figure 2.8, and the boron reactivity in Figure 2.9. We note that the Doppler feedback for the sensitivity case is less than for the reference case.

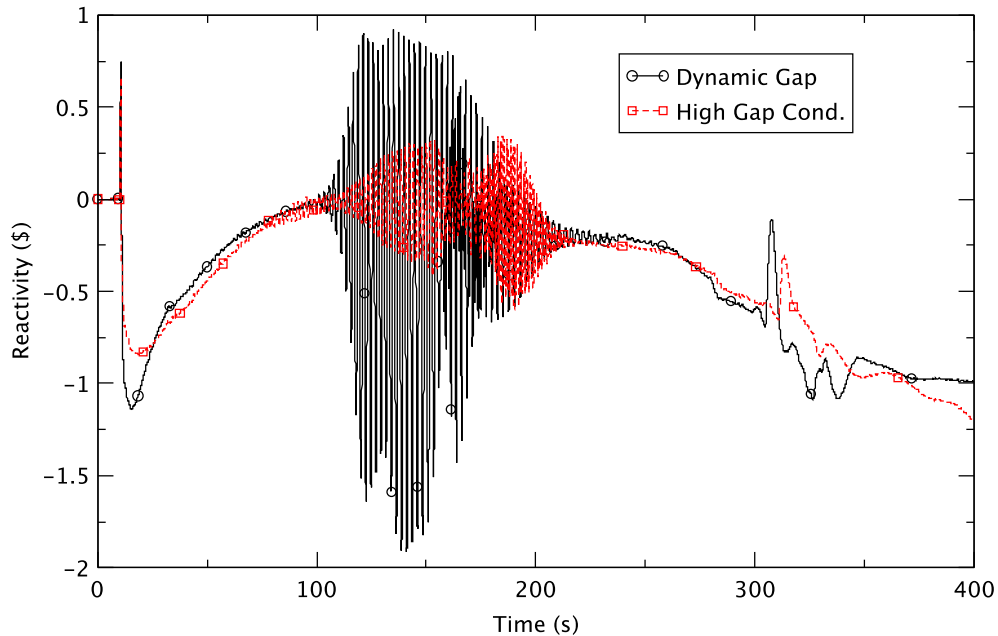


Figure 2.6 Total Reactivity for the Two PHE Cases

¹ A high gap conductance of $161,000 \text{ W/m}^2\text{-K}$ is likely only possible if the fuel pellet had swollen such as to come in contact with the clad. The thermal conductivity of the fuel pellet is expected to decrease significantly due to its growth. However, for the sensitivity analysis, the fuel pellet's conductivity is assumed to remain unchanged.

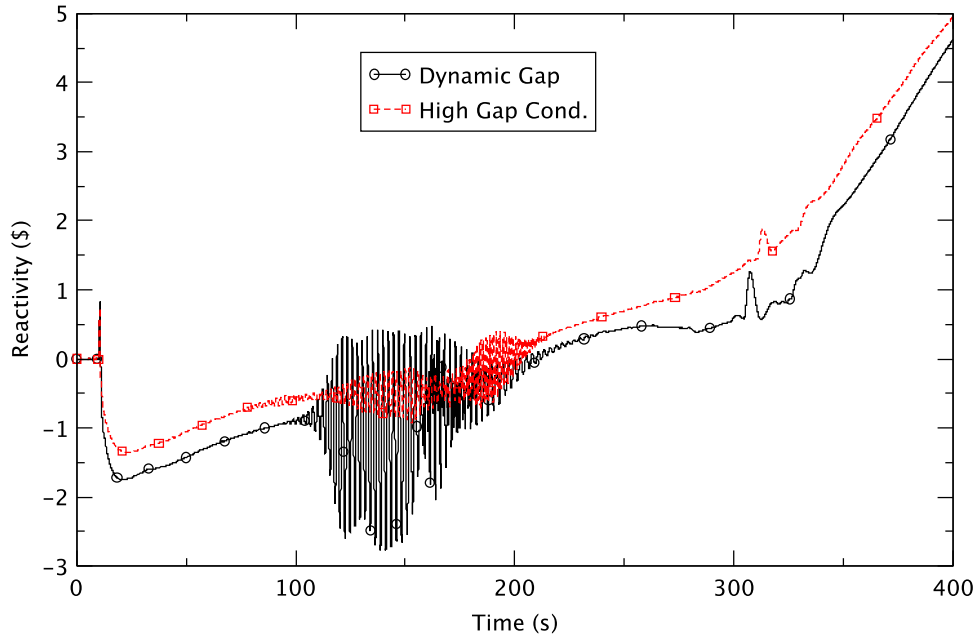


Figure 2.7 Moderator Reactivity for the Two PHE Cases

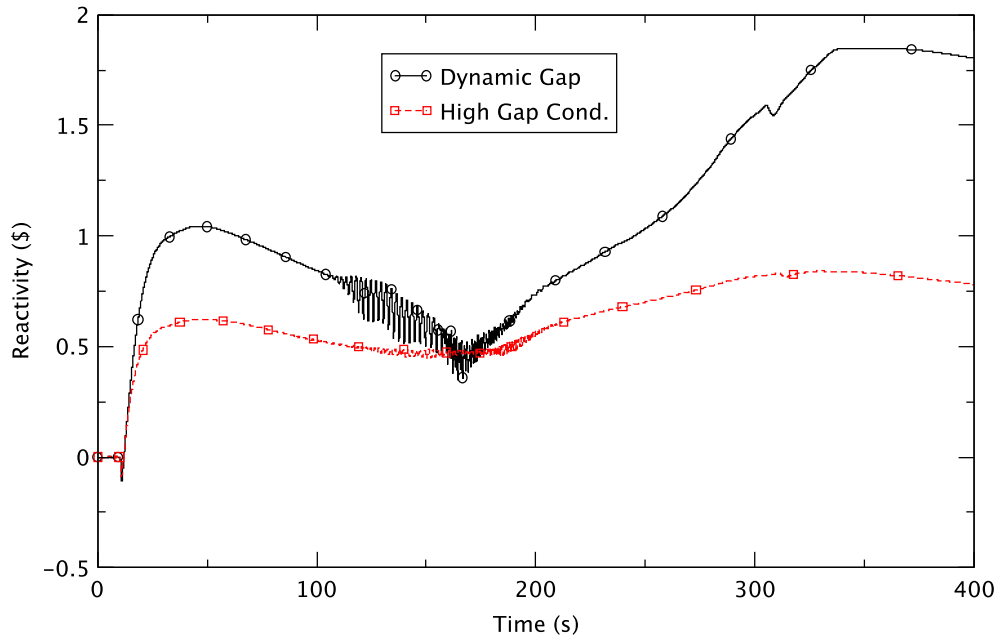


Figure 2.8 Doppler Reactivity for the Two PHE Cases

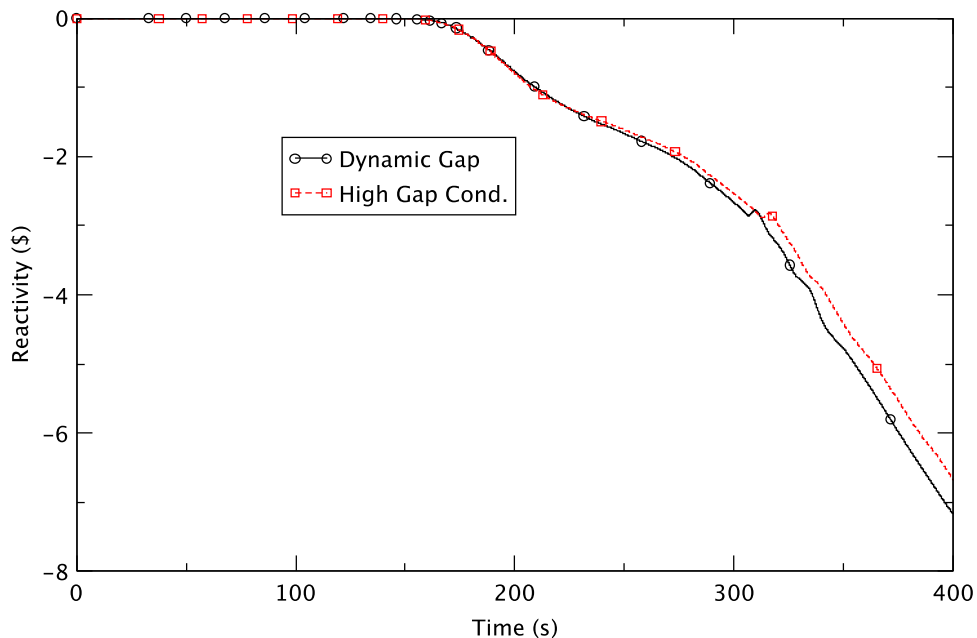


Figure 2.9 Boron Reactivity for the Two PHE Cases

This relatively low and stable power behavior with the high gas-gap conductance (the sensitivity case) can be explained by considering the Doppler reactivity feedback (the fuel temperature reactivity). Fuel centerline and cladding temperatures in Channel 245 and Channel 243 in the northeast quadrant are shown in Figure 2.10 for the BOC cases and in Figure 2.11 for the PHE cases. The axial node number 20 was chosen because its location is near the core's center. In the legend "tsurfi" and "tsurfo" are the temperature of the fuel centerline and cladding, respectively. When the low fixed conductance of $5,000 \text{ W/m}^2\text{-K}$ is considered, TRACE predicts that the fuel temperature behavior is very similar to that obtained with the dynamic conductance model (Figure 2.10). From this comparison as well as the reactor power behavior shown in Figure 2.3, we can deduce that the effect of the low fixed conductance on general system behavior is very similar to that with the dynamic gap model. However, in the case with high fixed conductance, the temperature of the fuel centerline is predicted to be much lower than the one with the dynamic conductance model while the cladding temperatures are almost the same until around 145 s (Figure 2.11).

Figure 2.12 depicts the changes in the temperature of the fuel centerline from time zero in the PHE cases. Consistent with expectation, the case with the high fixed gap conductance shows a lesser decrease in fuel temperature than the case with dynamic gap model, from about 16 s to 147 s. At higher gap conductance, the fuel pellet temperature remains closer to the coolant temperature; as such, there is a much smaller change in fuel temperature in the high gap conductance case. The smaller fuel temperature change means that the positive reactivity introduction by the Doppler effect is reduced in the high gap conductance case. This difference results in lower reactor power (Figure 2.4). This lower power, with additional effects, such as the lower subcooling at the core inlet and a lower ratio of power to the product of flow and enthalpy at the core inlet, leads to more stable reactor power behavior, as discussed in Section 2.1.8.

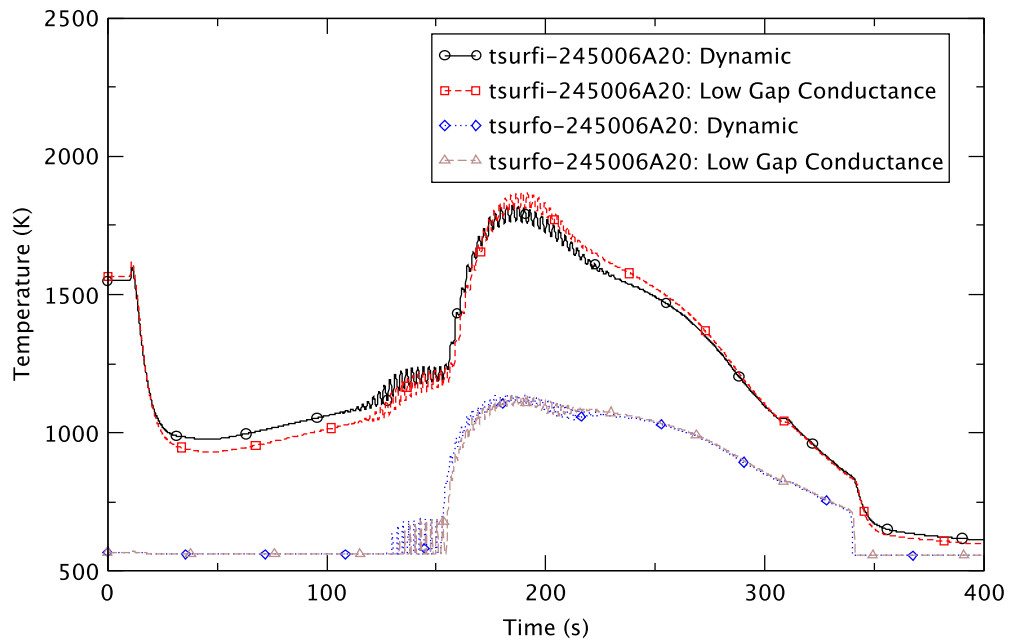


Figure 2.10 Fuel Centerline and Cladding Temperatures in Channel 245 at BOC

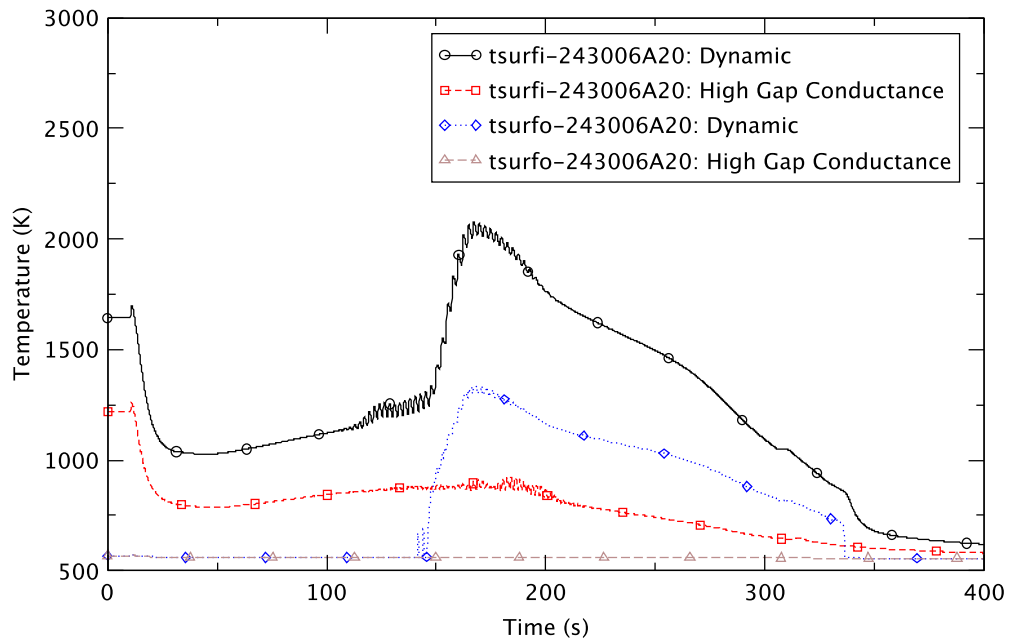


Figure 2.11 Fuel Centerline and Cladding Temperatures in Channel 243 at PHE

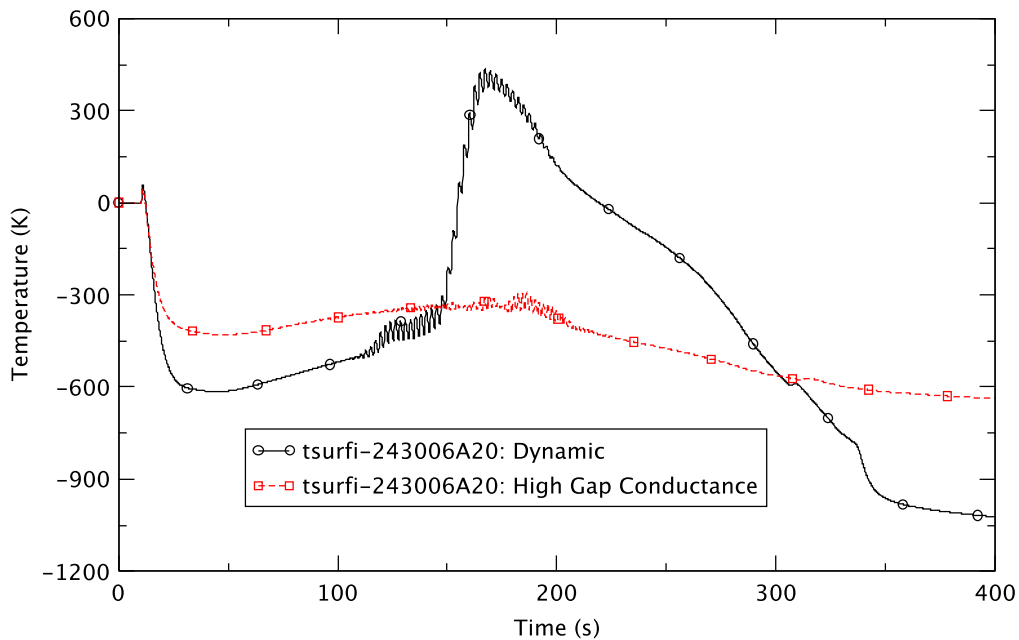


Figure 2.12 Change of Fuel Centerline Temperatures in Channel 243 in Northeast Quadrant at PHE

The general system pressure behavior is almost identical in the BOC cases and very similar in the PHE cases, as shown respectively in Figure 2.13 and Figure 2.14. A close examination of Figure 2.14 illustrates that the pressure is slightly lower with the high fixed conductance than with the dynamic gap model from around 12 s to 315 s. This difference mostly reflects the lower reactor power (Figure 2.4). However, the difference between the two pressures almost is negligible.

2.1.5 Core Flow

We compare the rates of core flow in Figure 2.15 for the BOC cases, and in Figure 2.16 for the PHE cases. The behavior of core flow basically is identical in the BOC and PHE cases. This is because the recirculation pumps' coast-down is the same, and the difference in gravity head between the downcomer and core essentially is the same after natural circulation is established.

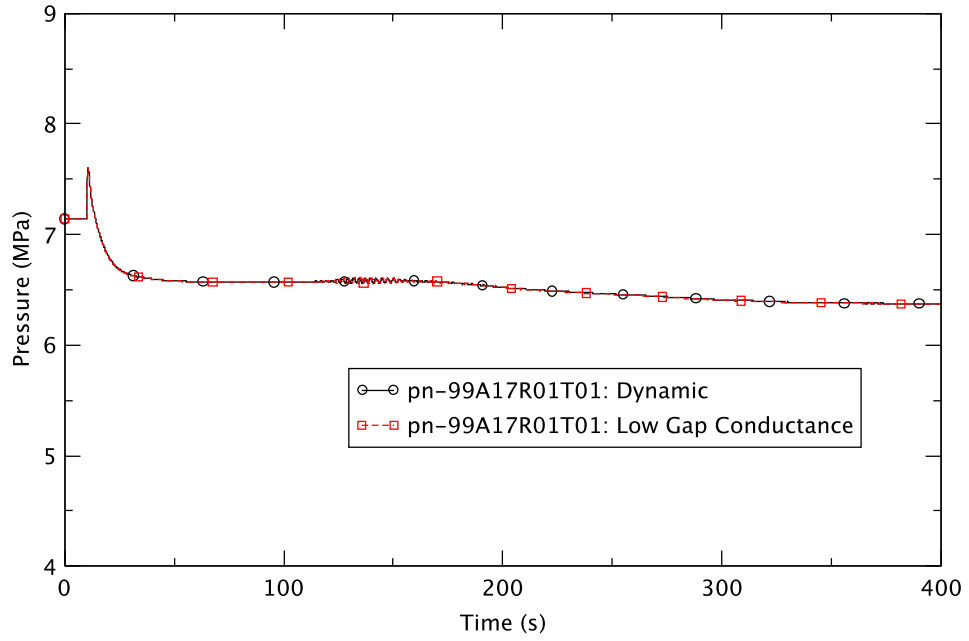


Figure 2.13 RPV Pressure - Effect of Low Gas-Gap Conductance at BOC

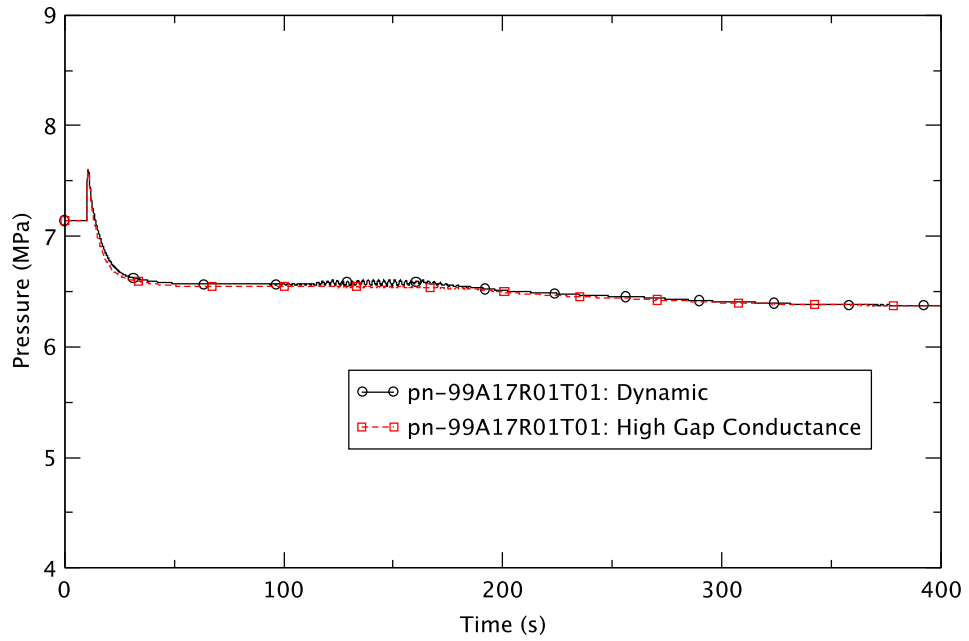


Figure 2.14 RPV Pressure - Effect of High Gas-Gap Conductance at PHE

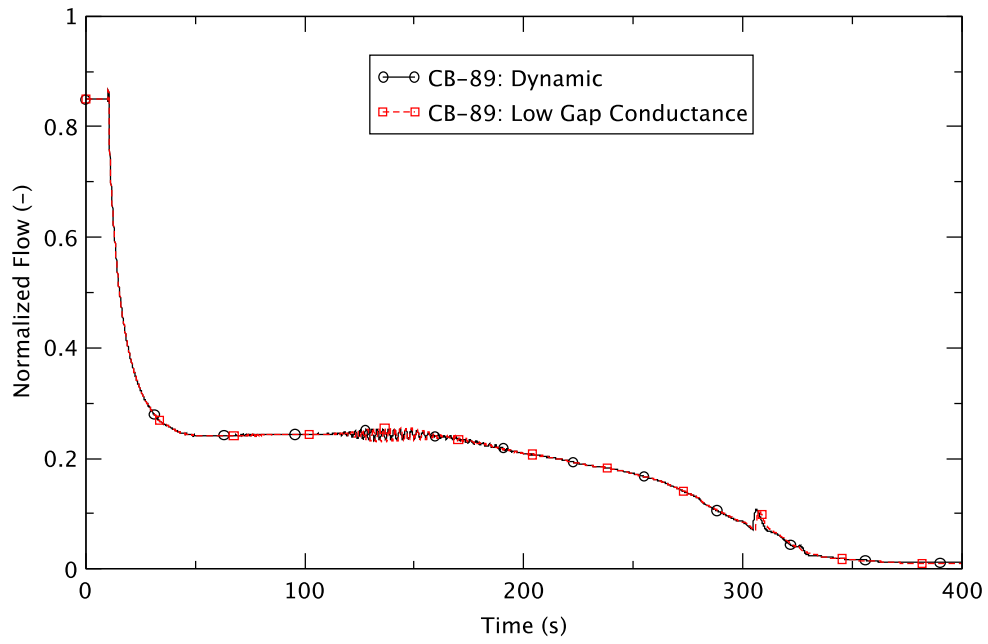


Figure 2.15 Core Flow Rate - Effect of Low Gas-Gap Conductance at BOC

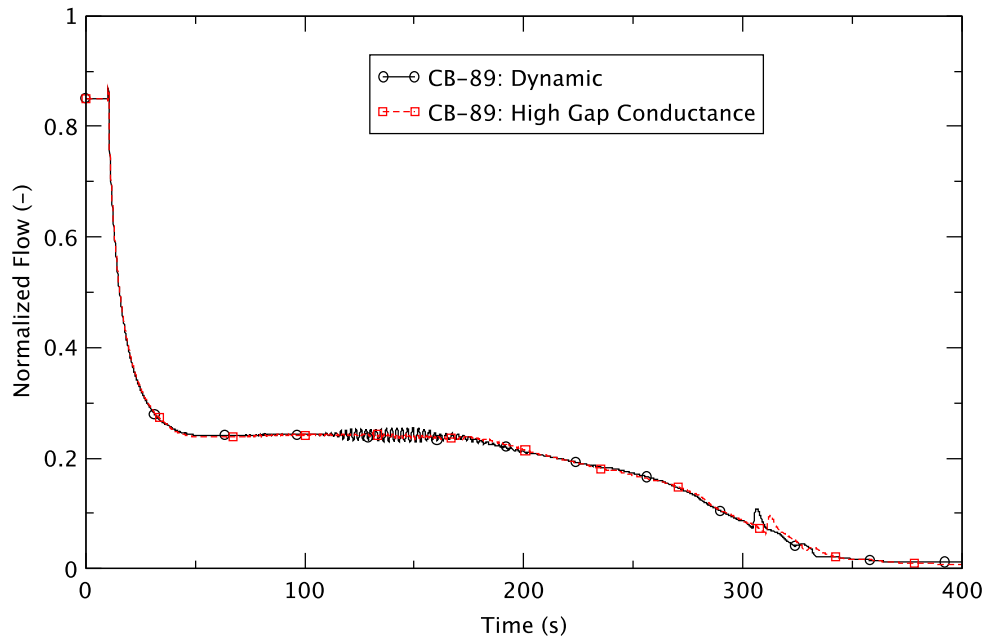


Figure 2.16 Core Flow Rate - Effect of High Gas-Gap Conductance at PHE

2.1.6 Feedwater Flow and RPV Water Level

The operator action for water level reduction to TAF is simulated at 120 s by reducing the flow of feedwater to decrease the mass flow into the core. Figure 2.17 and Figure 2.18 respectively compare the feedwater flow rates at BOC and PHE. As expected, the flow rates start decreasing faster from 120 s in all cases at both BOC and PHE. The comparisons reveal that while the behavior is almost identical in the BOC cases (in other words, the effect of the low gap conductance is almost the same as the one with the dynamic gap model), the feedwater (FW) flow becomes smaller with the high fixed conductance from around 13 s to 255 s. This is caused by less steam flow (see Figure 2.2) owing to the lower reactor power (see Figure 2.4).

Figure 2.19 and Figure 2.20 compare the behavior of the level of downcomer (DC) water. The general behavior of the DC water level is almost identical in all cases at both BOC and PHE, and this causes the core flow to behave similarly, especially after natural circulation is established (Figure 2.15 and Figure 2.16).

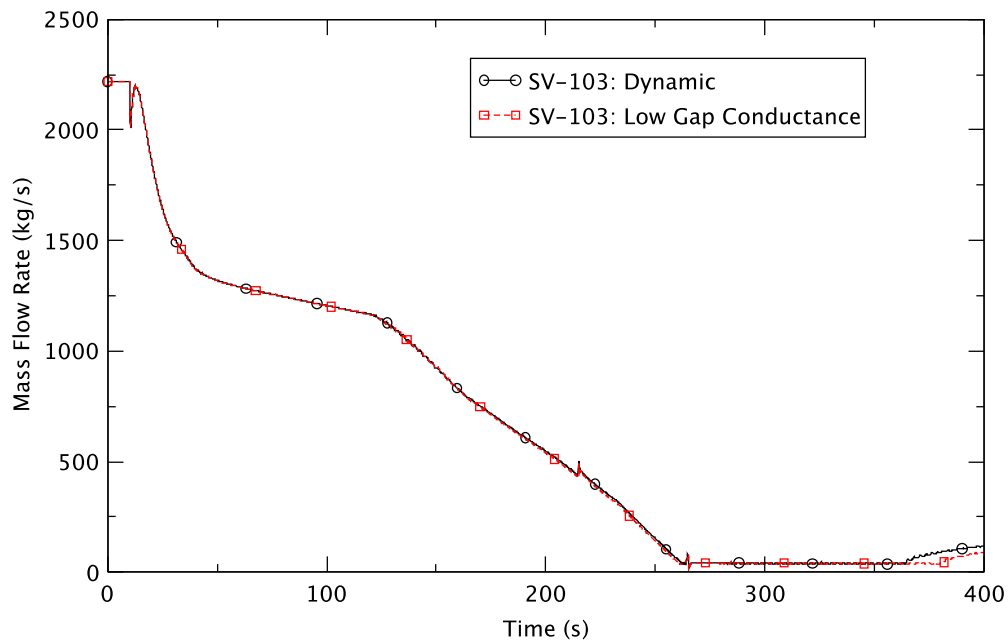


Figure 2.17 Feedwater Flow Rate - Effect of Low Gas-Gap Conductance at BOC

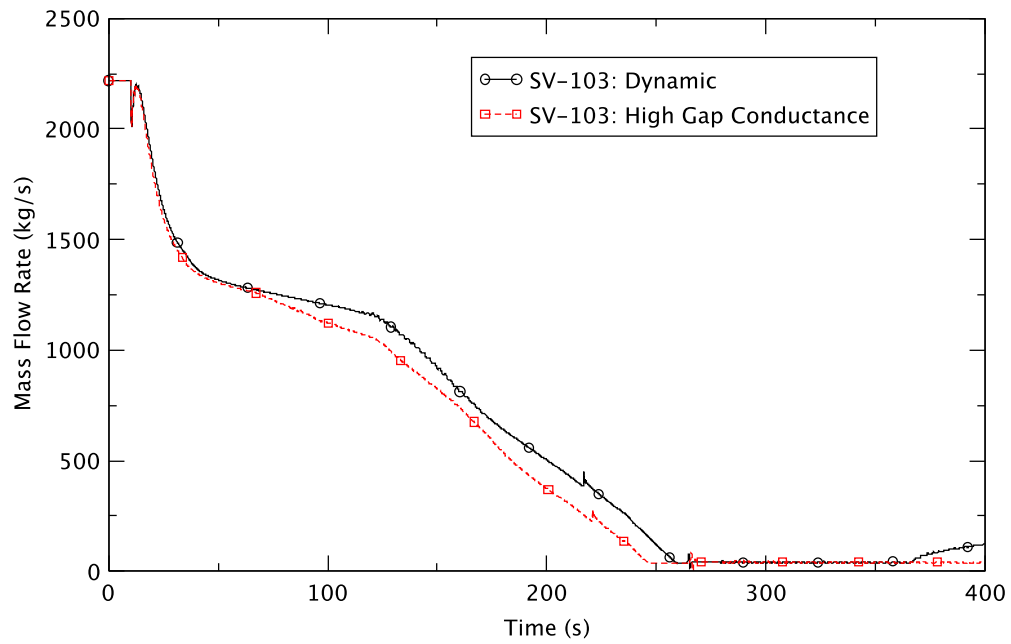


Figure 2.18 Feedwater Flow Rate - Effect of High Gas-Gap Conductance at PHE

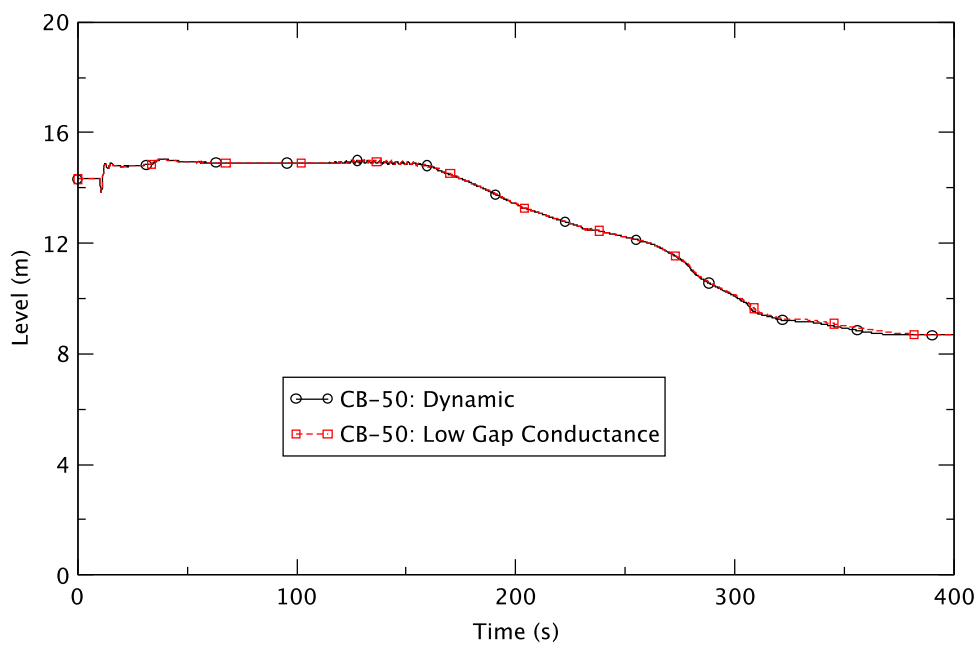


Figure 2.19 Downcomer Water Level - Effect of Low Gas-Gap Conductance at BOC

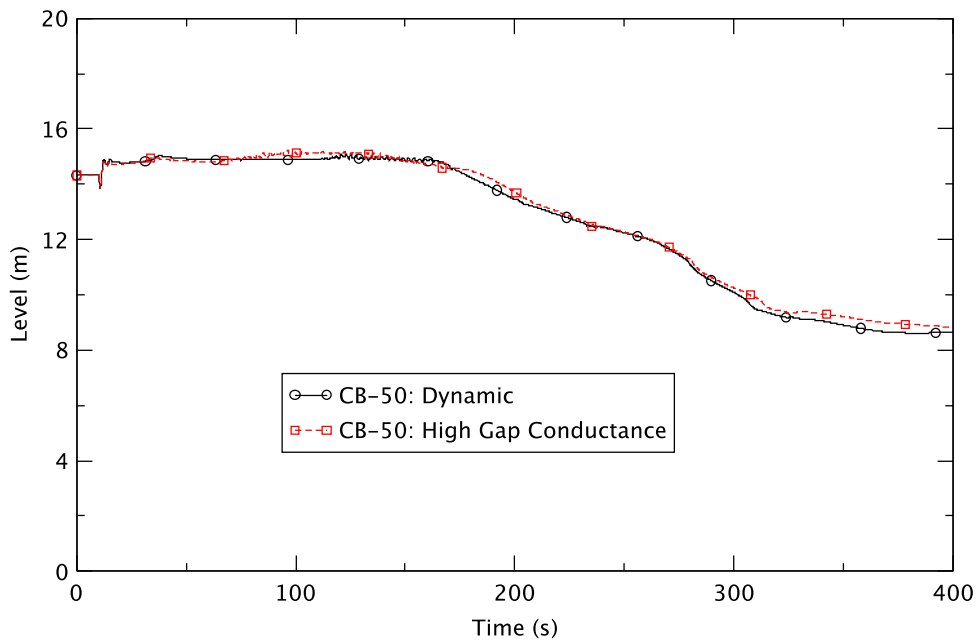


Figure 2.20 Downcomer Water Level - Effect of High Gas-Gap Conductance at PHE

As shown in Figure 2.19 and Figure 2.20, the DC level does not drop for a relatively long time (about 40 s in the BOC cases and about 43 s in the PHE cases) after the operator action at 120 s. Figure 2.20 illustrates that the DC level starts decreasing very slowly from around 131 s and then begins dropping noticeably from around 178 s at PHE with high fixed gap conductance. Because the change of the DC water level is very small from 131 s to 178 s, it can be said that the effect of the operator action to reduce the water level becomes evident around 178 s after a delay of 58 s.

2.1.7 Boron Inventory in Core

The standby liquid control system (SLCS) is initiated at 130 s; Figure 2.21 and Figure 2.22 compare the boron inventory in the core. As is evident, its behavior is the same in both cases at BOC and PHE, especially until around 300 s when the reactor power instability ends. Hence, boron injection does not contribute to the differences between the cases with different gap conductance.

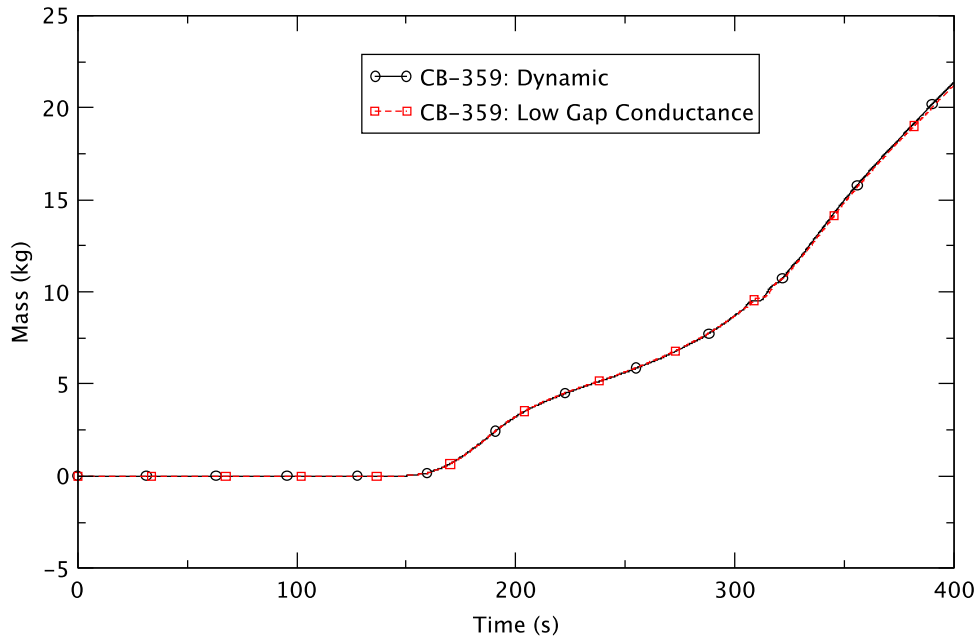


Figure 2.21 Boron Inventory in Reactor Core - Effect of Low Gas-Gap Conductance at BOC

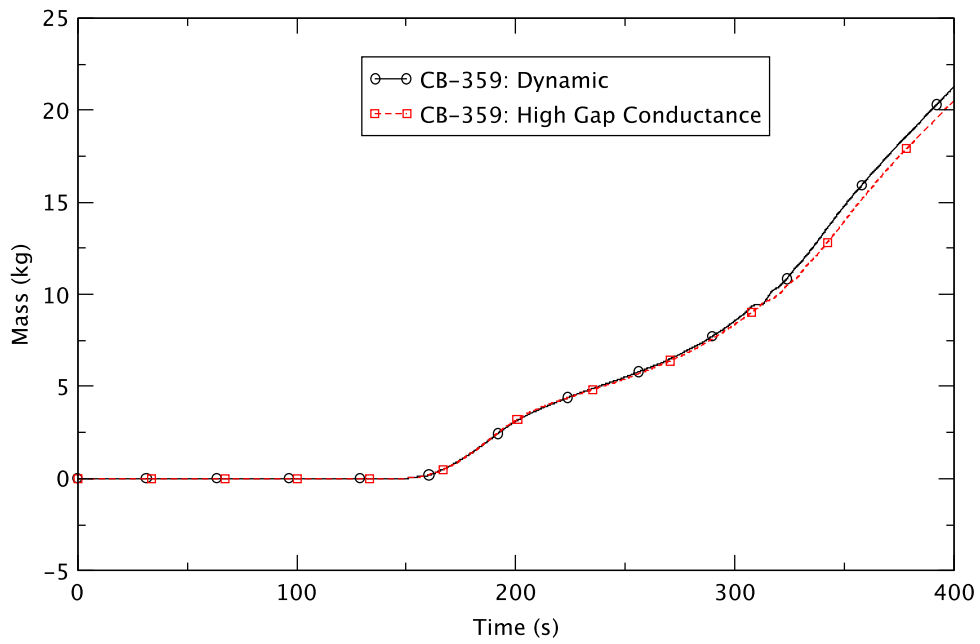


Figure 2.22 Boron Inventory in Reactor Core - Effect of High Gas-Gap Conductance at PHE

2.1.8 Liquid Subcooling of Core Flow

Figure 2.23 and Figure 2.24 illustrate the subcooling of the core inlet in ring 1 (see Chapter 2 of [2] that describes how the vessel is modeled). While it is almost identical in those cases with the low conductance and the dynamic gap model at BOC, subcooling lessens, especially from around 98 s, with a high fixed conductance relative to the dynamic gap model at PHE. Its diminution is explained by the fact that the core flow is almost the same (Figure 2.16) but the steam flow and FW flow are smaller (Figure 2.1 and Figure 2.18). More hot water returns to the DC from the separators, and is mixed with a smaller amount of the colder FW; this lowers subcooling in the DC and at the core inlet with the high fixed conductance at PHE.

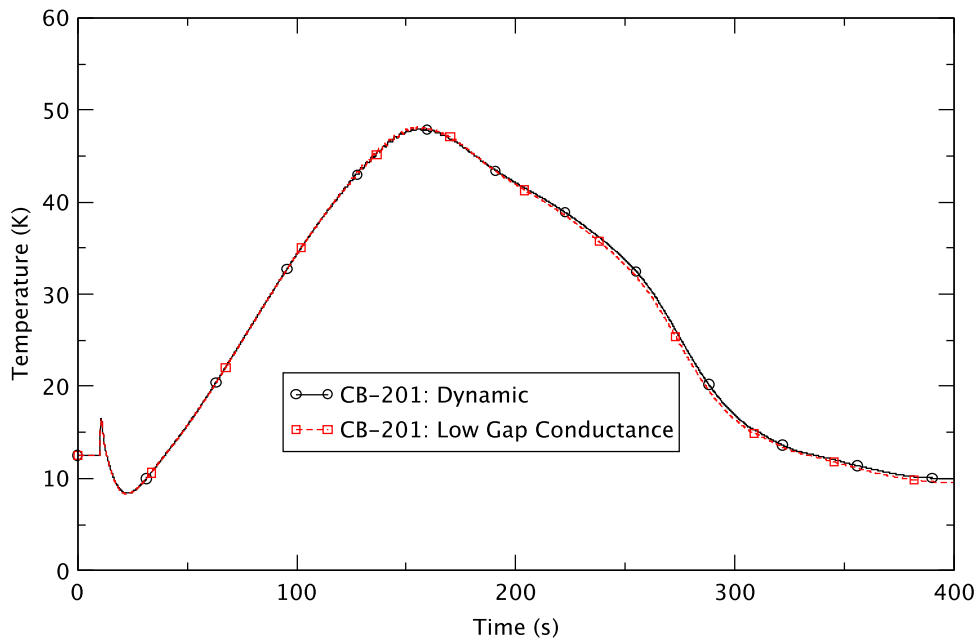


Figure 2.23 Liquid Subcooling at the Core Inlet - Effect of Low Gas-Gap Conductance at BOC

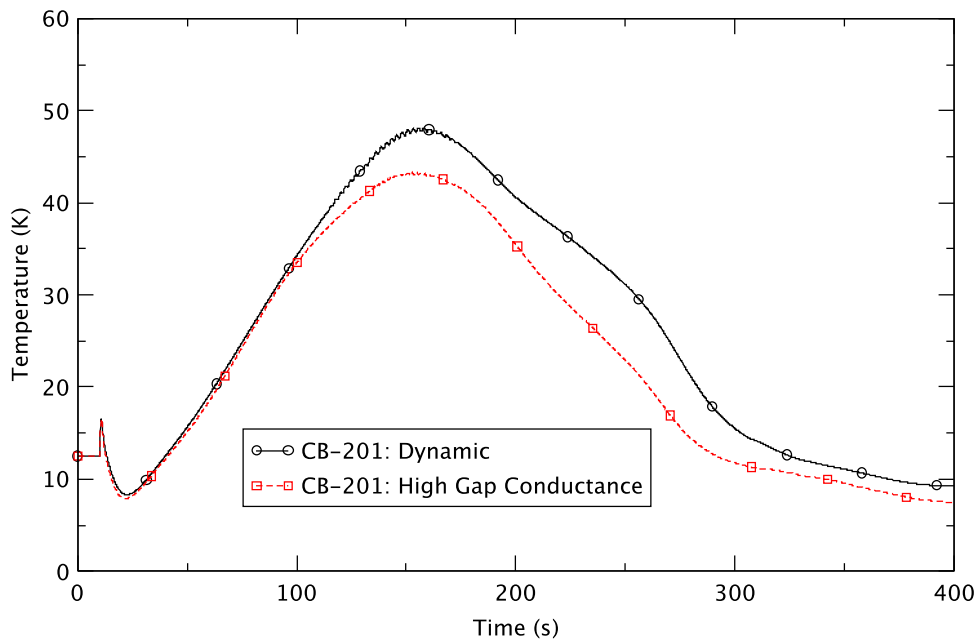


Figure 2.24 Liquid Subcooling at the Core Inlet - Effect of High Gas-Gap Conductance at PHE

2.1.9 Fuel Rod Cladding Temperature

The temperature of the fuel cladding is affected by oscillations in the core power and in the efficiency of heat transfer from the fuel to coolant; the latter reflecting the continuous changes in the void fraction and the flow rate of the coolant. Figure 2.25 and Figure 2.26 compare the maximum cladding temperature among all fuel bundles in the core for the different conductance models. The behavior of the cladding temperature is very similar at BOC. However, in the PHE cases, although it increases significantly from approximately 122 s with the dynamic gap model, the rise in cladding temperature is very small with a high fixed conductance (less than 70 K). This small increase reflects the relatively stable reactor power without large oscillations (Figure 2.4).

In one case the temperature is higher than 1,478 K (2,200°F); this value is used as an acceptance criterion for the purposes of this study because it is imposed as a limit in new plants [7]. Above this temperature, there is the possibility of damaging the clad that is not taken into account in the modeling.

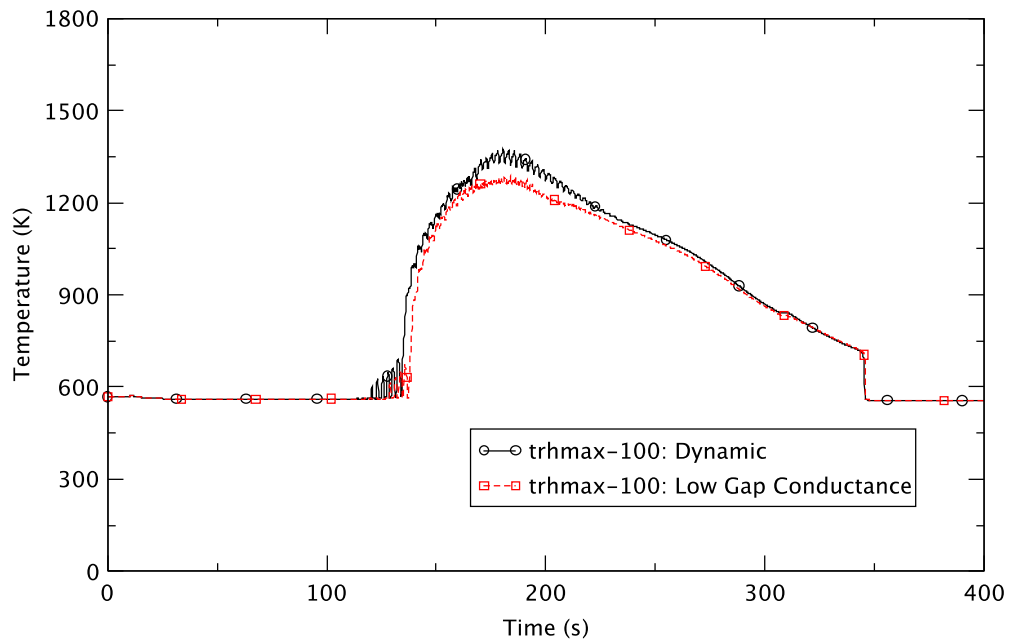


Figure 2.25 Maximum Cladding Temperature among all Fuel Bundles - Effect of Low Gas-Gap Conductance at BOC

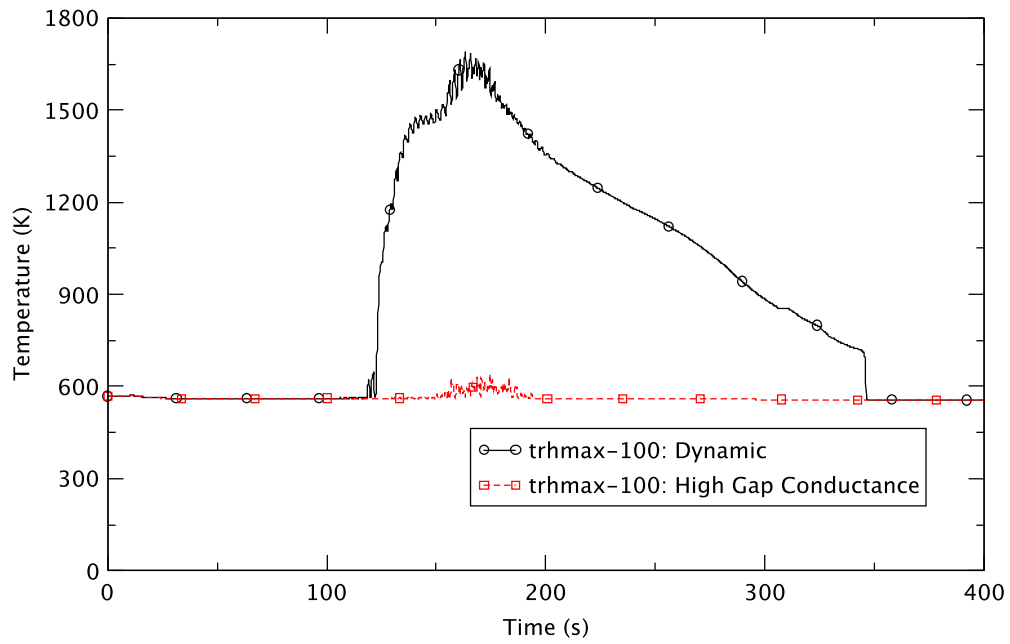


Figure 2.26 Maximum Cladding Temperature among All Fuel Bundles - Effect of High Gas-Gap Conductance at PHE

2.1.10 Ratio of Power to Product of Flow and Enthalpy

Several figures-of-merit (FOMs), discussed in [2], help to explain core behavior when the reactor is unstable. Figure 2.27 and Figure 2.28 compare the behavior of the ratio of power to the product of flow and enthalpy in the limiting bundles wherein the peak cladding temperature seems to be predicted. This variable was defined as FOM1 (other FOMs are discussed in Section 2.1.11). It is plotted for the early phase of the event where it is of interest to see how instability develops. The lower that this variable is, the more stable is the reactor. The figures show that this ratio increases with time in all cases. The large oscillatory behavior after around 95 s is caused by oscillatory bundle flow associated with unstable reactor power.

Figure 2.27 shows that in the BOC cases the behavior of this ratio is almost the same until 95 s. On the other hand, FOM1 is predicted to be lower, especially from approximately 11 s to 95 s, when the high fixed gas-gap conductance at PHE is considered (Figure 2.28). The effects of this figure-of-merit clearly appear in the behavior of the reactor power, as illustrated in Figure 2.3 and Figure 2.4. The degree of reactor power instability is almost the same at BOC but the amplitude of the power oscillation is much less at PHE when the FOM1 value is smaller with a high fixed-gap conductance.

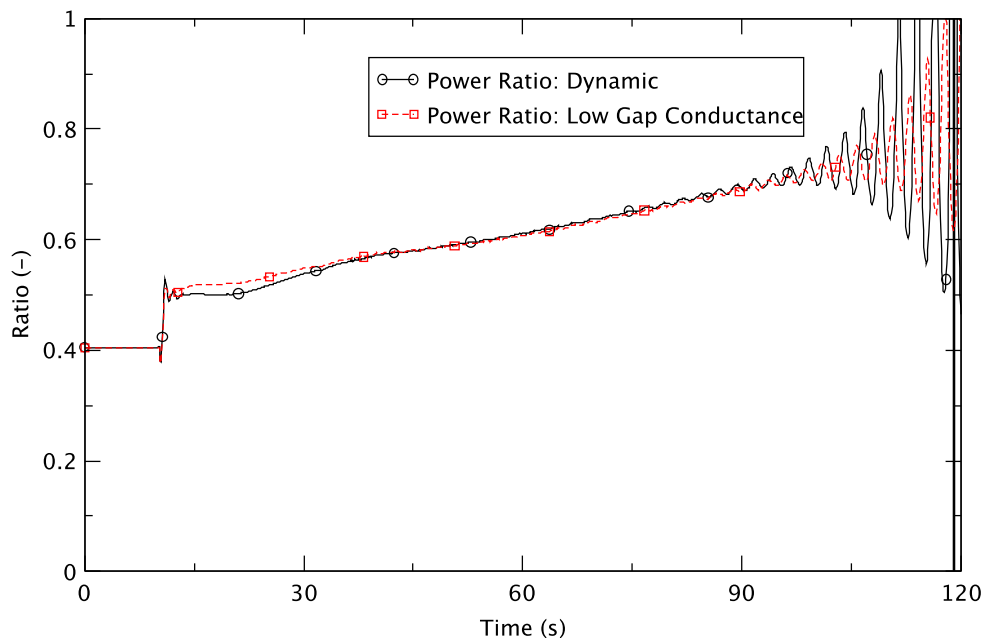


Figure 2.27 Ratio of Power to Product of Flow and Enthalpy (FOM1) in Limiting Bundles - Effect of Low Gas-Gap Conductance at BOC

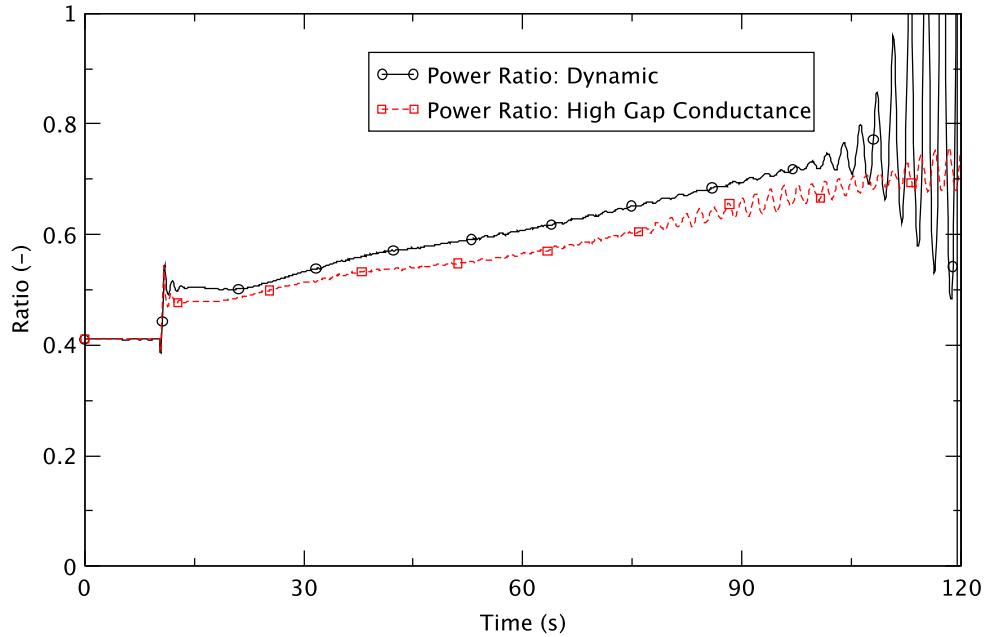


Figure 2.28 Ratio of Power to Product of Flow and Enthalpy (FOM1) in Limiting Bundles - Effect of High Gas-Gap Conductance at PHE

2.1.11 Additional Figures-of-Merit

Additional figures-of-merit were examined as denoted in Table 2.5. One observation is that for PHE, the larger that the gas-gap conductance is, the earlier the instability starts, even though it does not become more severe with high conductance. Table 2.5 also shows that the power oscillation mode evolves from fundamental to higher harmonic and then to first harmonic mode for the PHE cases, whilst, for the BOC cases, there is only one bi-modal power oscillation evolution from the fundamental to a higher harmonic mode.

Movies were generated showing the radial (x,y) assembly power versus time for the two sensitivity cases. Figure 2.29 and Figure 2.30 are snap shots from them showing the evolution of the power oscillation modes over time for the cases with fixed low and fixed high gap conductance, respectively.

Table 2.5 Figures-of-Merit Associated with the Evolution of Power Instability - Effect of Gas-Gap Modeling

Figure-of-Merit	BOC		PHE	
	Dynamic	Gap with 5,000 W/m ² -K	Dynamic	Gap with 161,000 W/m ² -K
Time of Onset of Reactor Instability (s)	95	102	95	77
Time of Onset of Bi-modal Power Oscillation	143 ¹	144 ¹	144 ¹ 160 ⁽²⁾	146 ¹ 169 ⁽²⁾
Time of Frequency Change (s)	154 (From 0.39 to 0.77 Hz)	154 (From 0.4 to 0.79 Hz)	157 (From 0.42 to 0.79 Hz)	166 (From 0.52 to 1.04 Hz)
Time of Onset of Oscillation Decay (s)	189	190	167	190

¹ The power oscillation evolves from the fundamental to a higher harmonic mode.

² The power oscillation evolves from a higher harmonic to the first harmonic mode.

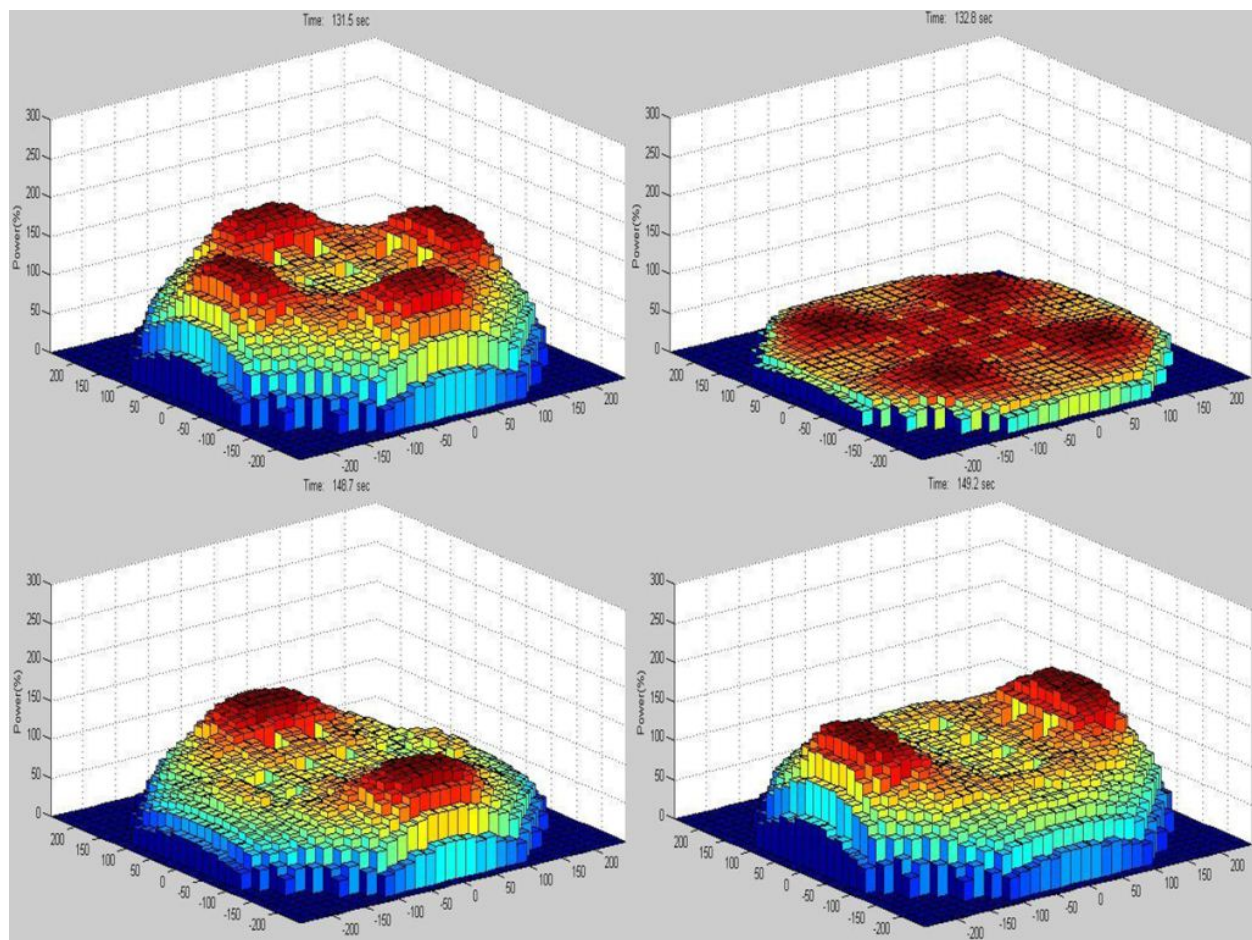


Figure 2.29 Power Oscillation Modes - Low Gas-Gap Conductance at BOC

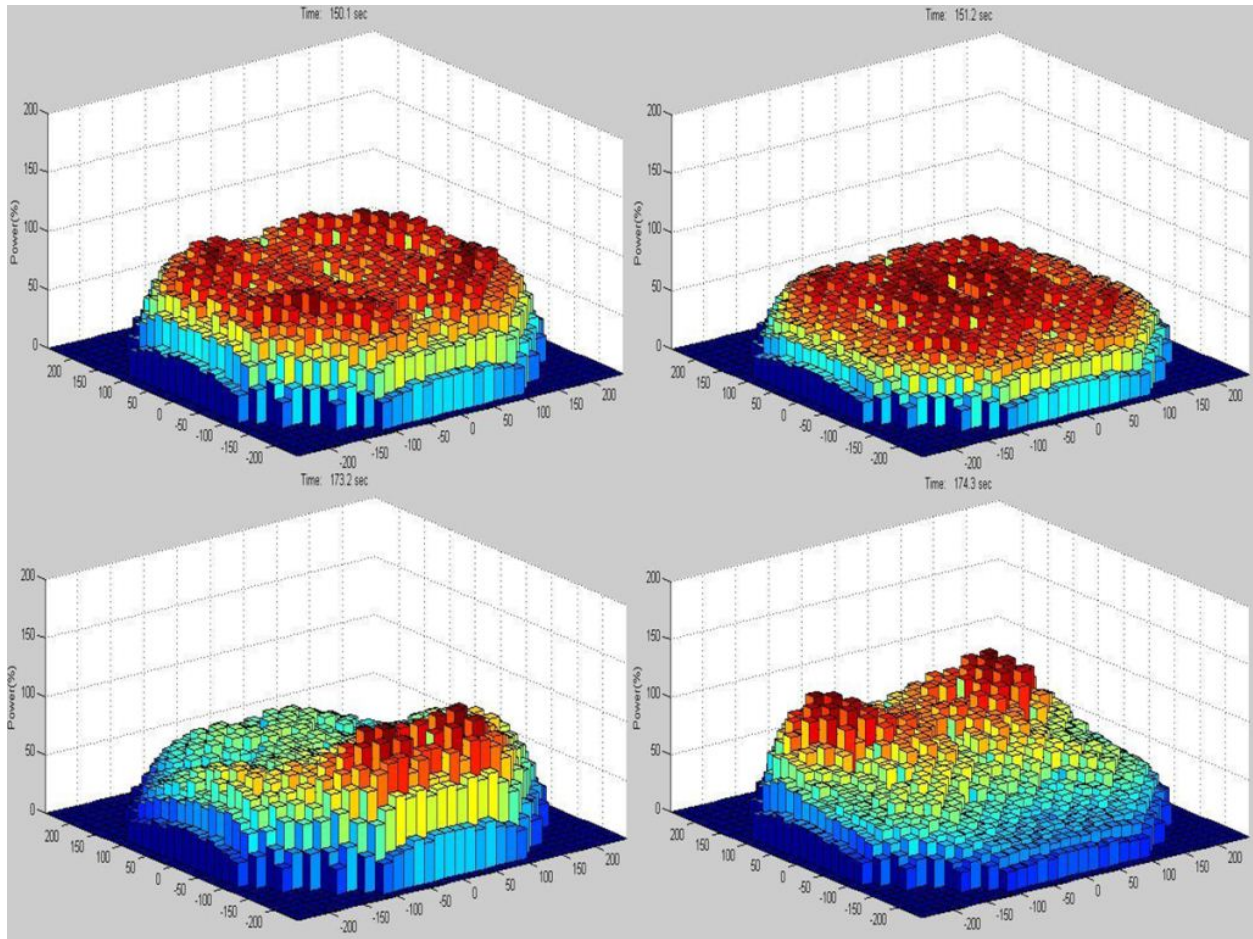


Figure 2.30 Power Oscillation Modes - High Gas-Gap Conductance at PHE

2.1.12 Summary

System behavior is very similar in the BOC cases using the dynamic gap model and a fixed low conductance for the gas-gap between the fuel pellet and the clad. This correspondence reflects that the assumed low value for gap conductance is similar in magnitude to the gap conductance predicted by the dynamic gap model. In fact, the assumed fixed gap conductance of 5,000 W/m²-K (based on results presented in [6]) is higher than the average effective gap conductance calculated by the dynamic gap model under initial steady-state conditions. This is evidenced in the lower steady-state average fuel temperature of the sensitivity case (Case 1C) compared with the reference case (Case 1).

However, in the PHE cases, while the dynamic gap model predicts the core as relatively unstable, with fixed high conductance the reactor power seemingly is much more stable, and there is no significant increase of cladding temperature during the transient period.

With high gap conductance, the fuel temperature remains closer to the coolant temperature than in the nominal case. Therefore, in response to a recirculation pump trip (2RPT) the change in fuel temperature is smaller compared to the nominal case. This is evident in Figure 2.12 that depicts the trajectory of temperature in the fuel centerline for a candidate hot rod.

While overall the fuel temperature is lower with high gap conductance, it is the combined effect of the fuel temperature and the magnitude of the Doppler reactivity coefficient that determines the contribution of reactivity from this temperature change. At the start of the transient, the reactor is treated as critical and, therefore, the initial temperature can be thought of as the “critical” fuel temperature. The change in fuel temperature in the high gap conductance case is smaller than in the nominal case. However, the magnitude of the Doppler coefficient is greater at lower temperatures. (The magnitude of the Doppler coefficient is proportional to the reciprocal of the square root of absolute temperature.) Therefore, we expect that the magnitude of the Doppler coefficient will be higher for the high gas-gap conductance scenario. The combination of these effects yields the difference in the Doppler feedback illustrated in Figure 2.8; the results show that with a higher gas-gap conductance, the positive reactivity insertion due to Doppler as the power decreases during the natural circulation phase (before 100 s) is about half that of the nominal case. This occasions a difference in the level of core power during the natural circulation phase. Figure 2.4 illustrates the trajectories of transient power and shows that after the 2RPT, the high gap conductance results in a slightly lower power level.

Compared to the nominal situation, the lower level of core power with high gap conductance entails a lower flow rate of the steam. Consequently, the feed flow rate necessary to maintain level also is lower than in the nominal case (Figure 2.18), that in turn means that less cold water is injected in the RPV. This difference in feed flow becomes important in changing inlet subcooling between the two cases around 100 s (Figure 2.24). The temperature of the core inlet is sensitive to the rate of FW injection since this water mixes with the return flow from the separators. As less cold water is injected in the case of high gap conductance, the inlet subcooling transient departs from the nominal case (Figure 2.24). Our high gap conductance calculations show lower inlet subcooling; lower inlet subcooling contributes to greater stability.

The results of our calculations suggest that a higher gap conductance can result in smaller reactor power oscillations primarily because of the effect of the fuel’s thermal response on such oscillations. The transient response of the fuel directly impacts the fuel’s temperature and the rate of energy transfer (heat flux) to the coolant. Thus, the dynamic response of the fuel is related to two reactivity feedback mechanisms, viz., the Doppler effect, and the moderator density (void) effect. It is known from fuel dynamic analyses [8] that the power-to-heat-flux transfer function adds almost a 90° phase delay (i.e., in addition to the phase delay due to the flow channel dynamics) to the total feedback to the response of reactor power. The destabilizing effect of fuel dynamics (due to this delay) is somewhat mitigated by a stabilizing effect inherent in the fuel’s thermal inertia that tends to filter out oscillations at frequencies higher than about 0.1 Hz (unstable oscillations in BWRs typically are observed at approximately 0.3 to 0.5 Hz [8], a range that agrees well with the results of the current analysis). Results for fixed high gap conductance suggests that the phase lag (heat flux is delayed with respect to power) is more important than the filtering effect. Another aspect of increasing the gap conductance is enhancing heat transfer from the fuel to the coolant. Thus, for a given power increase, the fixed high gap conductance triggers a higher rate of heat removal from the fuel and dampens the subsequent rise in the fuel’s temperature. The reduced sensitivity of fuel temperature to power oscillations is evident in the Doppler reactivity shown in Figure 2.8 where the fixed high gap conductance exhibits much lower magnitude of oscillation than does the dynamic-gap case.

2.2 Effect of Turbine Bypass Fraction at PHE

We explored the effect of turbine bypass fraction at PHE on the reactor's instability, considering cases with 10%, 25%, or 100% turbine bypass fractions. The general behavior of system parameters in all of them is very similar to that at BOC with different turbine bypass fractions as discussed in [2] except for the responses of reactor power. Detailed descriptions of the effect of turbine bypass fraction on the instability of the reactor's power at PHE are presented next.

2.2.1 Bypass Fractions

We considered three bypass fractions at PHE in our analysis: 10% (Case 2A), 25% (Case 2B), and 100% (Case 2, the reference case). The TSV is closed in 0.1 s on a turbine trip at 10 s of the simulation time, and reopens in 1.0 s to mimic the bypass paths with flow fractions given in the fifth column of Table 2.6 that lists the simulation conditions.

Table 2.6 Turbine Bypass Fractions and Simulation Conditions

Case ID	Exposure	Power, % of OLTP	Core Flow Rate, %	% Bypass Capacity ⁽¹⁾
2	PHE	120	85	100
2A	PHE	120	85	10
2B	PHE	120	85	25

¹ Bypass capacity (or bypass fraction) is percentage of normal steam flow to the turbine.

2.2.2 Initial Conditions

We compare in Table 2.7 the predicted initial values of some key thermal-hydraulic parameters from the TRACE/PARCS coupled null-transient calculation for 10 s to reference values and show the differences between them. As is evident, the calculated steady state values agree well with the reference ones.

Table 2.7 Comparison of Steady-State Thermal-Hydraulic Parameters - Effect of Turbine Bypass Fraction at PHE

Parameter	10%, 25%, and 100% Bypass			
	TRACE Value	Reference Value	Diff.	Diff. (%)
Core Power (MWt)	3988	3988	0	0
Steam Dome Pressure (kPa)	7141	7136	5	0.07
Main Steamline Flow (kg/s)	2218	2222	-4	-0.18
Total Core Flow (kg/s)	11617	11620	11	0.09
Feedwater Flow (kg/s)	2218	2222	-4	-0.18
Feedwater Temperature (K)	500	500	0	0
Downcomer Level (m)	14.32	14.46	-0.14	-0.97

2.2.3 Sequence of Events

The responses to variation of turbine bypass fraction at PHE are all very similar; furthermore, they are similar to the results of equivalent cases at BOC [2]. Table 2.8 shows the sequence of events; detailed discussions about system behavior are given in the following sections. In the table, we note where the sequence differs for different bypass fractions.

Table 2.8 Sequence of Events - Effect of Turbine Bypass Fraction at PHE

Time (s)	Event
0.0	<ul style="list-style-type: none"> Null transient simulation starts.
10.0	<ul style="list-style-type: none"> Null transient simulation ends. Turbine trip is initiated by closing the TSV. Recirculation pumps are tripped on the turbine trip. Feedwater temperature starts decreasing.
10.1	<ul style="list-style-type: none"> TSV closes completely and starts opening again to simulate turbine bypass fraction.
11.1	<ul style="list-style-type: none"> TSV (bypass) completes opening and its open area provides the predetermined fraction of steam flow shown in Table 2.6.
~11.4	<ul style="list-style-type: none"> Steam flow starts decreasing in Case 2. ~ 11.5 s in Case 2B. ~ 12.2 s in Case 2A.
~12.3	<ul style="list-style-type: none"> Feedwater flow starts decreasing in Case 2. ~14.2 s in Case 2A. ~14.3 s in Case 2B.
~65	<ul style="list-style-type: none"> Power oscillation (instability) starts in Cases 2A and 2B. ~ 95 s in Case 2.
~86	<ul style="list-style-type: none"> Noticeable bi-modal oscillation of the core power is initiated in Case 2A. ~104 s in Case 2B. ~144 s in Case 2.
120	<ul style="list-style-type: none"> Water level reduction is initiated and the setpoint of the control system for normal water level is reduced linearly to TAF over 180 s.
130	<ul style="list-style-type: none"> Boron injection is initiated and linearly ramped to full flow at 190 s.
~155	<ul style="list-style-type: none"> Downcomer water level begins falling noticeably in Cases 2A and 2B. ~ 163 s in Case 2.
~160	<ul style="list-style-type: none"> Boron starts accumulating in the core.
~161	<ul style="list-style-type: none"> Peak cladding temperature of ~1,552 K occurs in Case 2B. ~1,690 K at 163 s in Case 2. ~1,679 K at 164 s in Case 2A.
~230	<ul style="list-style-type: none"> Power oscillation ends in Case 2A. ~ 240 s in Cases 2 and 2B.
400	<ul style="list-style-type: none"> Simulation ends.

2.2.4 Steamline Flow and Dome Pressure

Figure 2.31 shows the steamline flow rates for the three cases at PHE with variation in the turbine bypass fraction. The general behavior of each case is similar. However, closer examination reveals that the average steam flow is slightly larger, from around 23 s to 200 s, when the bypass fraction is smaller (10% and 25%). This is caused by a higher average core

power with a smaller turbine bypass fraction that results in more steam generation in the core. The power behavior is discussed in the next section.

Figure 2.31 shows that the steam flow oscillates when the turbine bypass fraction is 10% and 25% while no oscillatory behavior is predicted with a bypass fraction of 100%. This reflects the continuous opening and closing of the safety relief valves (SRVs) to control system pressure in cases with small bypass fractions.

Figure 2.32 plots the system pressure behavior. As expected, TRACE predicts an oscillation of pressure with 10% and 25% bypass fractions. However, when the bypass fraction is sufficiently large (100%), the system pressure becomes almost constant from approximately 50 s to 165 s and then decreases almost negligibly as the core power begins dropping.

Figure 2.32 also shows that the system pressure varies inversely with the turbine bypass fraction after around 240 s. The pressure is almost the same for 10% and 25% bypass from around 50 s to 200 s because the SRVs maintain it. Figure 2.32 also shows that the system pressure reaches an asymptotic value faster when the bypass fraction is larger.

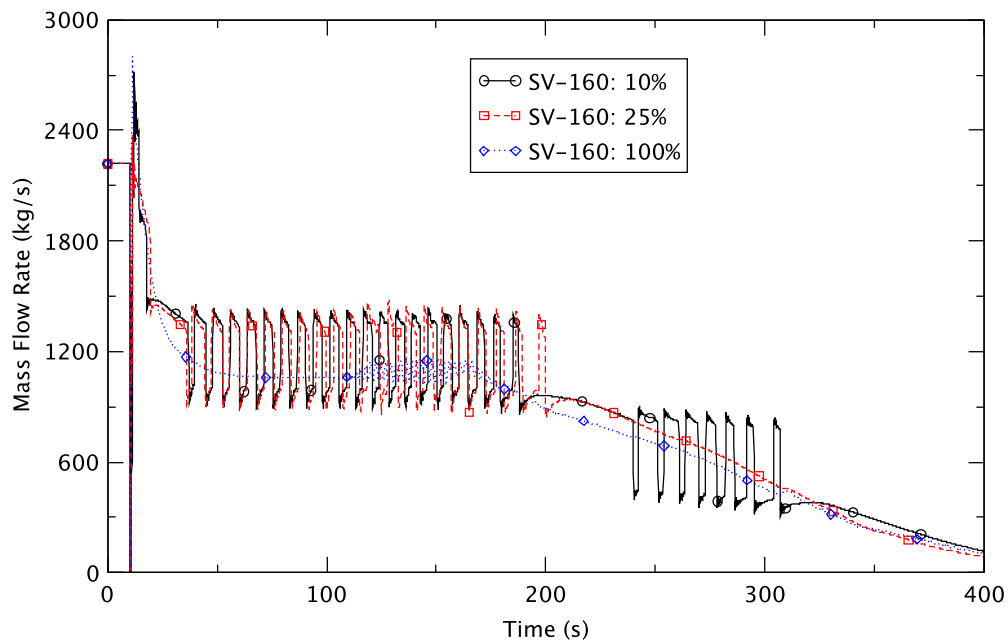


Figure 2.31 Steamline Mass Flow Rate - Effect of Turbine Bypass Fraction at PHE

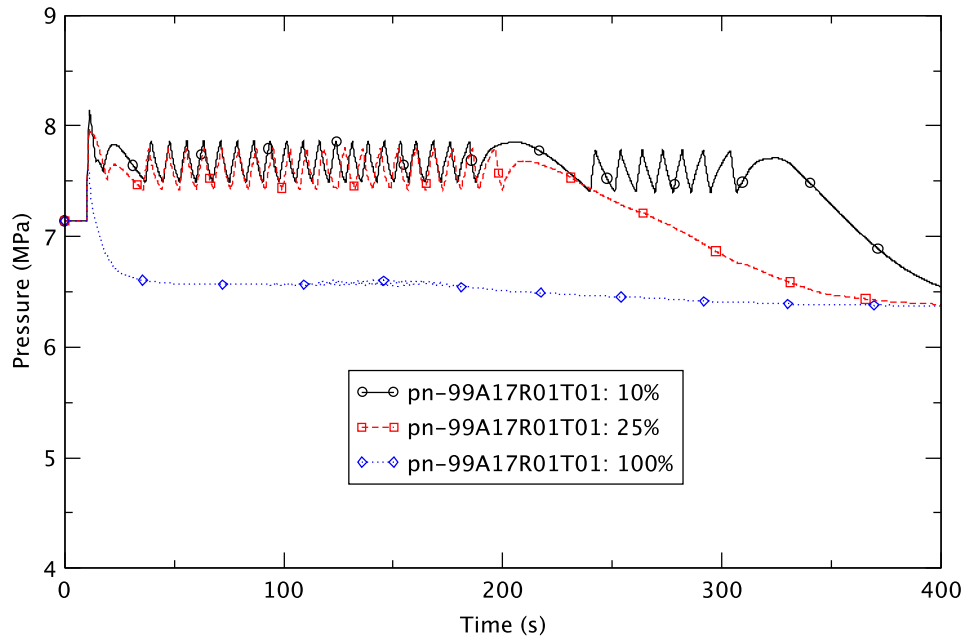


Figure 2.32 RPV Pressure - Effect of Turbine Bypass Fraction at PHE

2.2.5 Core Power

Figure 2.33 depicts the reactor core power for all three cases, whilst Figure 2.34, Figure 2.35, and Figure 2.36 show the reactor power for each case separately. The general behavior is similar for all three cases. However, large amplitude power oscillations are predicted from around 115 s to 130 s in the 25% case while they continue from approximately 117 s to 162 s in the 100% case. For the 10% bypass fraction, the amplitudes of the power oscillation are relatively small from about 110 s to 160 s. These power responses are different from those at BOC [2]. There, the power behavior is similar; the reactor power oscillates, its amplitude is large, and it continues for almost the same time, especially from 110 s to 200 s, with all sizes of the bypass fraction (Figure 2.37).

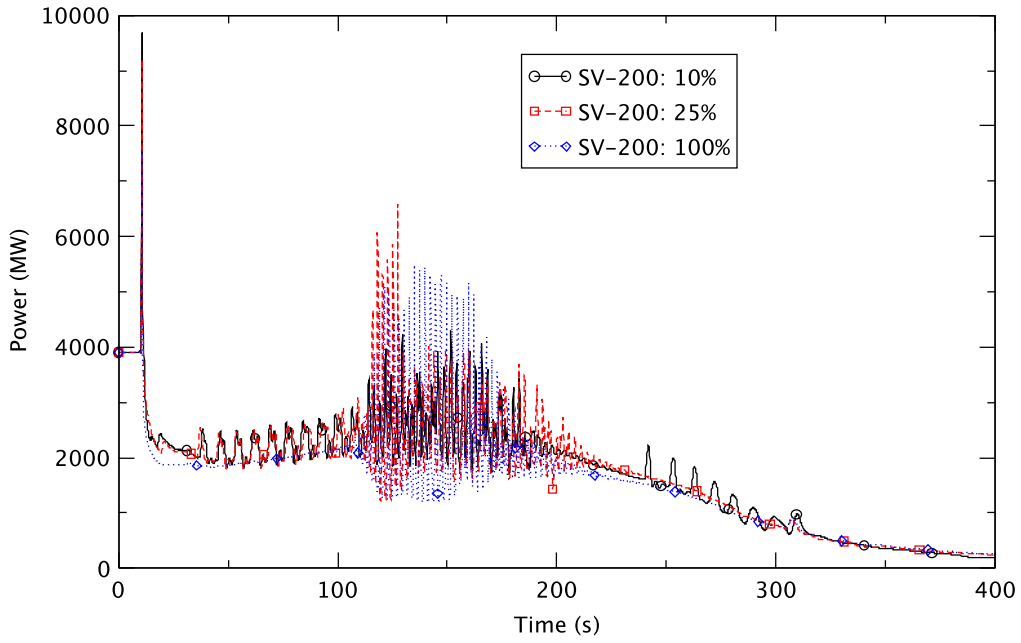


Figure 2.33 Core Power - Effect of Turbine Bypass Fraction at PHE

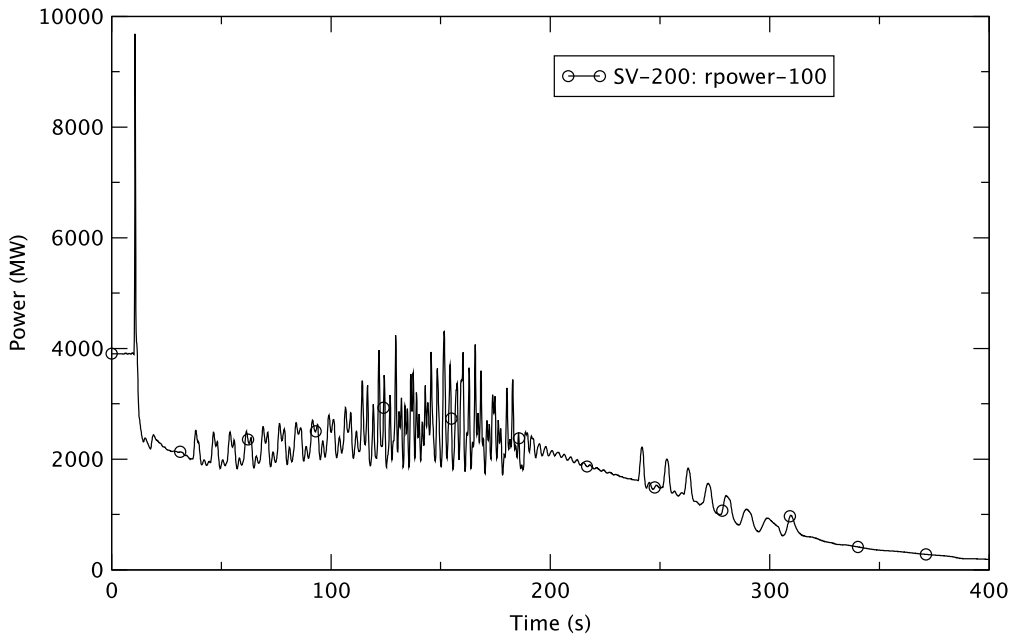


Figure 2.34 Core Power at PHE with 10% Bypass Fraction (Case 2A)

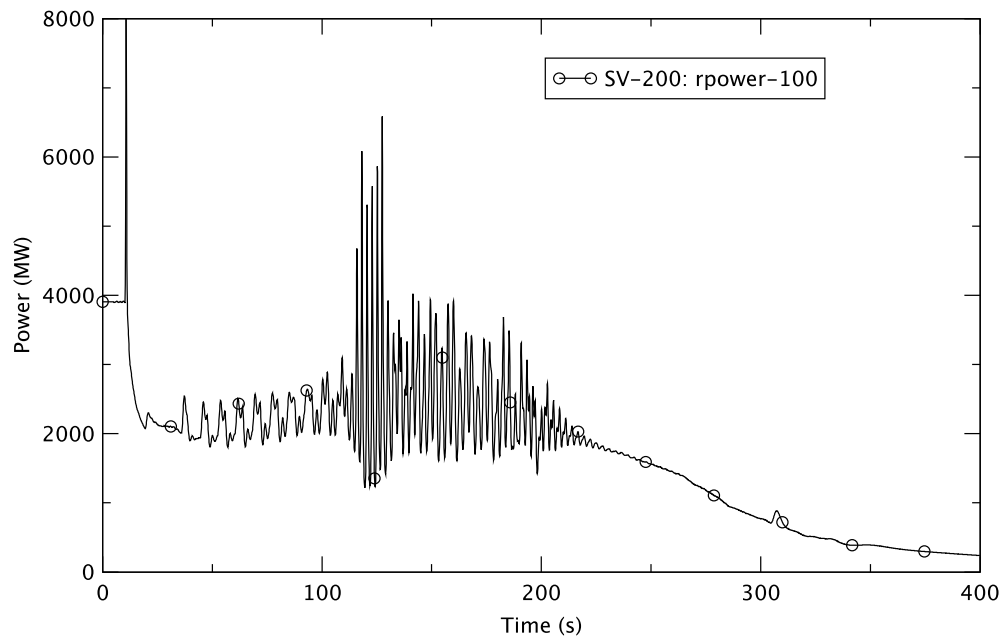


Figure 2.35 Core Power at PHE with 25% Bypass Fraction (Case 2B)

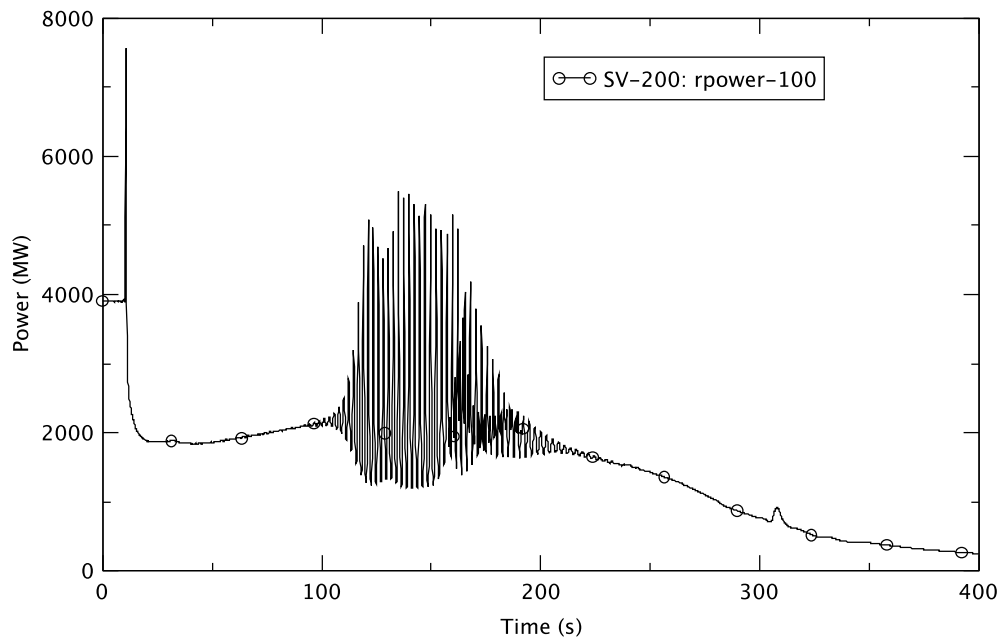


Figure 2.36 Core Power at PHE with 100% Bypass Fraction (Case 2)

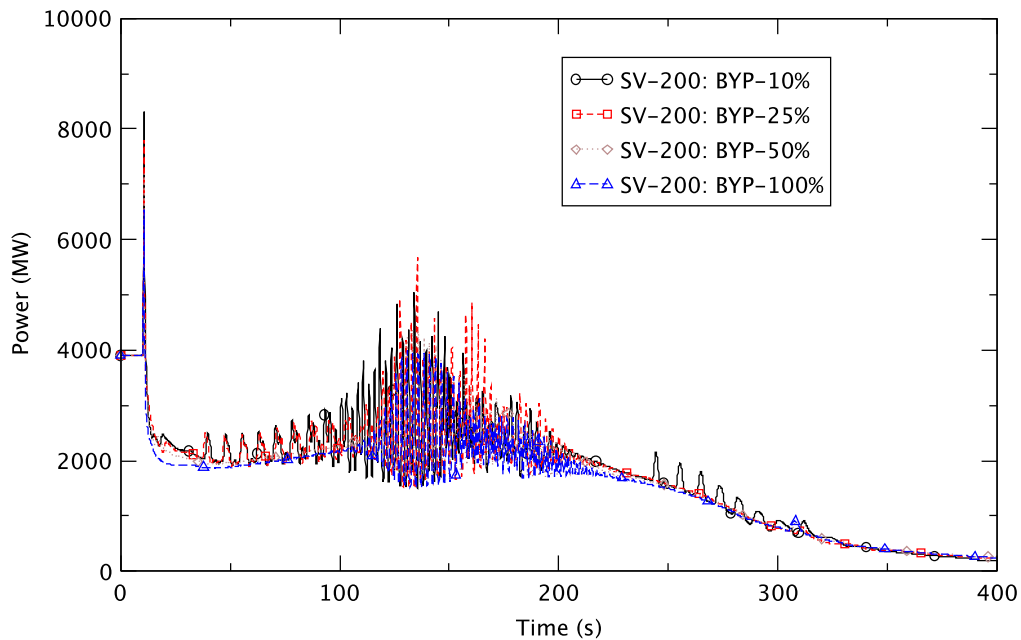


Figure 2.37 Core Power - Effect of Turbine Bypass Fraction at BOC

From Figure 2.33 we see that the average power is higher when the bypass fraction becomes smaller. This is caused by the system pressure behavior. As shown in Figure 2.32, the system pressure is higher with smaller bypass fraction and this leads to reduced void, a smaller negative void reactivity feedback, and a higher average core power.

It is observed in Figure 2.34 through Figure 2.36 that the power oscillations start earlier with smaller bypass fractions (10% and 25%) than with full bypass (100%). These early power oscillations, from around 35 s to 65 s, do not indicate reactor instability but are caused by moderator density changes due to the oscillatory behavior of the system pressure caused by SRV cycling (Figure 2.32). However, the oscillations become more irregular due to the perturbation caused by the SRVs when the reactor becomes unstable around 65 s.

As discussed above, there is a difference between BOC and PHE results. At BOC the reactor becomes more unstable as the system pressure becomes higher with smaller turbine bypass fractions. We did not observe a corresponding trend at PHE.

2.2.6 Core Flow

Core flow rates are compared in Figure 2.38. They behave very similar to each other except for some oscillatory behavior from around 40 s to 110 s with small bypass fractions (10% and 25%) due to SRV cycling (see Section 2.2.4).

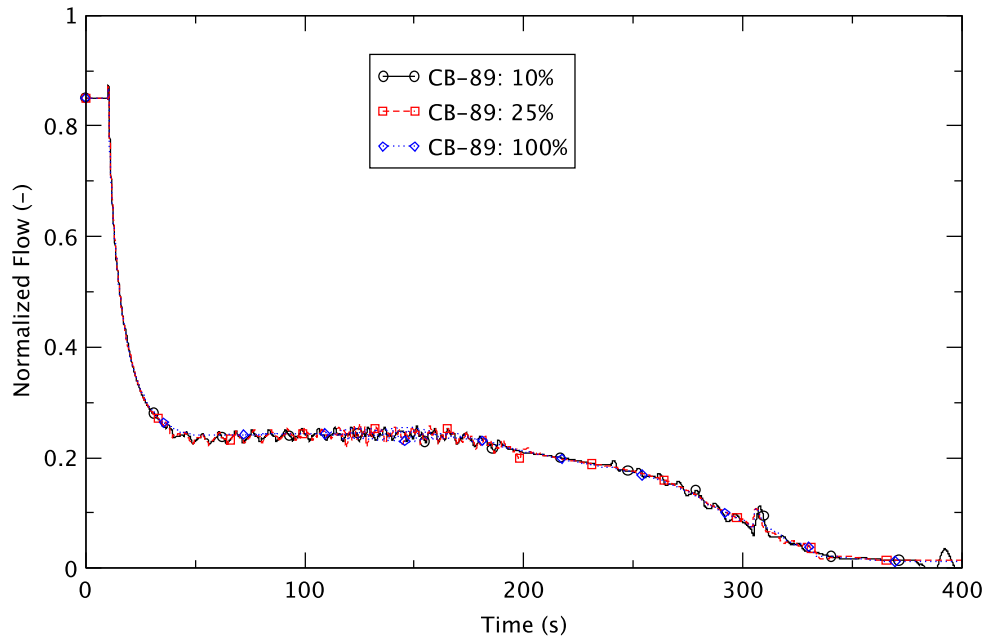


Figure 2.38 Core Flow Rate - Effect of Turbine Bypass Fraction at PHE

2.2.7 Feedwater Flow and RPV Water Level

The operator action of level reduction to TAF to decrease the mass flow into the core is simulated at 120 s by reducing the flow of feedwater. Figure 2.39 compares the feedwater flow rates. As expected, they start decreasing from 120 s in all cases. This comparison illustrates that as the turbine bypass fraction lessens, the recovery of the feedwater flow rate also becomes smaller at around 14 s when the TBV is open, but the flow rate is slightly larger from approximately 24 s until it becomes zero at around 270 s. This larger FW flow is due to the larger steam flow with smaller bypass fraction (Figure 2.31). However, the general behavior is similar for each case.

The DC water levels do not drop until around 170 s with all bypass fractions (Figure 2.40). This unexpected behavior was discussed in detail in [2]. The general behavior of the level is very similar in all cases. The delay of the reduction in the DC water level results in the late onset of the decline in core flow (Figure 2.38), that starts decreasing from around 170 s for all cases.

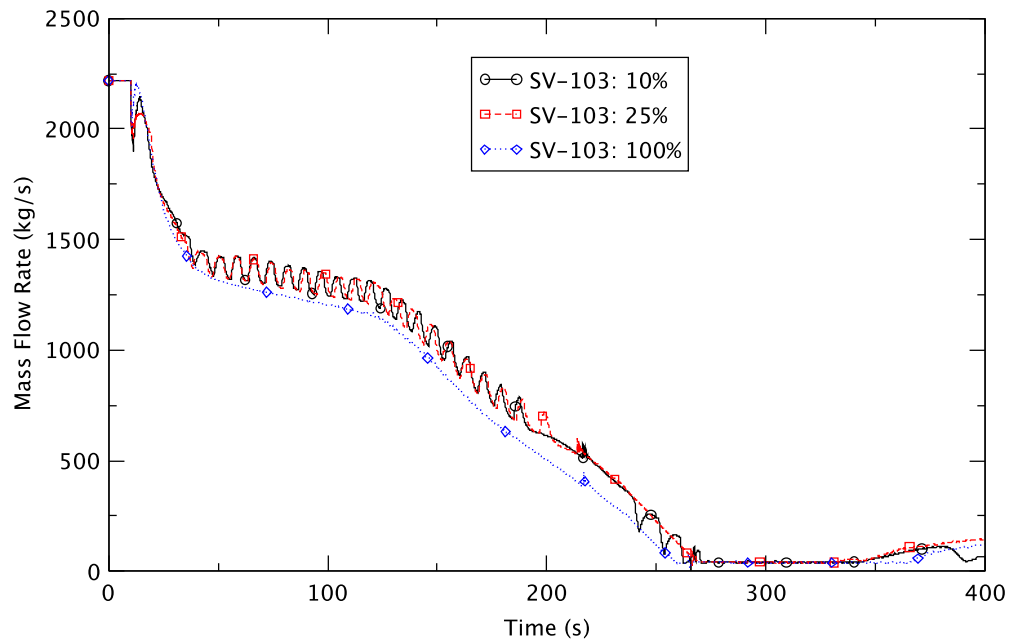


Figure 2.39 Feedwater Flow Rate - Effect of Turbine Bypass Fraction at PHE

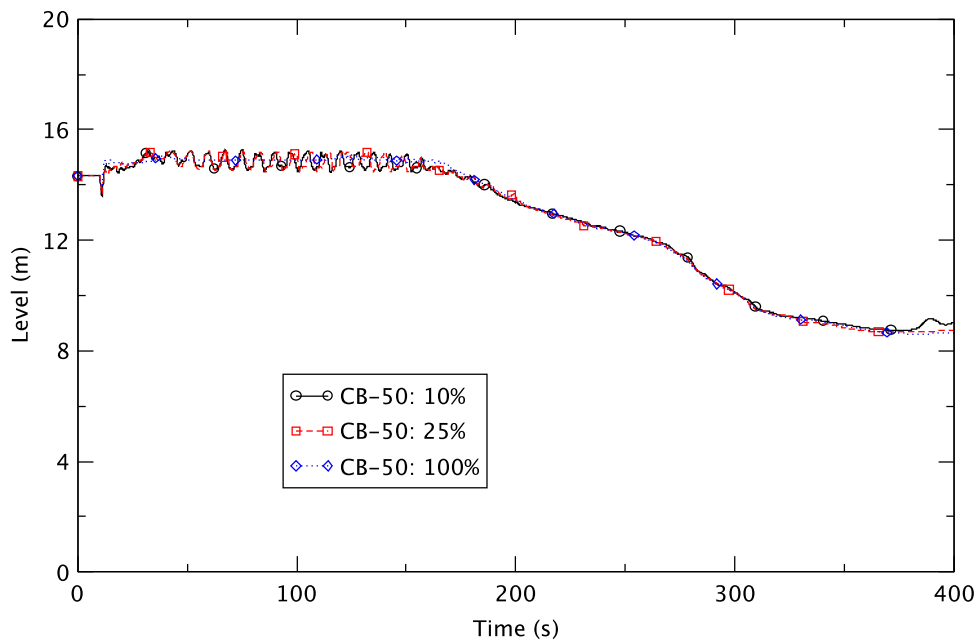


Figure 2.40 Downcomer Water Level - Effect of Turbine Bypass Fraction at PHE

2.2.8 Boron Inventory in Core

Operation of the SLCS is initiated at 130 s, and Figure 2.41 compares the boron inventory in the core. It is almost the same in all cases, especially until around 260 s when the reactor instability has practically ended. Hence, boron injection does not contribute to the differences between the cases with different bypass fractions.

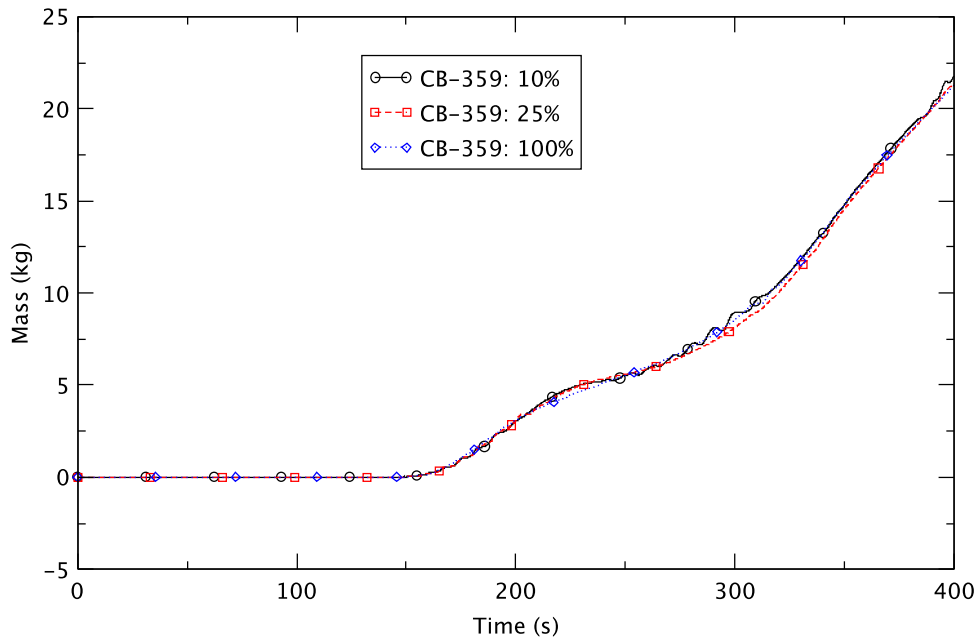


Figure 2.41 Boron Inventory in Reactor Core - Effect of Turbine Bypass Fraction at PHE

2.2.9 Liquid Subcooling of Core Flow

Figure 2.42 shows core inlet subcooling in ring 1 that becomes larger as the turbine bypass fraction becomes smaller (10% and 25%). This is due to the system's pressure being higher with a smaller bypass fraction (Figure 2.32), and it entails a higher saturation temperature and higher liquid subcooling at the core inlet. In addition, the larger flows of steam and feedwater increase subcooling.

The severity of the power oscillation is not associated with the degree of the core inlet subcooling (actually, the size of turbine bypass) at PHE, as shown in Figure 2.33 to Figure 2.36, while a correlation between the amplitude of the power oscillation and turbine bypass fraction can be observed in the BOC cases [2]. We do not know the reason why the reactor's power response, especially the amplitude of the power oscillation, is different at the two different fuel cycle times, BOC and PHE. One of the plant's responses that contributes to the oscillatory power behavior is the cycling of SRVs in cases where the steam bypass capacity is less than 50%. The current analyses were performed with a model that lumps all SRVs into one single effective valve. This approximation has known limitations in simulating the individual lifting of

different banks of SRVs and the modeling of pressure losses in partially open valves. The application of an improved model [3] is outside the scope of this study.

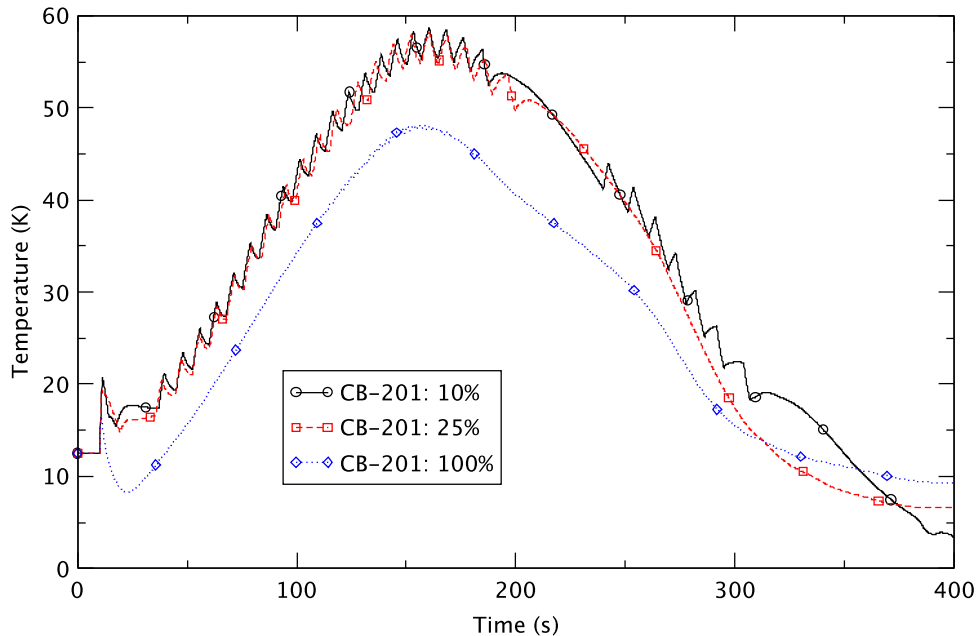


Figure 2.42 Liquid Subcooling at Core Inlet - Effect of Turbine Bypass Fraction at PHE

2.2.10 Fuel Rod Cladding Temperature

Core power oscillations affect the temperature of the fuel cladding due to the changes of the power and the efficiency of heat transfer from the fuel to coolant; the latter occurs because of the continuous change of the void fraction and coolant flow in the core. Figure 2.43 compares the maximum cladding temperature among all bundles in the core. The cladding temperature suddenly increases around 120 s and except for the behavior from around 150 s to 190 s, all cases exhibit very similar behavior. The peak cladding temperatures of 1,679 K, 1,552 K, and 1,690 K take place at approximately 164 s with 10% bypass fraction, 161 s with 25% bypass fraction, and 163 s with 100% bypass fraction. They all are higher than 1,478 K (2,200°F), which can be used as an acceptance criterion for this study because it is imposed as a limit in new plants [7]. We also note that the simulation does not model potential fuel damage at excessive temperatures.

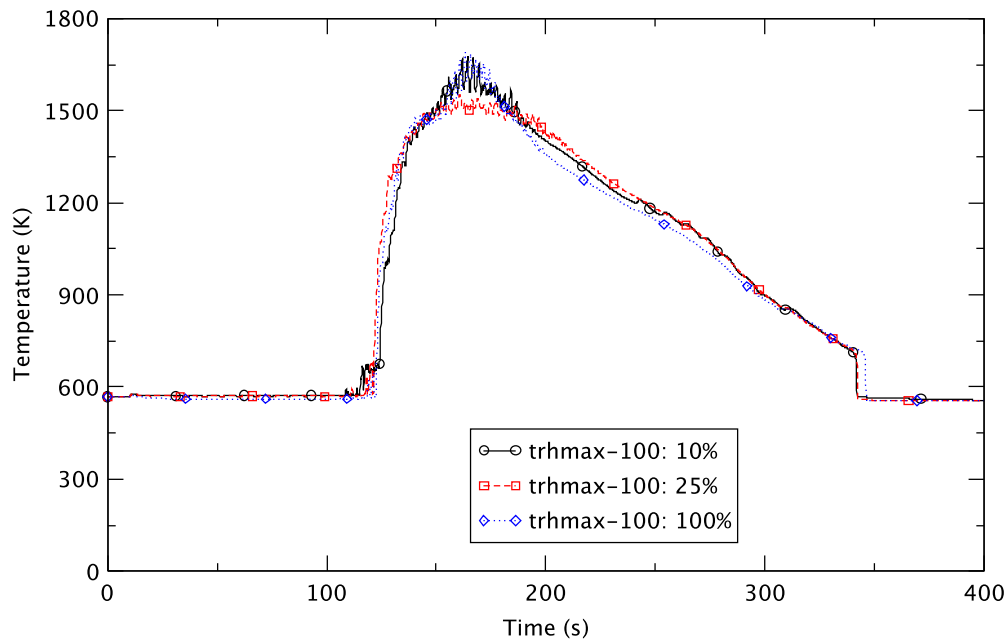


Figure 2.43 Maximum Cladding Temperature among All Fuel Bundles - Effect of Turbine Bypass Fraction at PHE

2.2.11 Ratio of Power to Product of Flow and Enthalpy

Figure 2.44 compares the behavior of the ratio of power to the product of flow and enthalpy (FOM1) in the limiting bundles where the peak cladding temperature seems to be predicted for the early part of the transient. The figure shows that this ratio increases with time in all cases. It also shows that this variable is generally larger with smaller bypass fraction than with 100% bypass, but it is difficult to detect any clear correlation between the severity of the power instability and the relative magnitude of this variable. In the figure, the large oscillatory behavior after around 100 s is caused by oscillatory bundle flow that correlates with unstable reactor power.

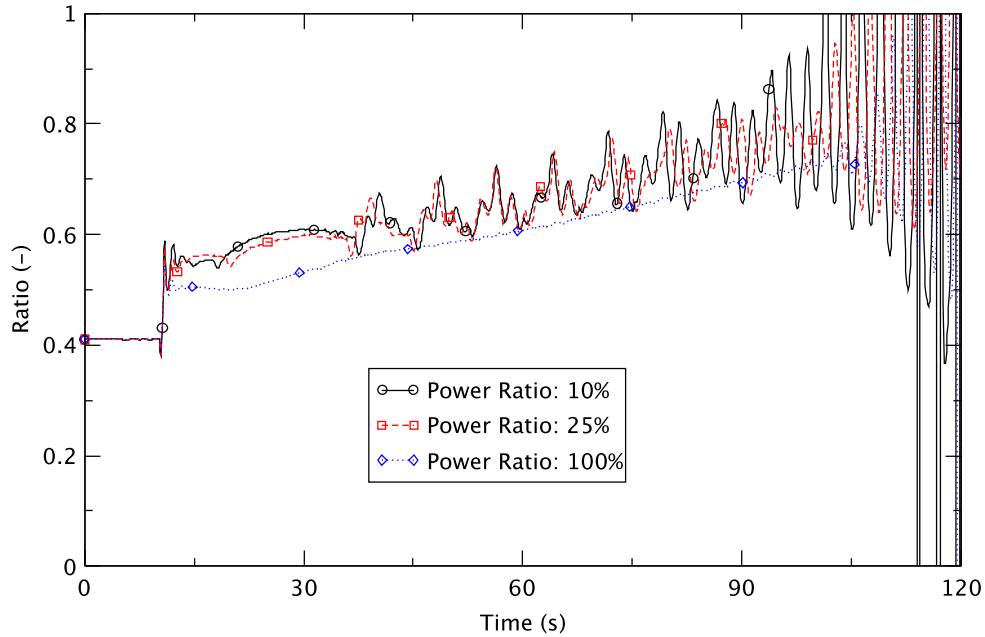


Figure 2.44 Ratio of Power-to-Product-of-Flow-and-Enthalpy (FOM1) in Limiting Bundles - Effect of Turbine Bypass Fraction at PHE

2.2.12 Additional Figures-of-Merit

Additional figures-of-merit are shown in Table 2.9. The reactor instability starts early and there are multiple evolutions of bi-modal power oscillation when the turbine bypass fraction is small. This is best observed in the movies of radial (x,y) power versus time. Snapshots from the movies, depicted in Figure 2.45 and Figure 2.46, illustrate the various modes of oscillation for 10% and 25% turbine bypass, respectively.

Table 2.9 Figures-of-Merit Associated with Evolution of Power Instability - Effect of Turbine Bypass Fraction at PHE

Figure-of-Merit	10%	25%	100%
Time of Onset of Reactor Instability (s)	65	65	95
Time of Onset of Bi-modal Power Oscillation	107 ¹ 166 ²	130 ¹ 182 ²	144 ¹ 154 ²
Time of Frequency Change (s)	NA ³ (From 0.4 to 0.75 Hz)	NA ⁽³⁾ (From 0.36 to 0.77 Hz)	157 (From 0.42 to 0.79 Hz)
Time of Onset of Oscillation Decay (s)	169	196	167

¹ The power oscillation evolves from the fundamental mode to a higher harmonic mode.

² The power oscillation evolves from higher harmonic to the first harmonic mode.

³ It is difficult to determine the timing of change of frequency because of the continuous opening and closing of the SRVs. However, information on frequency doubling is obtained via a Fourier transform [2].

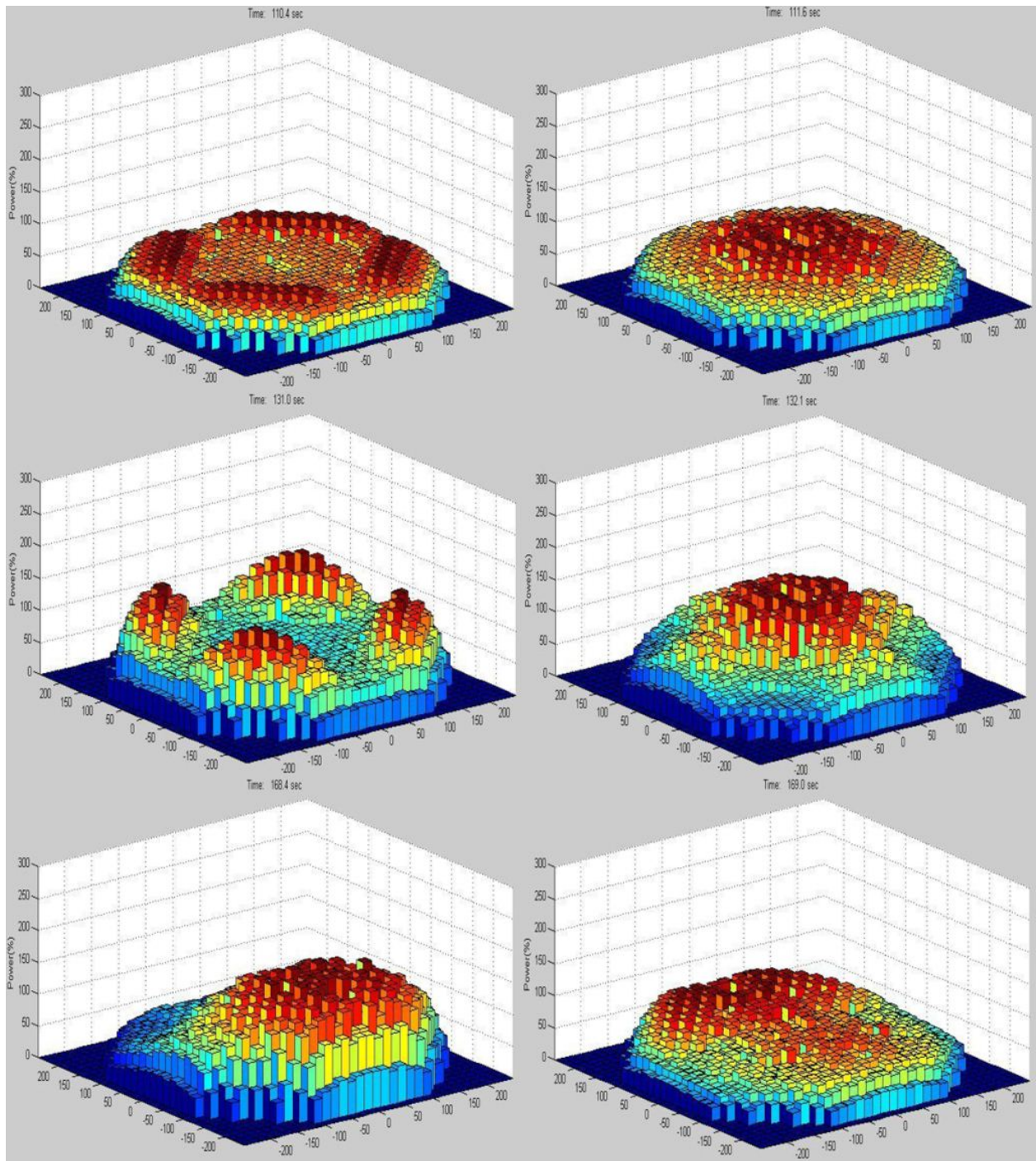


Figure 2.45 Power Oscillation Modes - 10% Turbine Bypass at PHE

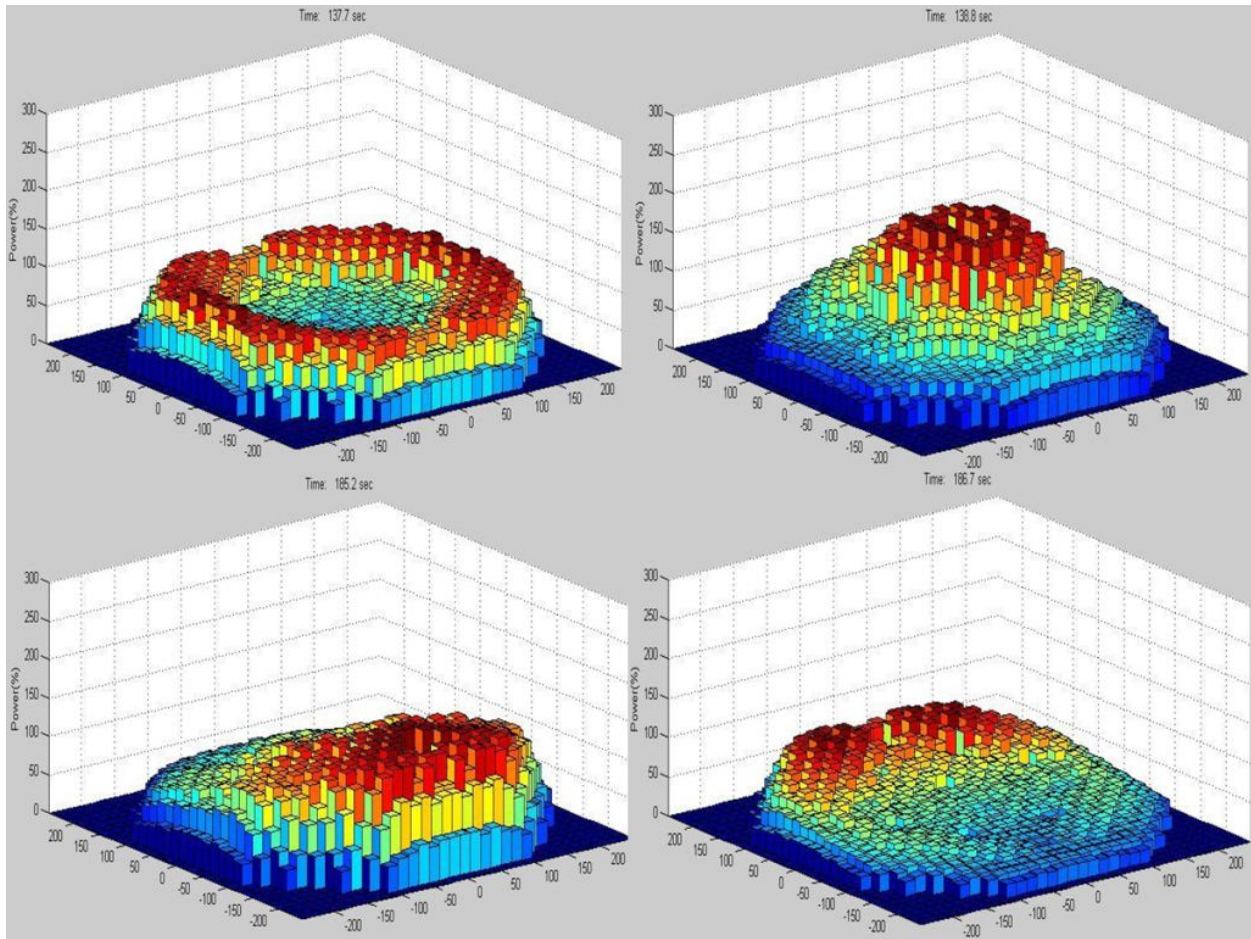


Figure 2.46 Power Oscillation Modes - 25% Turbine Bypass Fraction at PHE

2.2.13 Summary

At PHE with different turbine bypass fractions, the general behavior of the system parameters is similar to the behavior at BOC with several bypass fractions. For example, the core inlet subcooling and the ratio of power to the product of flow and enthalpy are larger when the turbine bypass fraction is smaller. However, the power responses differ at the two different fuel cycle times. While TRACE predicts a more unstable reactor condition at BOC as the turbine bypass fraction falls, the amplitude of the power oscillation due to the reactor instability does not show any obvious trend associated with the size of the bypass fraction at PHE, even though power instability is observed in all cases. Different cases exhibiting different oscillation modes further complicates the ability to understand the trends of the results.

The reasons for the different trends in reactor power responding to variations in the turbine bypass fraction at BOC and PHE are unknown. Subsequent to this analysis, a revised SRV model and a new boron transport model, which may offer more detailed modeling of the plant, were incorporated in the BWR/5 model that is used to study ATWS events with emergency depressurization [3]. The new SRV model addresses the known limitations of the simplified SRV model that we used in the current analysis. The new boron transport scheme eliminates the lower plenum flow control valve whose presence is known to create flow disturbances that are non-physical.

2.3 Effect of Initial Core Flow Rate at PHE

2.3.1 Core Flow Rates at PHE

To understand the effect of core flow rate on reactor instability, two cases are analyzed: PHE with 85% initial core flow rate (Case 2, the reference case) and PHE with 75% initial core flow rate (Case 2H, the sensitivity case). Both cases have 100% turbine bypass capacity and start from 100% power. The TSV is closed in 0.1 s on a turbine trip at 10 s into the simulation time, and then reopens in 1.0 s to simulate the bypass paths with 100% turbine bypass. The simulation conditions are shown in Table 2.10.

Table 2.10 Initial Core Flow Rate at PHE and Simulation Conditions

Case ID	Exposure	Power	Core Flow Rate	Bypass Capacity
2	PHE	100%	85%	100%
2H	PHE	100%	75%	100%

2.3.2 Initial Conditions

Table 2.11 displays the predicted initial values of some key thermal-hydraulic parameters from the TRACE/PARCS null transient calculation up to 10 s and the difference to the reference values. As is evident, the calculated steady state values agree well with the reference ones.

Table 2.11 Comparison of Steady-State Thermal-Hydraulic Parameters - Effect of Core Flow Rate at PHE

Parameter	85% Flow (Case 2)		75% Flow (Case 2H)	
	TRACE Value	Diff. (%)	TRACE Value	Diff. (%)
Core Power (MWt)	3988	0	3988	0
Steam Dome Pressure (kPa)	7141	0.07	7141	0.07
Main Steamline Flow (kg/s)	2218	-0.18	2219	-0.14
Total Core Flow (kg/s)	11631	0.09	10250	-0.03
Feedwater Flow (kg/s)	2218	-0.18	2219	-0.14
Feedwater Temperature (K)	500	0	500	0
Downcomer Level (m)	14.32	-0.97	14.32	-0.97

2.3.3 Sequence of Events

The timing of the sequence of events is similar in both cases, as Table 2.12 shows. Detailed discussions about the system behavior are given in the following sections. In the table, it is noted where the sequence differs for the sensitivity case.

Table 2.12 Sequence of Events - Effect of Core Flow Rate at PHE

Time (s)	Event
0.0	<ul style="list-style-type: none"> Null transient simulation starts.
10.0	<ul style="list-style-type: none"> Null transient simulation ends. Turbine trip is initiated by closing the TSV. Recirculation pumps are tripped on the turbine trip. Feedwater temperature starts decreasing.
10.1	<ul style="list-style-type: none"> TSV closes completely and starts opening again to simulate 100% turbine bypass flow.
11.1	<ul style="list-style-type: none"> TSV (bypass) completes opening and its open area provides the predetermined steam flow fraction of 100% shown in Table 2.10.
~11.4	<ul style="list-style-type: none"> Steam flow starts decreasing.
~12.3	<ul style="list-style-type: none"> Feedwater flow starts decreasing.
~87	<ul style="list-style-type: none"> Power oscillation (instability) starts in Case 2H. ~95 s in Case 2.
~103	<ul style="list-style-type: none"> Noticeable bi-modal oscillation of the core power is initiated in Case 2H. ~144 s in Case 2.
120	<ul style="list-style-type: none"> Water level reduction is initiated by reducing the setpoint of the normal water level control system linearly to TAF over 180 s. Downcomer water level begins decreasing due to operator action in Case 2H. At ~163 s the DC level starts dropping in Case 2.
130	<ul style="list-style-type: none"> Boron injection is initiated and linearly ramped to full flow at 190 s.
~156	<ul style="list-style-type: none"> Peak cladding temperature of ~1,759 K occurs in Case 2H. ~1,690 K at 163 s in Case 2.
~160	<ul style="list-style-type: none"> Boron starts accumulating in the core.
~240	<ul style="list-style-type: none"> Power oscillation ends in Case 2. ~255 s in Case 2H.
400	<ul style="list-style-type: none"> Simulation ends.

2.3.4 Steamline Flow

Figure 2.47 compares steamline flow rates for the two cases. The behavior is similar in both except that steam flow is higher with 75% initial core flow from around 20 s to 360 s. This is caused by higher core power during that period. We discuss the core power in the following section.

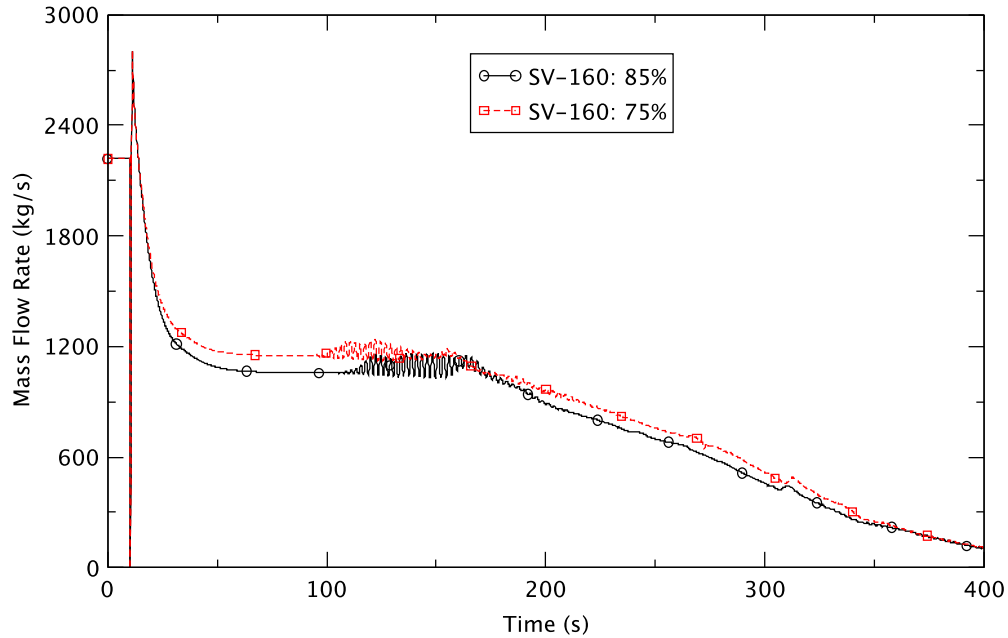


Figure 2.47 Steamline Mass Flow Rate - Effect of Core Flow at PHE

2.3.5 Core Power and Dome Pressure

Figure 2.48 compares the reactor core powers. With 75% core flow, the core power is predicted to be higher than with 85% flow after it decreases at around 11 s due to the opening of the turbine bypass valve. The reason for the higher power with 75% core flow is that a relatively smaller negative void reactivity is introduced after around 13 s (Figure 2.49). In comparing the responses of the void reactivity after the recirculation pump trip for the two cases, we note that the 75% flow case involves a relatively smaller reduction in core flow from its initial value compared to the 85% case (see Section 2.3.6). It also is evident in Figure 2.48 that reactor instability starts earlier with 75% core flow (at around 87 s) relative to that with 85% flow (at around 95 s).

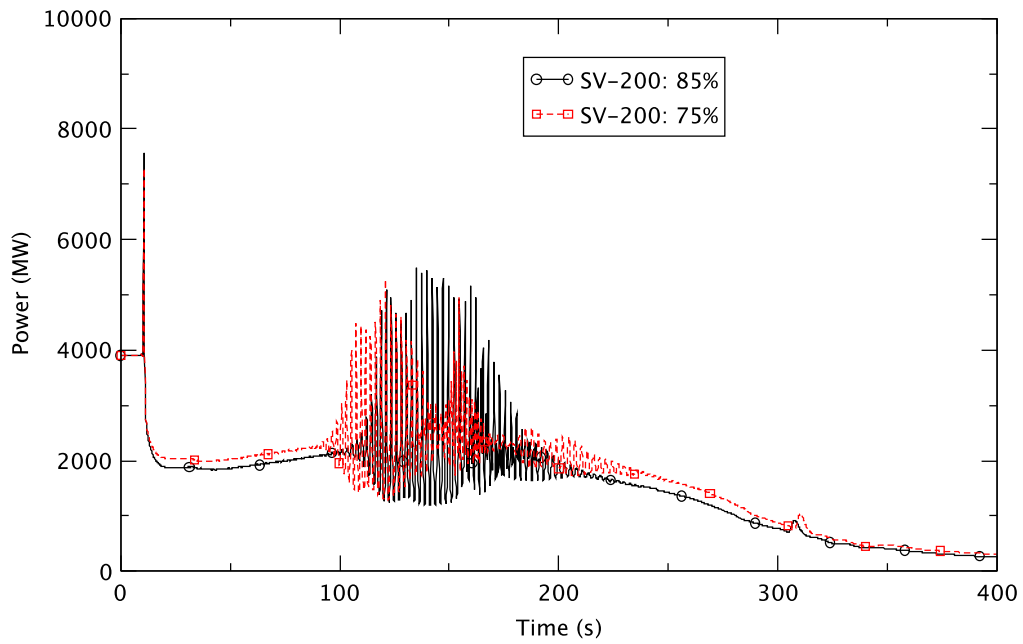


Figure 2.48 Core Power - Effect of Core Flow at PHE

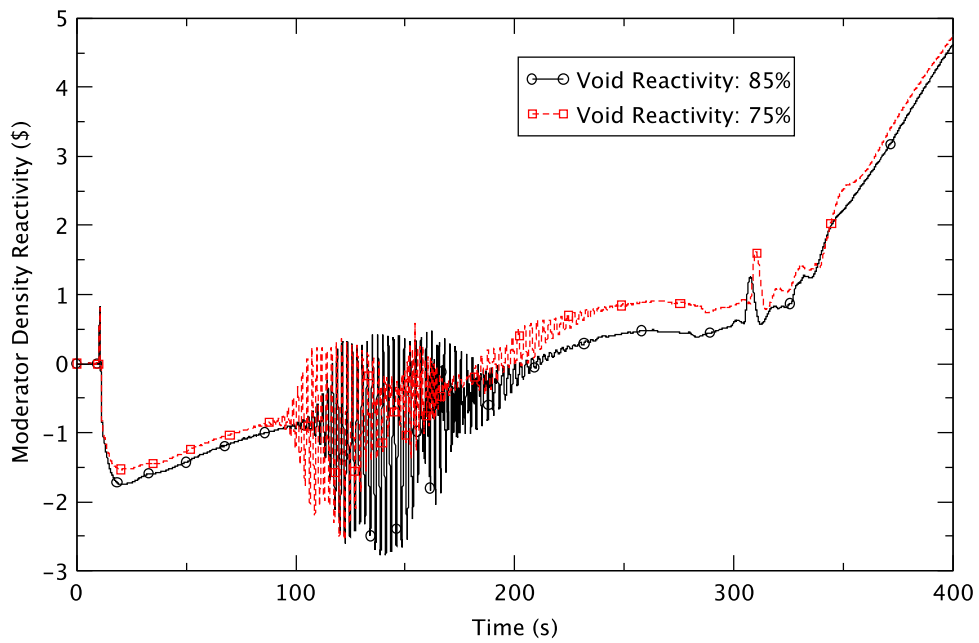


Figure 2.49 Void Reactivity - Effect of Core Flow at PHE

The system pressure is very similar in each case (Figure 2.50) but marginally higher for 75% flow than for 85% flow from around 20 s to 360 s. This is consistent with the behavior of steam flow and power, although the difference between the two pressure traces is small.

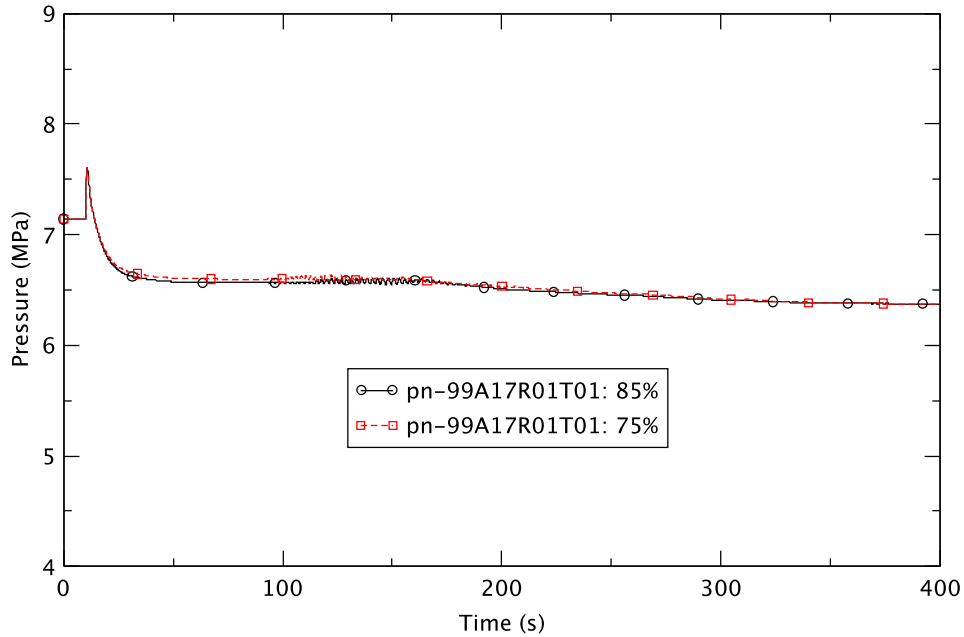


Figure 2.50 RPV Pressure - Effect of Core Flow at PHE

2.3.6 Core Flow

Core flow rates are compared in Figure 2.51. The initial core flow is 75% and 85% of rated flow as shown in the figure. As the recirculation pumps coast down after 10 s, the behavior of the core flow becomes alike because of the similar behavior of the pump's coast down and the difference in the gravity head between the core and downcomer after natural circulation is established. Figure 2.51 shows that the flow is slightly larger with 85% initial core flow during the recirculation pump coast down (from about 10 s to 50 s), and this is caused by the initially higher flow rate. From around 120 s to 220 s, TRACE predicts a slightly smaller core flow for the instance of 75% initial core flow wherein the downcomer water level is predicted to be a little lower, as discussed in Section 2.3.7.

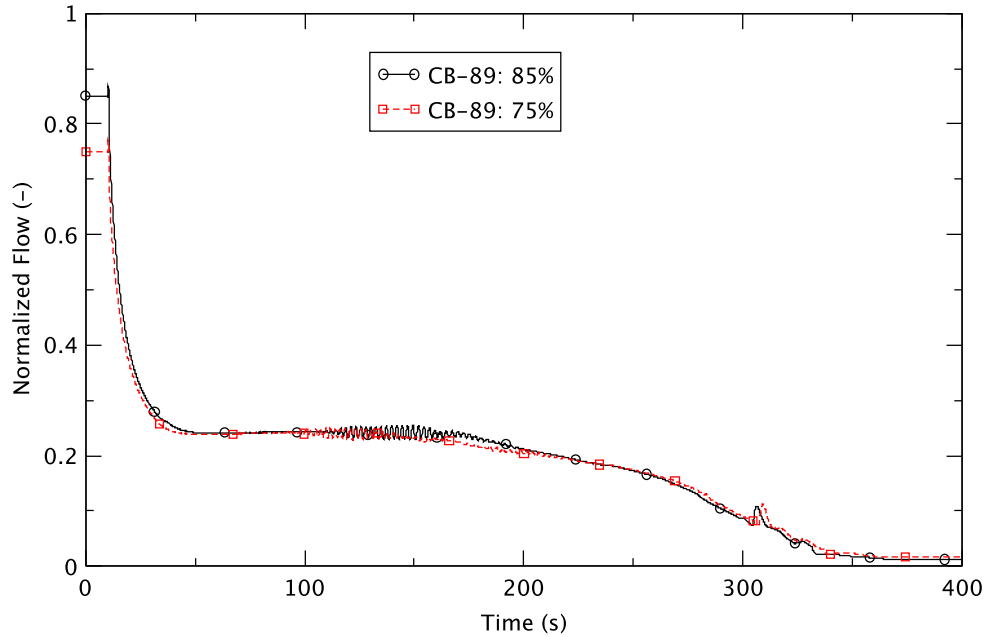


Figure 2.51 Reactor Core Flow Rate - Effect of Core Flow at PHE

2.3.7 Feedwater Flow and RPV Water Level

Operator action for reducing the water level to TAF is simulated at 120 s by reducing the flow of feedwater to decrease the mass flow into the core. Figure 2.52 compares the feedwater flow rates. As expected, in both cases the flow rates start decreasing faster after 120 s. The comparison shows that TRACE predicts larger FW flow for the 75% core flow case from approximately 20 s onwards. This difference is attributed to a larger steam flow rate in that case (Figure 2.47), causing the FW controller to try to match the FW flow with the steam flow so to maintain the DC water level until 120 s, after which the FW flow starts decreasing further. The FW flow becomes zero at around 259 s with 85% flow, and at ~270 s with 75% flow. From those times onward, water flows into the vessel only from the RCIC and the FW restarts flowing at around 321 s in the 75% flow case and ~ 365 s with 85% flow.

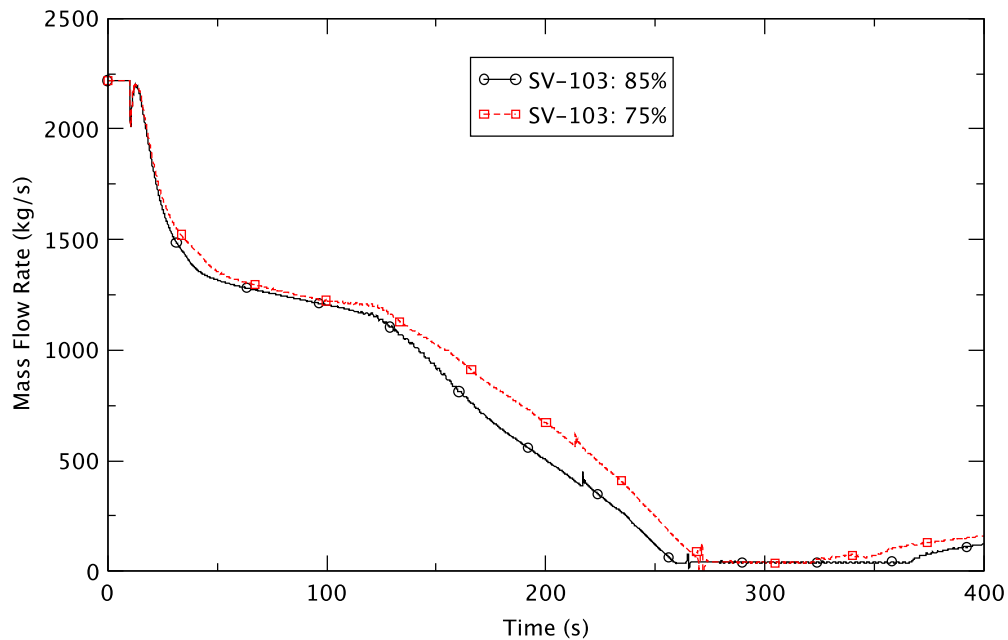


Figure 2.52 Feedwater Flow Rate - Effect of Core Flow at PHE

Figure 2.53 compares the DC water level. With 75% core flow, the DC water level behaves differently from the 85% flow case as well as from the other cases discussed in [2]. While it does not drop for a relatively long time (about 43 s) after the operator action at 120 s in the 85% case, the DC level starts declining just after the operator action with 75% core flow. This different behavior seems to be caused by the different behavior of the coolant mass in the separators. Figure 2.54 compares the coolant mass in the separators in ring 1. As shown, there is no noticeable accumulation of coolant in the separators with 75% flow while coolant mass accumulates with 85% flow from around 37 s to 122 s, and then starts to be released to the RPV until around 170 s (see Section 4.2.9 in [2] for detailed discussions about this separator behavior). In the latter, this mass release compensates for the reduction in FW flow and keeps the DC level at almost the same elevation from 122 s to 163 s. However, in the former case, basically no excessive mass is accumulated and released from the separators during that time, so resulting in a decrease of the DC water level from around 120 s and a lower level from about 120 s to 220 s. This lower DC level causes smaller core flow from approximately 120 s to 220 s (Figure 2.51).

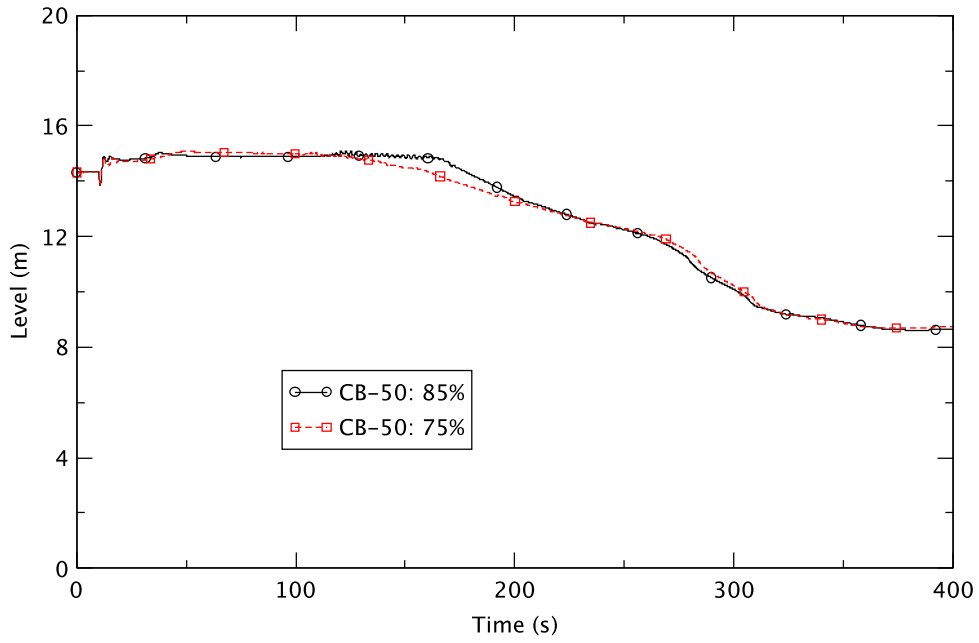


Figure 2.53 Downcomer Water Level - Effect of Core Flow at PHE

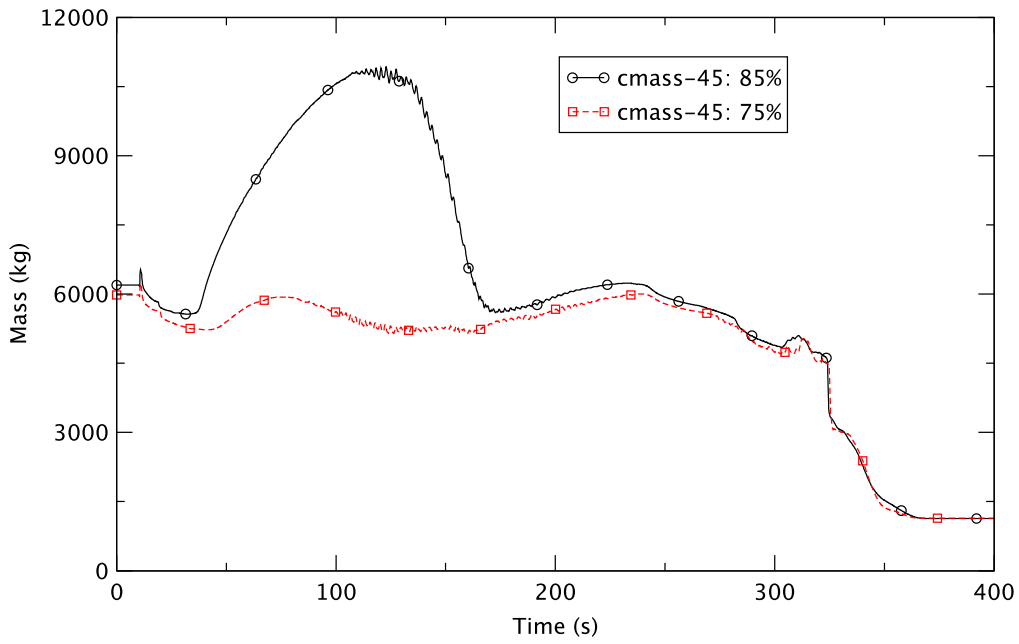


Figure 2.54 Coolant Mass in Ring 1 Separators - Effect of Core Flow at PHE

2.3.8 Boron Inventory in Core

SLCS is initiated at 130 s and Figure 2.55 compares the boron inventory in the core for both cases. It is almost the same; hence, boron injection does not contribute to the differences between cases with different initial flow rates.

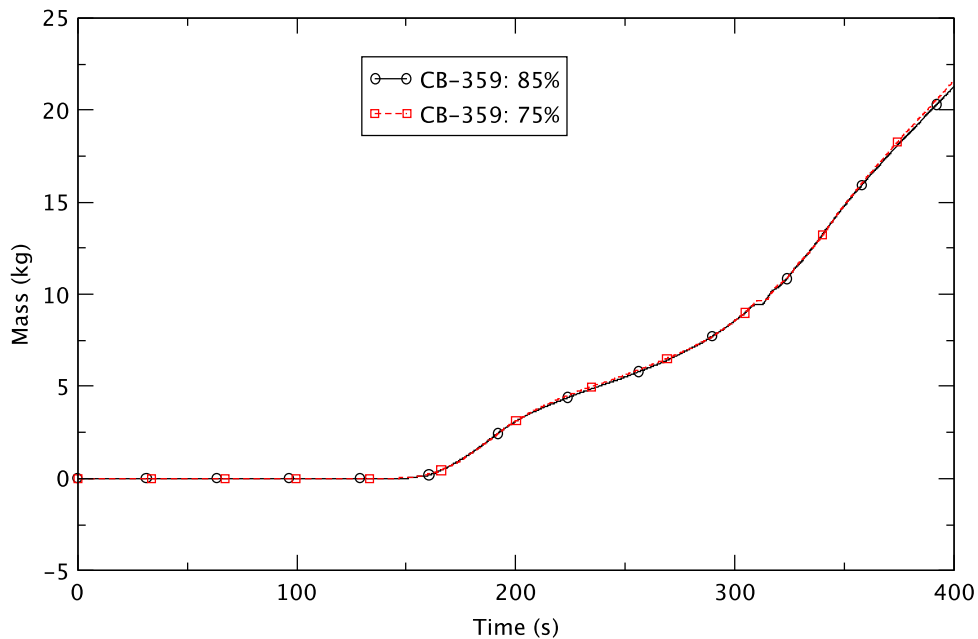


Figure 2.55 Boron Inventory in Reactor Core - Effect of Core Flow at PHE

2.3.9 Liquid Subcooling of Core Flow

Figure 2.56 shows core inlet subcooling in ring 1. The subcooling is larger initially by around 1.3 K with 75% core flow. This reflects the fact that the steam flow and the feed flow are the same initially in both cases (see Figure 2.47) but the core flow is smaller with 75% flow (Figure 2.51). During normal operation, a 75% core flow would return a smaller amount of hot liquid to mix with the cold feedwater and this leads to a lower liquid temperature for the core flow.

The initial subcooling difference between the two cases is maintained until around 140 s, and then the difference rises until around 250 s, and from thereon it starts declining. The subcooling difference, becoming noticeably larger from around 155 s, is accounted for by relatively larger FW flow from around 130 s for a 75% flow (Figure 2.52). The drop in the subcooling difference from around 250 s seems to result from the core flow becoming larger with 75% flow relative to that for 85% flow from about 230 s; the difference of the FW flow between the two cases begins dropping from around 220 s. The change of the liquid subcooling in the downcomer appears at the core inlet around 20 s later (Figure 2.56), because the coolant takes time to reach the core inlet from the downcomer.

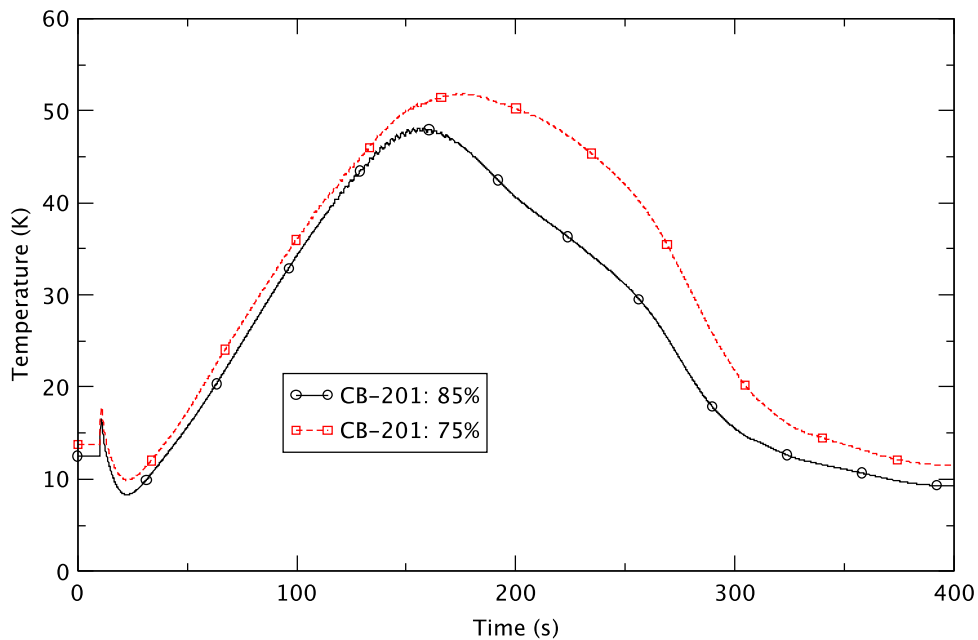


Figure 2.56 Liquid Subcooling at Core Inlet - Effect of Core Flow at PHE

2.3.10 Fuel Rod Cladding Temperature

The core power oscillations can affect the temperature of the fuel cladding due to the changes in the power and the efficiency of heat transfer from the fuel to the coolant. The variation in heat transfer is affected by the continuous change of void fraction and coolant flow in the core. Figure 2.57 compares the maximum cladding temperature among all bundles in the core. It suddenly increases at around 108 s and 122 s, respectively, for the 75% flow and 85% flow cases. This behavior seemingly is caused by the early start of the power oscillations at around 87 s in the former case (Figure 2.48). Figure 2.57 also shows that the cladding is quenched later in the 75% flow case, due to a later start in the decay of the power oscillation as well as a higher power (Figure 2.48).

In addition, the case with 75% core flow predicts a peak cladding temperature of 1,759 K at around 156 s; in contrast, 1,690 K is predicted at approximately 163 s for the 85% flow case. In both, the cladding temperature becomes higher than the ad hoc limit of 1,478 K (2,200°F) (Section 2.2.10). The highest cladding temperature is related to the relative local peak power (and not the total power) as shown in Figure 2.58. The relative local peak power for the 75% flow case is slightly higher (around 9.4 at 154 s) than that for the 85% flow case (around 9.3 at 161 s), showing consistent behavior with peak cladding temperatures. However, the general behavior of the cladding temperature is similar in both cases.

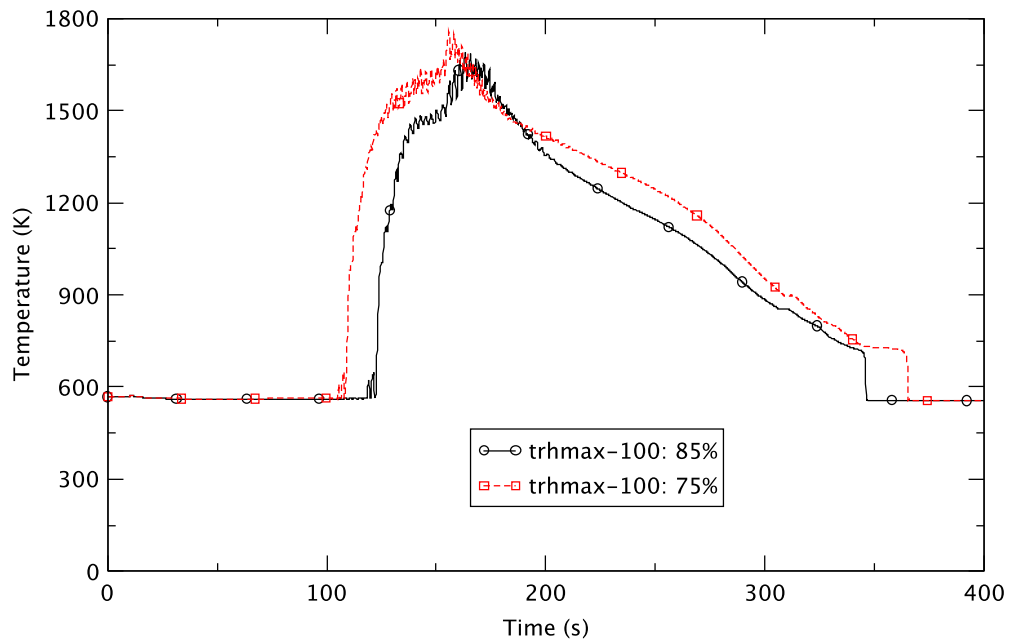


Figure 2.57 Maximum Cladding Temperature among all Fuel Bundles - Effect of Core Flow at PHE

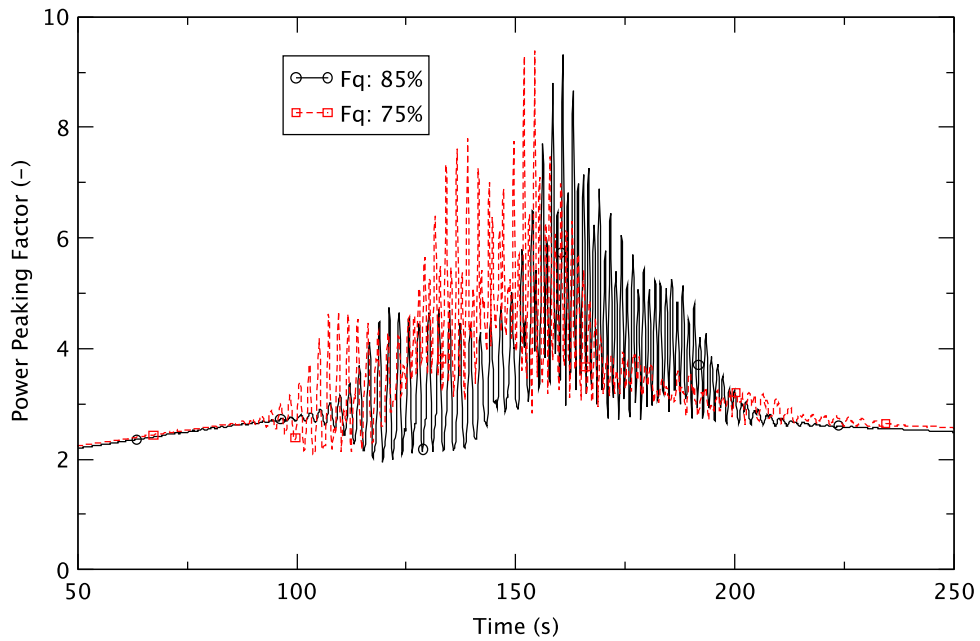


Figure 2.58 Local Peak Power - Effect of Core Flow at PHE

2.3.11 Ratio of Power-to-Product-of-Flow-and-Enthalpy

Figure 2.59 compares the behavior of the ratio of power to product of flow and enthalpy (FOM1) in the limiting bundles wherein the peak cladding temperature seems to be predicted. From the figure, we observe that this ratio continues to increase with time for both cases. Furthermore, it is evident that this variable is generally larger for the smaller core flow (75%). This effect, with the higher reactor power and core inlet subcooling for the 75% flow case, causes more severe instability and a higher peak cladding temperature.

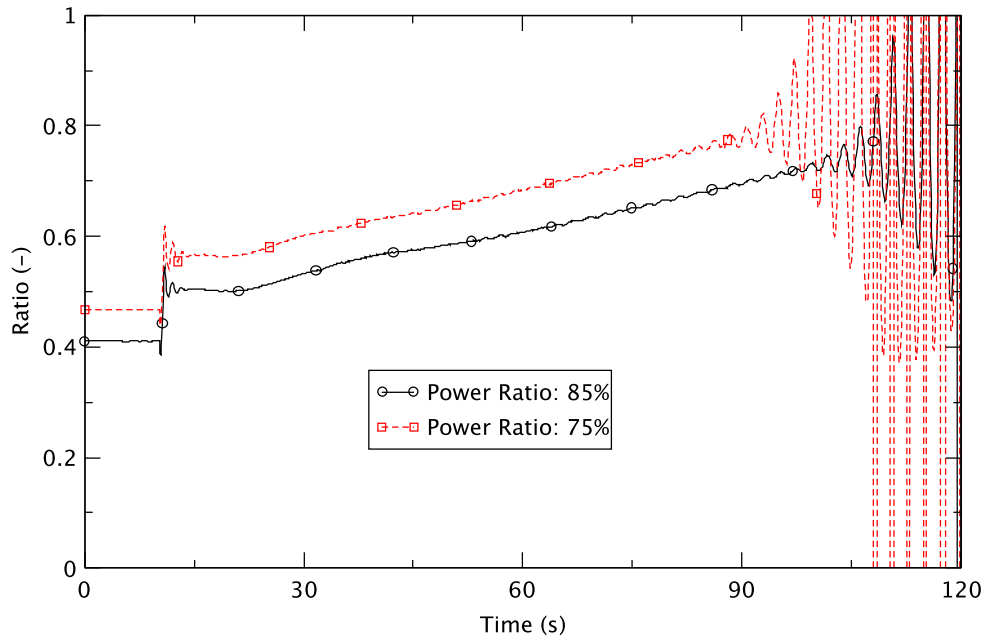


Figure 2.59 Ratio of Power to Product of Flow and Enthalpy (FOM1) in Limiting Bundles - Effect of Core Flow at PHE

2.3.12 Additional Figures-of-Merit

Additional figures-of-merit were examined (Table 2.13). When the initial core flow is 75%, the onset of reactor instability occurs earlier and power oscillation evolves from one mode to another multiple times. This can best be seen in the radial (x,y) power versus time movies. The snapshots from the movies in Figure 2.60 illustrate the modes of oscillation for 75% initial core flow.

Table 2.13 Figures-of-Merit Associated with Evolution of Power Instability - Effect of Core Flow Rate at PHE

Figure-of-Merit	75% Core Flow	85% Core Flow
Time of Onset of Reactor Instability (s)	87	95
Time of Onset of Bimodal Power Oscillation	118 ¹ 154 ²	144 ¹ 154 ²
Time of Frequency Change (s)	131 (From 0.43 to 0.84 Hz)	157 (From 0.42 to 0.79 Hz)
Time of Onset of Oscillation Decay (s)	158	167

¹ The power oscillation evolves from the fundamental to a higher harmonic mode.

² The power oscillation evolves from higher harmonic to the first harmonic mode.

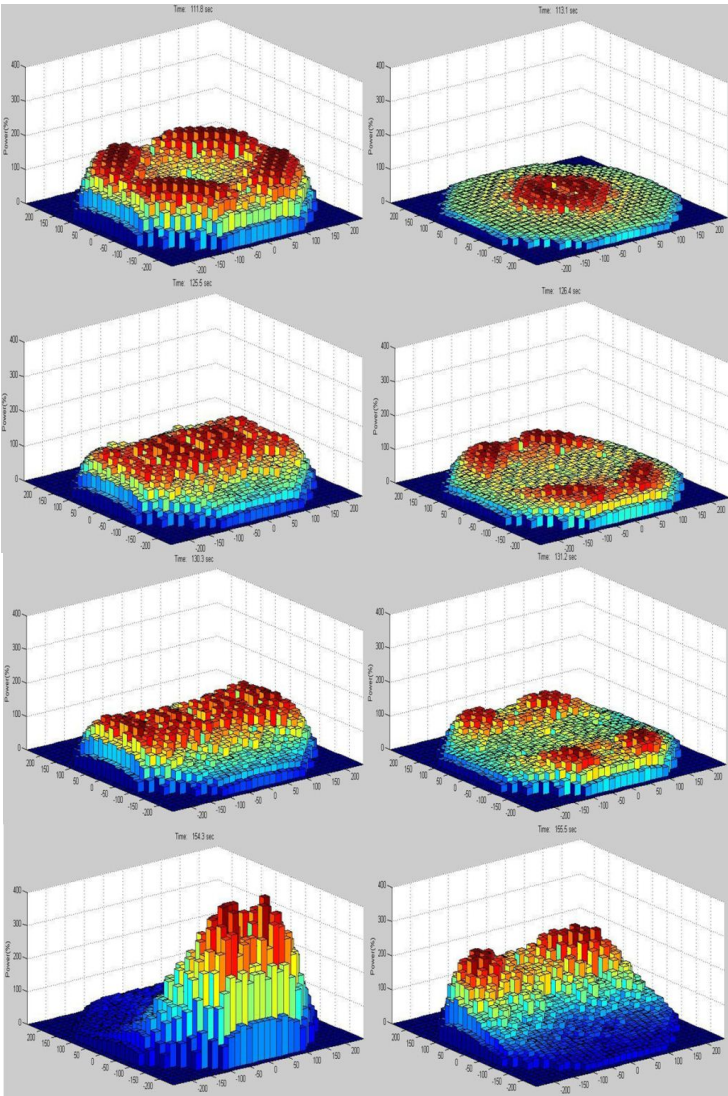


Figure 2.60 Power Oscillation Modes - 75% Core Flow at PHE

2.3.13 Summary

The general behavior of the core power is similar at PHE with 75% and 85% initial core flows. However, for 75% flow, TRACE/PARCS predicts a relatively smaller negative moderator reactivity due to the relatively larger core flow rate compared to the initial one after the recirculation pumps coast down. This results in higher core power during the transient. Subcooling of the core inlet and the ratio of power to the product of flow and enthalpy are larger for 75% flow; all these parameters seem to cause slightly more severe instability and result in higher maximum cladding temperature.

It is predicted that when the initial core flow is 75%, the downcomer water level starts decreasing around 120 s. This behavior seems to be reasonable and differs from that with 85% initial core flow as well as the other cases discussed in [2]. The behavior of other variables including system pressure and boron inventory in the core are predicted to be very similar in general for a 75% and 85% initial core flow.

3 SUMMARY AND CONCLUSIONS

We completed a study of ATWS events initiated by turbine trip with the reactor initially in the MELLLA+ extended operating domain. The events considered complement those documented in a previous study [2]. (That report also discussed the modeling used in the present study.) In the present study, the sensitivity to gas-gap conductance modeling, turbine bypass fraction at PHE, and initial core flow at PHE were considered. The intent of the current scope of work has been to study reactor instability events and the consequences that may result from such scenarios. The results of the studies are summarized below.

The system behavior is very similar in the BOC cases using the dynamic gap model and a low fixed conductance for the gas-gap between the fuel pellet and the clad. This correspondence is because the assumed magnitude of the value of the low gap conductance is similar to that predicted by the dynamic gap model. However, in PHE cases, while the core is relatively unstable with the dynamic-gap model, the reactor power is predicted to be much more stable and there is no significant increase in cladding temperature during the transient period with a high fixed conductance. The high conductance in the gas-gap effectively reduces the time lag between reactor power and heat flux to the coolant. It also tempers the temperature response of the fuel to power fluctuations. The net result is a smaller change in the fuel temperature for a given change in power. A smaller decline in fuel temperature results in relatively more neutrons being absorbed in the fuel pellet (specifically, in ^{238}U) and fewer being available for fission due to the characteristics of the Doppler effect. The fuel dynamics, as manifested in the reduced Doppler effect, with additional parameters such as the lower subcooling at the core inlet and the lower ratio of power to the product of flow and enthalpy, seems to lead to more stable behavior at PHE with the fixed high gap conductance.

At PHE with different turbine bypass fractions, the general behavior of the system parameters is similar to the behavior at BOC under the same conditions. For example, the core inlet subcooling and the ratio of power to the product of flow and enthalpy are larger when the turbine bypass fraction is smaller. However, the power responses differ at the two different fuel cycle times. While TRACE predicts a more unstable reactor condition at BOC when the turbine bypass fraction lessens, the amplitude of the power oscillation due to the reactor instability does not show any obvious trend associated with the size of the bypass fraction at PHE, even though the power instability is observed in all cases.

The general behavior of the core power is similar at PHE with 75% and 85% initial core flows. However, for the former, TRACE/PARCS predicts relatively smaller negative moderator reactivity feedback due to relatively larger core flow rate compared to the initial one after the recirculation pumps coast down. This results in higher core power during the transient. The core inlet subcooling and the ratio of power to the product of flow and enthalpy become larger for the 75% flow case. All these parameters seem to cause slightly more severe instability and result in higher maximum cladding temperature in that case.

The TRACE analysis shows that when the initial core flow is 75%, the level of downcomer water starts decreasing from around 120 s, right after the reduction in water level is initiated. This behavior seems to be reasonable and differs from that with 85% initial core flow, as well as the other cases discussed in the initial study [2]. The behavior of other variables, including system pressure and boron inventory in the core, are predicted to be very similar in general for a 75% and 85% initial core flow.

The following conclusions are drawn from the analysis presented in Chapter 2.

- The reactor power becomes relatively lower than the base case and much more stable with a fixed high gap conductance of 161,000 W/m²-K, while TRACE predicts very similar system behavior with fixed low gap conductance of 5,000 W/m²-K, compared to the predictions with the dynamic gas-gap model. For the fixed high gap conductance, the peak cladding temperature does not increase much (less than 70 K).
- The similarity in the transient responses in the sensitivity case for gap conductance at BOC and the reference case is due to the fixed low gap conductance value of 5,000 W/m²-K being within the range of values calculated by the dynamic gas-gap model for the reference case.
- The high conductance in the gas-gap between the fuel pellet and clad causes less decrease of the fuel temperature during the transient, and results in relatively more neutrons being absorbed by the ²³⁸U in the fuel pellet and fewer neutrons being available for fission due to the characteristics of the Doppler coefficient (fuel temperature coefficient of reactivity).
- The lower power due to the fuel's dynamic response, as manifested in the reduced Doppler effect, seems to be the major reason for the more stable behavior at PHE with the fixed high gap conductance. Some parameters contribute to stabilizing the reactor more, such as the lower core inlet subcooling and the lower FOM1 (ratio of power to product of flow and enthalpy).
- At PHE with different turbine bypass fractions, the general behavior of the system parameters is very similar to the behavior at BOC with different bypass fractions, but the trend of the power responses to the bypass fractions is different.
- While TRACE predicts a more unstable reactor condition at BOC with a smaller turbine bypass fraction, the amplitude of the power oscillation due to reactor instability does not show any obvious trend associated with the size of the bypass fraction at PHE, even though the power instability is observed in all cases (10%, 25%, and 100% bypass fractions).
- The reasons are unknown for different trends at BOC and PHE, for reactor power responding to variations in the turbine bypass fraction. Subsequent to this analysis, a revised SRV model and a new boron transport model, that may provide more detailed modeling of the plant, were incorporated in the BWR/5 model that was used to study ATWS events with emergency depressurization [3]. The new SRV model addresses the known limitations of the simplified SRV model utilized in this current analysis. The new boron transport scheme eliminates the flow control valve at the lower plenum whose presence is known to create non-physical flow disturbances.
- At PHE, a higher transient core power is predicted for the case with 75% initial flow rate relative to that with an 85% initial flow rate because there is more (negative) moderator feedback in the latter resulting from the larger change in flow rate after 2RPT.
- The core inlet subcooling and the FOM1 value become larger for the case of smaller initial core flow (75%) and these parameters together with higher power seem to cause

slightly more severe instability of the reactor power and higher maximum cladding temperature than with the higher initial core flow (85%).

- When the initial core flow is at 75%, TRACE predicts the expected response of the downcomer water level starting to decrease shortly after the operator's action at 120 s. In the other cases, including that with 85% core flow at PHE, the DC level does not drop for a relatively long time (about 35 s to 45 s) after the operator's action due to the calculation of liquid accumulation in the separators.
- We observed that for the PHE cases, the reactor instability starts early and power oscillations evolve from the fundamental to higher harmonic mode, and then to the first harmonic mode when the gas-gap conductance is high, the turbine bypass fraction is small, and the initial core flow is small.
- In many cases, power oscillations evolve from the fundamental to higher harmonic modes. However, PARCS does not output modal reactivities, eigenvalue separations, or higher harmonic shapes. (A PARCS output file (xxx.parcs_pow) will have information on how the power oscillations can be decomposed between fundamental and first harmonic (only) modes, but this capability is not working in the version used for this study.)
- The sensitivity study demonstrated the effects of turbine bypass capacity and initial core flow on the ATWS instabilities in a BWR. Thus, it is prudent, for each plant-specific application, to model each plant under its proposed licensed limit condition.

4 REFERENCES

1. J. Harrison, GE Hitachi, letter to U.S. Nuclear Regulatory Commission, "Accepted Version of GE Licensing Topical Report NEDC-33006P-A, Revision 3 (TAC No. MD0277)," MFN 09-362, June 19, 2009, ADAMS Accession No. ML091800512.
2. L-Y. Cheng et al., "BWR Anticipated Transients Without Scram in the MELLLA+ Expanded Operating Domain – Part 1: Model Development and Events Leading to Instability," NUREG/CR-7179, BNL-NUREG-105323-2014, Brookhaven National Laboratory, March 3, 2014.
3. L-Y. Cheng et al., "BWR Anticipated Transients Without Scram in the MELLLA+ Expanded Operating Domain – Part 3: Events Leading to Emergency Depressurization," NUREG/CR-7181, BNL-NUREG-105328-2014, Brookhaven National Laboratory, April 22, 2014.
4. L-Y. Cheng et al., "BWR Anticipated Transients Without Scram in the MELLLA+ Expanded Operating Domain – Part 4: Sensitivity Studies for Events Leading to Emergency Depressurization," NUREG/CR-7182, BNL-NUREG-105330-2014, Brookhaven National Laboratory, April 25, 2014.
5. P. Yarsky, "Applicability of TRACE/PARCS to MELLLA+ BWR ATWS Analyses, Revision 1," U.S. Nuclear Regulatory Commission, Office of Nuclear Regulatory Research, November 18, 2011, ADAMS Accession No. ML113350073.
6. G.M. O'Donnell, H.H. Scott and R.O. Meyer, "A New Comparative Analysis of LWR Fuel Designs," NUREG-1754, U.S. Nuclear Regulatory Commission, Office of Nuclear Regulatory Research, December 2001.
7. NRC, "Standard Review Plan," Section 15.8, NUREG 0800, U.S. Nuclear Regulatory Commission, March 2007.
8. J. March-Leuba and J. Rey, "Coupled Thermalhydraulic-Neutronic Instabilities in Boiling Water Nuclear Reactors: A Review of the State of the Art," *Nucl. Eng. Des.*, 145, 97-111, 1993.

APPENDIX A

MODELING OF GAP CONDUCTANCE

Two of the ATWS-I sensitivity cases call for a low and a high value for the gap conductance for the fuel rod. The NRC staff provided guidance to use NUREG-1754 [1] to support the selection of the gap conductance. The NUREG report offers calculated gap conductance as a function of average burnup (GWd/t) for a BWR 10x10 fuel rod with initial peak power of 5, 7, 9, and 11 kW/ft. The results are reported in four figures, Figures 7-3 (5 kW/ft), 7-9 (7 kW/ft), 7-15 (9 kW/ft) and 7-21 (11 kW/ft) (placed with original numbering below). In all of them, the gap conductance reaches the minimum early in the burnup and attains the maximum near middle of the range. For the ATWS-I sensitivity calculations, the minimum from the figures is used as the fixed low value and the maximum from the figures is used as the fixed high value; namely, 5 kW/m²-K and 161 kW/m²-K, respectively.

The implementation of constant gap conductance in the TRACE fuel rod model necessitates the following two changes to the CHAN component inputs:

- 1) turning off the dynamic gas-gap model in TRACE, and,
- 2) specifying the rod gas-gap heat transfer coefficient (gap conductance)

Turning off the dynamic gas-gap model involves modifying or deleting the following input variables² for the CHAN component.

In Card Set Number 5 set **NFCI** = 0 (dynamic gas-gap model is off)

Delete Card Set Number 12 (**UCRPDOWN**, **UFSWELL**, **RFCLAD**)

Retain Card Set Number 58 (**GMIX**). The mole fraction of gap-gas constituents is not used if **NFCI** = 0 but must be input.

Retain Card Set Number 59 (**PGAPT**). The average initial gap-gas pressure is not used if **NFCI** = 0 but must be input.

Card Set Numbers 60 (**BURN**) and 61 (**GADC**) are retained for use by the modified fuel conductivity model.

The TRACE input for the gap conductance is in Card Set Number 15,

HGAPO = 5 kW/m²-K

HGAPO = 161 kW/m²-K

² TRACE input variable names are in bold type.

REFERENCES

1. G.M. O'Donnell, H.H. Scott and R.O. Meyer, "A New Comparative Analysis of LWR Fuel Designs," NUREG-1754, U.S. Nuclear Regulatory Commission, Office of Nuclear Regulatory Research, December 2001.

(Figures 7-3, 7-9, 7-15 and 7-21 with original numbering from this reference are placed below).

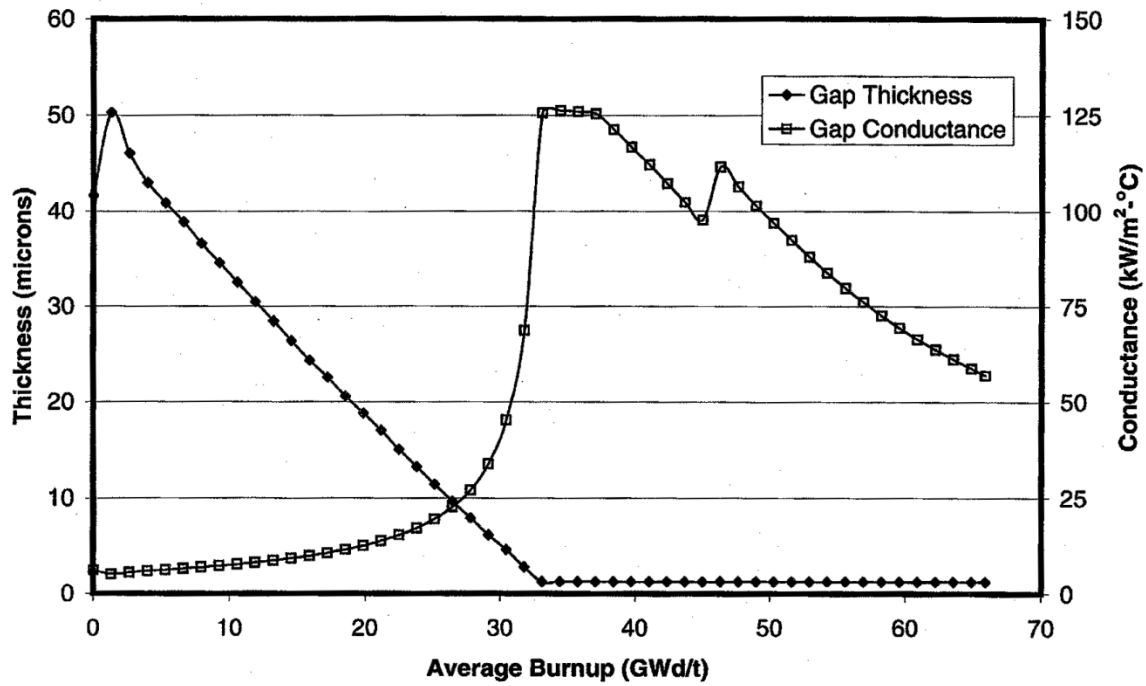


Fig. 7-3. Gap thickness and gap conductance for a BWR 10x10 fuel rod with initial peak power of 5 kW/ft.

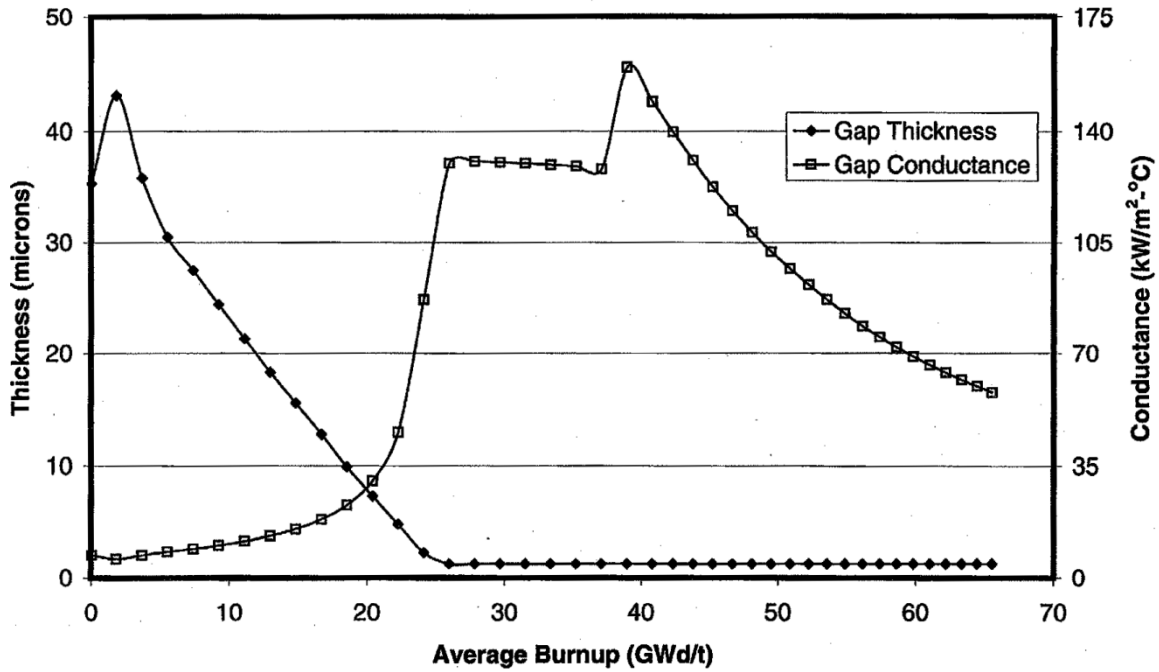


Fig. 7-9. Gap thickness and gap conductance for a BWR 10x10 fuel rod with initial peak power of 7 kW/ft.

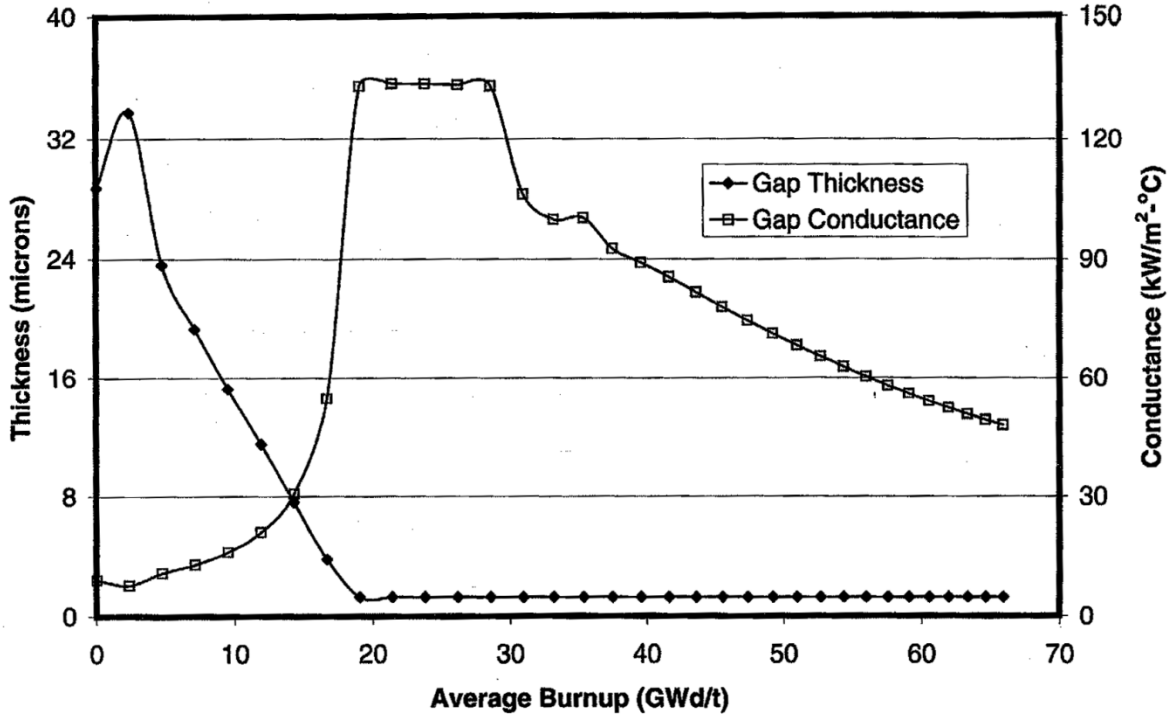


Fig. 7-15. Gap thickness and gap conductance for a BWR 10x10 fuel rod with initial peak power of 9 kW/ft.

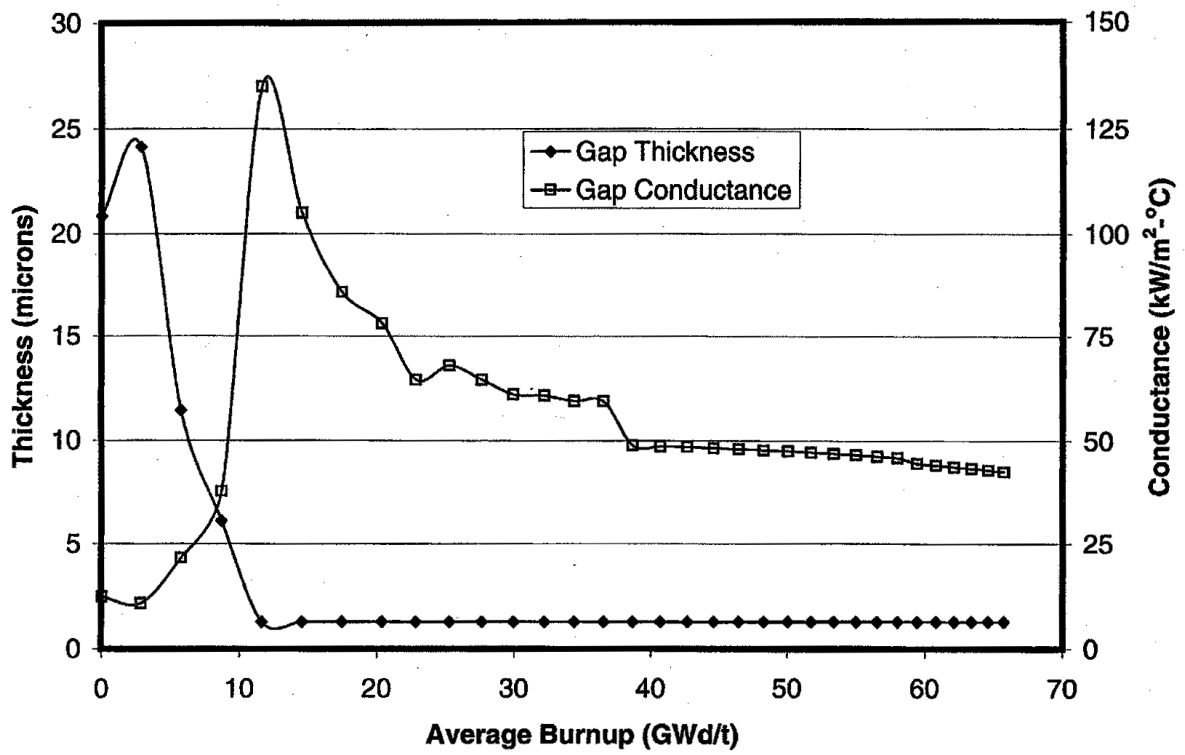


Fig. 7-21. Gap thickness and gap conductance for a BWR 10x10 fuel rod with initial peak power of 11 kW/ft.

<p>NRC FORM 335 (12-2010) NRCMD 3.7</p> <p style="text-align: center;">U.S. NUCLEAR REGULATORY COMMISSION</p> <p style="text-align: center;">BIBLIOGRAPHIC DATA SHEET <i>(See instructions on the reverse)</i></p>	<p>1. REPORT NUMBER (Assigned by NRC, Add Vol., Supp., Rev., and Addendum Numbers, if any.)</p> <p style="text-align: center;">NUREG/CR-7180 BNL-NUREG-105327-2014</p>				
<p>2. TITLE AND SUBTITLE</p> <p>BWR Anticipated Transients Without Scram in the MELLLA+ Expanded Operating Domain Part 2: Sensitivity Studies for Events Leading to Instability</p>	<p>3. DATE REPORT PUBLISHED</p> <table border="1" style="width: 100%;"> <tr> <td style="width: 50%;">MONTH</td> <td style="width: 50%;">YEAR</td> </tr> <tr> <td style="text-align: center;">June</td> <td style="text-align: center;">2015</td> </tr> </table> <p>4. FIN OR GRANT NUMBER</p> <p style="text-align: center;">V6150 / F6018</p>	MONTH	YEAR	June	2015
MONTH	YEAR				
June	2015				
<p>5. AUTHOR(S)</p> <p>Lap-Yan Cheng, Joo-Seok Baek, Arantxa Cuadra, Arnold Aronson, David Diamond, Peter Yarsky</p>	<p>6. TYPE OF REPORT</p> <p style="text-align: center;">Technical</p> <p>7. PERIOD COVERED (Inclusive Dates)</p> <p style="text-align: center;">6/1/10 - 6/30/15</p>				
<p>8. PERFORMING ORGANIZATION - NAME AND ADDRESS (If NRC, provide Division, Office or Region, U. S. Nuclear Regulatory Commission, and mailing address; if contractor, provide name and mailing address.)</p> <p>Nuclear Science & Technology Department Brookhaven National Laboratory Upton, NY 11973-5000</p>					
<p>9. SPONSORING ORGANIZATION - NAME AND ADDRESS (If NRC, type "Same as above", if contractor, provide NRC Division, Office or Region, U. S. Nuclear Regulatory Commission, and mailing address.)</p> <p>Division of Systems Analysis Office of Nuclear Regulatory Research U.S. Nuclear Regulatory Commission Washington, DC 20555-0001</p>					
<p>10. SUPPLEMENTARY NOTES</p> <p>Tarek Zaki, NRC Project Manager</p>					
<p>11. ABSTRACT (200 words or less)</p> <p>This is the second in a series of reports on the response of a BWR/5 boiling water reactor, operating in the expanded operating domain "MELLLA+," to anticipated transients without reactor scram (ATWS). Herein, ATWS events initiated by a turbine trip are considered at two points in the fuel cycle: the beginning of cycle (BOC), and at peak hot excess reactivity (PHE, close to the middle of the cycle). We evaluate the effects of modeling the gap conductance (between the fuel pellet and clad), the turbine bypass fraction, and the initial core flow rate. We compare two limiting fixed values of gas-gap conductance, a low value of 5,000 W/sq.m-K at BOC and a high value of 161,000 W/sq.m-K at PHE with corresponding base cases that utilize a dynamic gas-gap model. We analyze two turbine bypass fractions, viz., 10% and 25% at PHE, and compare them with the 100% bypass base case. A reduced core flow of 75% of the rated core flow is analyzed at PHE and compared with the base case of 85%. The simulations were carried out using the TRACE/PARCS code system and models developed for a previous study with all relevant BWR/5 systems. Modeling in the core is particularly detailed (four types of fuel rods are included in each fuel assembly, and 382 thermal-hydraulic channels to represent all assemblies, taking into account half-core symmetry) so as to capture the complex neutronic thermal-hydraulic coupling during periods of instability. The study offers insights into the behavior of the reactor during these events, including the impact of the operator's assumed actions on its oscillatory behavior due to instabilities in the reactor, and on its eventual shutdown. It shows the effect of gap conductance, turbine bypass fraction, and initial flow rate.</p>					
<p>12. KEY WORDS/DESCRIPTORS (List words or phrases that will assist researchers in locating the report.)</p> <p>TRACE/PARCS; Anticipated Transients Without Scram (ATWS); Boiling Water Reactor (BWR); operator action; safety analysis; stability analysis; Maximum Extended Load Line Limit Analysis Plus (MELLLA+)</p>	<p>13. AVAILABILITY STATEMENT</p> <p style="text-align: center;">unlimited</p> <p>14. SECURITY CLASSIFICATION</p> <p>(This Page) unclassified</p> <p>(This Report) unclassified</p> <p>15. NUMBER OF PAGES</p> <p>16. PRICE</p>				



Federal Recycling Program



**UNITED STATES
NUCLEAR REGULATORY COMMISSION**
WASHINGTON, DC 20555-0001

OFFICIAL BUSINESS



NUREG/CR-7180

**BWR Anticipated Transients Without Scram in the MELLLLA+ Expanded
Operating Domain, Part 2**

June 2015